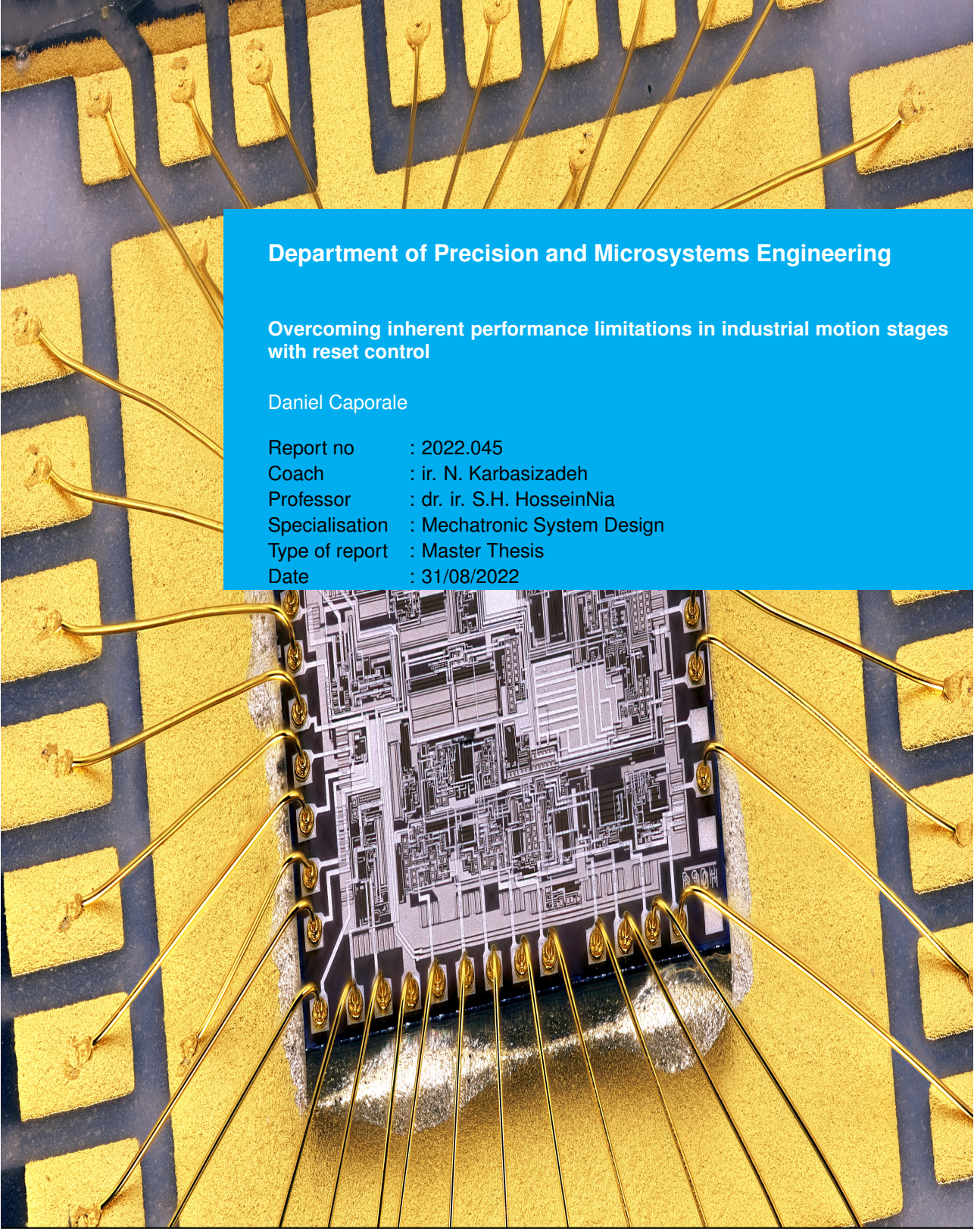

Department of Precision and Microsystems Engineering

Overcoming inherent performance limitations in industrial motion stages with reset control

Daniel Caporale

Report no	: 2022.045
Coach	: ir. N. Karbasizadeh
Professor	: dr. ir. S.H. HosseinNia
Specialisation	: Mechatronic System Design
Type of report	: Master Thesis
Date	: 31/08/2022

TU Delft Delft University of Technology

Challenge the future

OVERCOMING INHERENT PERFORMANCE LIMITATIONS IN INDUSTRIAL MOTION STAGES WITH RESET CONTROL

A GENERAL APPROACH TO THE DESIGN AND IMPLEMENTATION OF RESET CONTROLLERS VALIDATED ON AN ASMPT AB383 WIRE BONDER

by

Daniel CAPORALE

Master Thesis

in partial fulfillment of the requirements for the degree of

Master of Science
in Mechanical Engineering

at the Delft University of Technology,

to be defended publicly on 31/08/2022

Supervisors:	dr. ir. S.H. HosseinNia	(TU Delft)
	ir. N. Karbasizadeh	(TU Delft)
	ir. L.F. van Eijk	(ASMPT)
	ir. S. Beer	(ASMPT)
	dr. ir. D. Kostić	(ASMPT)
Thesis committee:	dr. ir. S.H. HosseinNia	(TU Delft)
	ir. N. Karbasizadeh	(TU Delft)
	dr. ir. L. Peternel	(TU Delft)
	dr. ir. C. Della Santina	(TU Delft)
	ir. L.F. van Eijk	(ASMPT)

TU Delft Delft University of Technology

ASM Pacific Technology

ABSTRACT

Linear time-invariant controllers are undoubtedly the most popular type of regulators used in industrial applications, with the overwhelming majority of companies employing them. The reason is mainly given by their simple design methods. In particular, frequency domain predictive performance analysis and stability methods allow the use of loopshaping techniques. Nevertheless, inherent limitations affecting linear controllers pose constraints on their performance that can only be overcome through the adoption of nonlinear control schemes. Promising findings in recent literature suggest that with reset control, a nonlinear control technique, it is possible to overcome these limitations. At the same time, reset control could also potentially allow the use of straightforward design techniques, thus making it suitable for industrial applications. The main goal of this work is to bring together the different concepts scattered in literature, in order to initialize the construction of a general framework for the design and analysis of reset controllers suitable for an industrial setting. Tuning guidelines for different structures using two classes of reset controllers, the first order reset element and the proportional Clegg integrator, were presented. Two frequency domain methods, namely open-loop higher order sinusoidal input describing functions (HOSIDFs) and pseudosensitivities computed through analytically derived (approximate) closed-loop HOSIDFs, were effectively applied to predict steady-state performance. Stability was (when possible) analysed through the frequency domain Nyquist stability vector method, which could also be implemented in the design process. The frequency domain analysis methods allowed the use of loopshaping techniques similar to LTI control for the design of reset controllers. The controllers, implemented digitally on an ASM Pacific Technology wire bonding machine, show that through reset control a significant decrease in the root mean square of the settling error compared to an equivalent LTI controller could be achieved. The existing frequency domain analysis methods, its straightforward implementation and the increase in performance achieved in experiments validate the potential of reset control as a suitable alternative to LTI control for industry. Nevertheless, limitations in the explored reset control structures still exist and further work is required in order to achieve the full potential that this technique has to offer. Some recommendations on further work are given in the conclusion.

PREFACE

This work is dedicated towards the fulfillment of the degree of Master of Science in Mechanical Engineering at the Precision and Microsystems Engineering group of Delft University of Technology (TU Delft), with specialization in Mechatronic System Design. The research has been conducted under the expert guidance and supervision of mentors at TU Delft and ASM Pacific Technology.

CONTENTS

1

INTRODUCTION

ASM Pacific Technology Ltd. (ASMPT) is one of the world's leading suppliers of semiconductor assembly and surface-mount technology equipment [1]. One of the products in the company's franchise is the AB383 wire bonder, which creates interconnections between chips and their packaging (Fig. 1.1). In order to succeed in this increasingly competitive market, every high-tech company is required to perpetually increase the speed and precision of their machines. One way ASMPT aims at increasing the performance of their products is through improving their control systems. As the overwhelming majority of commercial products, the motion of the ASMPT AB383 wire bonder is currently regulated by a fully linear-time-invariant (LTI) control strategy. Due to inherent limitations such as the *waterbed effect* and *Bode's gain phase relationship* [2] it is impossible to push the performance beyond a certain point relying solely on LTI control. For this reason, for the last few decades nonlinear control has been given great consideration in literature. Nevertheless, adoption in industry is still scarce [3]. One of the reasons is that for most techniques, it is relatively complex, if not impossible, to get any indication on the performance of the system in the frequency domain. This is however not necessarily true for all methods. Some, such as reset control, pose an exception. Another drawback of nonlinear systems is given by their complicated stability analysis which often require exact knowledge of the plant to be reliable, due to the lack of robustness analysis techniques. Recent studies have proven that the stability of some reset controllers can be determined without knowledge of the parametric description of the plant, thus overcoming this issue.

Reset control appeared the first time in literature more than 60 years ago [5]. However, it is only recently that the field has been given enough attention to be considered a potentially reliable alternative to linear control [6]. This particular category of nonlinear controllers shares much of the design process with linear control, while also allowing to

Figure 1.1: AB383 wire bonder (reproduced with permission from [4]).

overcome the inherent limitations of linear control, which makes it attractive in industry. Nevertheless, the adoption in industry is still in its infancy and literature on synthesis and implementation of reset controllers in industrial applications is scarce. ASMPT has already conducted research on the implementation of reset control on the motion platform of the AB383 wire bonder [4]. Although reset control proved to increase performance compared to its linear counterparts, some open issues prevented the adoption of reset control on the wire bonder. Specifically, the lack of frequency domain analysis tools prevented analysing the controllers in terms of predictive performance and stability. New research such as [7], [8], [9], [10], [11] and [12] opened new possibilities in terms of design, stability analysis and performance analysis of reset controllers. Therefore, this research aims to use these findings to solve the open issues.

The majority of the previously cited literature works are focused on the 'Constant in gain-lead in phase' (CgLp) element [13]. This structure has high versatility, as it can be used in combination with any LTI controller, increasing its robustness without loss in performance. However, being a nonlinear technique, reset controllers introduce unwanted higher order harmonic in the response. Recently, it was proven that the performance of a CgLp element can be potentially further improved by suppressing its nonlinearity in certain frequency bands. Two techniques that achieve that have shown promising results. The CgLp can be used in a series continuous reset (CR) structure [11], or in combination with a shaping filter [12]. However, different structures exist for which these techniques have yet to be studied. One example is the Proportional Clegg Integrator (PCI) [14] which allows a larger low frequency open-loop gain compared to an equivalent LTI Proportional integrator (PI) system, for the same phase margin. This leads to increased disturbance suppression when paired with an LTI controller, thus potentially increasing the tracking performance of the system. Furthermore, literature on synthesis and implementation of reset controllers in industrial applications is lacking. The potential issues

of CR or shaping filters in a digital implementation were for example never studied.

The main goal of the thesis is to utilize the concepts developed in this new research to begin with the construction of a general framework on the design and analysis of reset controllers for an industrial setting. This requires a reliable and straightforward method to predict the performance of the system as well as assure stability. Additionally, at least a qualitative understanding of the robustness of the system against plant uncertainties is necessary. Furthermore, the controller must be easily implementable digitally. The findings, when possible, are validated on an AB383 wire bonder motion stage. Since literature on reset control is already vast [15], one can assume an ample number of different reset controllers exists already in literature. It is not feasible to study the effects of all existing reset controllers within the scope of the project. It was thus necessary to investigate what type of reset controllers would suit an industrial motion system like the AB383 wire bonder better, based on what predictive performance and stability/robustness analysis methods can be applied. It was also necessary to investigate the issues that prevented ASMPT from adopting reset controllers in their products [4], in order to assure these issues are overcome. Based on findings presented in the explored literature, a collection of MATLAB/Simulink tools to easily analyse reset controllers were developed. These were extensively used in combination with Simulink simulations to analyse the selected types of reset controllers, understand their behaviour and accordingly devise design guidelines. Finally, once the behaviour of an analyzed reset controller was deemed satisfactory, it could be implemented on the AB383 wire bonder motion's stage to perform experiments and validate the design guidelines.

The layout of this thesis is as follows. Chapter 1 establishes the need for this project and its relation to the AB383 wire bonder. In Section 1.1 the limitations of LTI feedback control are presented. Section 1.2 illustrates how the inherent limitations affect the performance of a wire bonder. Subsequently, in Section 1.3, the dynamics of the AB383 wire bonder are studied. Moreover, it is examined how the AB383 wire bonder is controlled currently. In Chapter 2 the basics of reset control are presented. Section 2.1 includes the necessary theory on stability analysis and predictive performance indicators for reset systems. Some schemes from literature are also be presented. Based on that knowledge, the issues that arose in [4] are studied in Section 2.2. In Section 2.1 it is also proposed that the CgLp and PCI are the two most suitable reset control structures for industrial applications and should thus be studied further. The use of a CgLp for a non-collocated mass-spring-damper system with high frequency dynamics with similar dynamics of a stage of the AB383 wire bonder is explored in Chapter 3. This type of plant is very common for motion stages, including the AB383 wire bonder. It is concluded that the CgLp is not suitable for these type of plants. Chapter 4 presents the most relevant findings in this thesis in a standalone paper format. The use of a PCI for industrial applications is studied within the aforementioned CR architecture. The systems presented in this chapter showed the most promising results in terms of industrial applicability and could in

fact be implemented on the wire bonder motion stage to perform experiments. Next, the use of a shaping filter in combination with a PCI system is investigated in Chapter 5. The resulting system shows promises when it comes to performance, however stability could not be guaranteed, hence not allowing experiments. In the following chapter (Chapter 6) the results of simulations is shown. Finally, the relevant conclusions and future recommendations are summed up in Section 7.1.

1.1. LIMITATIONS OF LTI FEEDBACK CONTROL

1.1.1. BASICS OF LTI FEEDBACK CONTROL

Figure 1.2 depicts a typical control system, where C_{fb} is the feedback controller, C_{ff} is the feedforward controller, G is the plant, $r \in \mathbb{R}$ is the reference, $u \in \mathbb{R}$ is defined as the controller output, $d \in \mathbb{R}$ is the disturbance, $n \in \mathbb{R}$ is the sensor noise, $y \in \mathbb{R}$ is the true output, y^* is the measured output, $e = r-(y+n)$ is the error and $v = u+d$ is the plant input. Assuming no feedforward control and assuming C_{fb} and G are LTI single-input single-output (SISO) systems, the open-loop transfer function is defined as $L(s) = C_{fb}(s)G(s)$, with $s \in \mathbb{C}$ representing a complex frequency. Moreover, the sensitivity transfer function $S(s)$ and the complementary sensitivity transfer function $T(s)$, are respectively defined as

$$S(s) = \frac{\mathscr{L}\{y\}}{\mathscr{L}\{d\}}\frac{1}{G(s)} = \frac{\mathscr{L}\{e\}}{\mathscr{L}\{r\}} = \frac{1}{1+L(s)}, \tag{1.1}$$

$$T(s) = \frac{\mathscr{L}\{y\}}{\mathscr{L}\{r\}} = -\frac{\mathscr{L}\{y\}}{\mathscr{L}\{n\}} = \frac{L(s)}{1+L(s)}, \tag{1.2}$$

with $\mathscr{L}\{x\} \in \mathbb{C}$ being the Laplace transform of $x \in \mathbb{R}$.

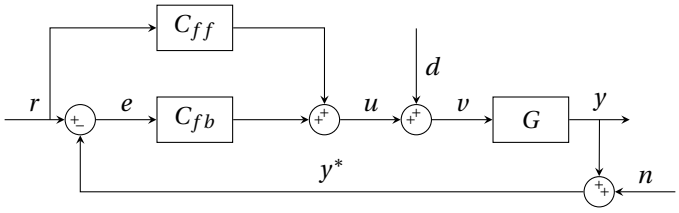

Figure 1.2: Standard control system architecture.

The goal of a control system is to track a desired reference signal while attenuating a possible unknown disturbance as well as the sensor's noise. In other terms, the ideal control system will result in $y = r$. Attenuating disturbances would require $|S(j\omega)| \approx 0$, with $j = \sqrt{-1}$ and the frequency $\omega \in \mathbb{R}$, which can be achieved only when $|L(j\omega)| \gg 1$, since G cannot be altered. Good tracking requires $|T(j\omega)| \approx 1$, also leading to $|L(j\omega)| \gg 1$. On the

other hand, noise cancellation necessitates $|T(j\omega)| \approx 0$, thus constraining $|L(j\omega)| \ll 1$. It is clear that these relations cannot be achieved simultaneously for all ω. However, assuming the fact that the noise acts at high frequencies, whereas disturbances act at lower frequencies, which is usual for mechanical systems [16], it is obvious how it is desirable to keep $|L(j\omega)|$ large for low frequencies and small for high frequencies. In fact, through the final value theorem, one can determine that to achieve 0 steady-state error, $\lim_{t\to\infty} e(t) = e_{ss}$, with $t \in \mathbb{R}$ representing time, an infinite gain at the frequency of 0 Hz is necessary. This can be achieved through the addition of an integrator (pole at 0 Hz), to the feedback controller if this is not already present in the plant. The number of integrators required to drive e_{ss} to 0 for a polynomial reference or disturbance signal is related to the order of the polynomial itself and can be computed through the final value theorem [2].

Loopshaping is a controller design technique in which the desired closed loop performance is achieved by shaping the open and closed loop transfer functions in the frequency domain [16]. Fig. 1.3 shows a typical shape of $S(s)$ and $T(s)$ that that is required to achieve the aforementioned trade off between disturbance suppression, noise rejection and reference tracking. At the peak of the sensitivity function $M_S = ||S(j\omega)||_\infty \geq 1$, and control actually degrades the performance of the system since disturbances are amplified. Apart from performance, M_S gives an indication on the robustness of the system. In fact, $\frac{1}{M_S}$ is the shortest distance to the critical point [-1,0j] on the Nyquist plot. A rule of thumb states that the controller should be tuned such that $M_S \leq 6$ dB [2].

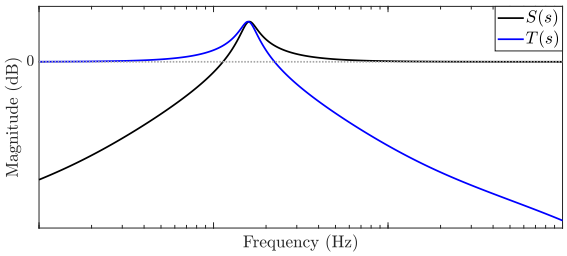

Figure 1.3: Magnitude characteristics of $S(s)$ and $T(s)$ of a typical motion system.

The lowest frequency at which $|L(j\omega)| = 0$ dB will be referred as the bandwidth frequency ω_{BW}. The bandwidth frequency is positioned between the frequency at which $|S(jw)| = -3$ dB and the frequency at which $|T(jw)| = -3$ dB [2]. The bandwidth is a fundamental concept in feedback control both in terms of performance as well as stability. Higher bandwidth corresponds to a faster rise time, as control is effective on a wider range of frequencies, but also corresponds to higher sensitivity to noise [2]. The phase margin $PM = \angle L(j\omega_{BW}) + 180°$, obtained from the phase at the bandwidth frequency, provides information on the performance, stability and robustness of the system. According to Bode's stability criteria, an open-loop stable system requires a positive phase

margin to be stable in closed-loop [2]. In the time domain, PM is related to the overshoot and settling time of a system [2]. A low PM will in fact increase the overshoot as well as the oscillations in the response. A rule of thumb is to design a controller that achieves at least $PM = 30°$ in order to guarantee a certain level of robustness against plant uncertainties [2]. The next subsection will demonstrate how many of these parameters are related in LTI systems, hence leading to inherent performance limitations.

1.1.2. INHERENT PERFORMANCE LIMITATIONS OF LTI FEEDBACK CONTROL

The fact that using LTI controllers for feedback results in inherent performance limitations is anything but unfamiliar. Already in 1945 H.W. Bode described the *waterbed effect* [17]. This phenomenon can be comprehended at best by making use of Bode's sensitivity integral, expanded to both $S(s)$ and $T(s)$ in [18] and given by

$$\int_0^\infty \log|S(j\omega)|\mathrm{d}\,\omega = \pi \sum_{i=1}^{m} \mathrm{Re}(p_i), \tag{1.3}$$

$$\int_0^\infty \log|T(1/j\omega)|\mathrm{d}\,\omega = \pi \sum_{i=1}^{n} \mathrm{Re}\left(\frac{1}{z_i}\right), \tag{1.4}$$

where $\mathrm{Re}(p_i) \in \mathbb{R}$ is the real part of one of the $m \in \mathbb{Z}^+$ open-loop right half plane (OLRHP) poles and $\mathrm{Re}(z_i) \in \mathbb{R}$ is the real part of one of the $n \in \mathbb{Z}^+$ OLRHP zeros. One should note that (1.3) and (1.4) are valid only when $L(s)$ has at least two more poles than zeros. This holds true for most industrial plants, including the wire bonder as will be discussed in Section 1.3. It is clear that (1.3) and (1.4) impose a constraints on the sensitivities transfer functions. Fig. 1.3 can be utilized to picture this constraint. For instance, assuming $L(s)$ has no unstable poles or zeroes, the area of $S(s)$ underneath the 0 dB line and the area above the line have to be equal. This means that an improvement in one range of frequencies comes at the cost of a worsening performance at all other frequencies. In case of unstable poles or zeros the area above the 0 dB line must be greater than the one underneath for S or T respectively, which would decrease performance thus making the constraints become even more strict.

From the previous subsection, it could already be comprehended that $S(s)$ and $T(s)$ are interdependent. In fact the complementarity constraint states that $S(s) + T(s) = 1 \ \forall s$ [19]. This leads to a necessary trade-off between noise suppression and disturbance rejection or tracking at each frequency.

A further limitation is given by *Bode's phase-gain relationship*

$$\begin{aligned} \angle L(j\omega_0) &= \frac{1}{\pi}\int_{-\infty}^{\infty} \frac{\mathrm{d}\ln|L(j\omega)|}{\mathrm{d}\ln(\omega)} \left|\frac{\omega+\omega_0}{\omega-\omega_0}\right| \frac{\mathrm{d}\,\omega}{\omega}, \\ \angle L(j\omega_0) &\approx 90° \cdot N_L(\omega_0), \end{aligned} \tag{1.5}$$

where $N_L \in \mathbb{R}$ is the slope of $L(s)$. It should be noted that this equation holds true only if $L(s)$ is a minimum-phase system. However, since non-minimum-phase systems have

an additional phase lag, the constraint is even stricter. Equation (1.5) also shows how the phase can be approximated from N_L. It should also be noted that this approximation is good only if the slope in the range close to $\omega = \omega_0$ is constant. This constraint translates directly to the shape of the magnitude of $L(s)$. It would be beneficial to have a steep negative slope in the range $\omega \approx \omega_{BW}$, to quickly go from good tracking to good noise rejection, however in order to allow $PM \geq 30°$, it is required that $N_L \geq -1.67$. A typical $L(s)$ will then look like Fig. 1.4, with a steep negative slope at low and high frequencies and a moderate slope in the crossover region. In case of non-minimum-phase systems the constraints are even more severe [20]. Every real life system is to some degree non-minimum-phase, as it suffers from time delay. Time delay will cause a linear decrease in the phase of the system as a function of frequency, which also causes the bandwidth to be upper-bounded. A rule of thumb states that in case of a time delay $\tau \in \mathbb{R}$, the bandwidth should be chosen as $\omega_{BW} \leq 1/\tau$ [2].

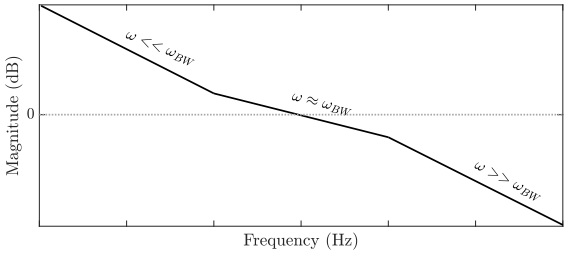

Figure 1.4: Magnitude characteristics of $L(s)$ of a typical motion system.

1.2. WIRE BONDER TRACKING PROBLEM

A wire bonder is a machine utilized for the fabrication of semiconductor devices. It is used to create electrical interconnections between a microchip and the terminals of a chip package or other integrated circuits [21]. Fig. 1.5 illustrates the typical cycle undergone for each wire connection. A thin wire is initially attached to the end-effector of the wire bonder's motion stage (Fig. 1.5-1). The end-effector then travels to the bonding location on the silicon chip, where a bond is created through the application of thermal or ultrasonic energy (Fig. 1.5-2). The end-effector then moves to the second bonding location where another bond is created (Fig. 1.5-3 and Fig. 1.5-4). The connection between the bonded wire and the end-effector is finally broken (Fig. 1.5-5) and the wire bonding cycle can restart. In terms of control, the operation requires the end-effector to track a desired path. A typical reference signal resembles a trajectory required to move the end-effector to a bonding location. After reaching the desired position, the wirebonder needs to settle such that bonding can occur. Fig. 1.6 shows an example reference signal. As can

be seen, there are strict requirements on the error bounds dependent on the stage of the operation.

At the tracking stage (1), characterized by the motion of the end-effector, the bounds are necessary to avoid contact between the end-effector and nearby, already bonded, wires. These bounds are required for the same purpose in the settling region (2), encompassing the time during which the end-effector has reached the desired position, however oscillations are still present. When these oscillations decrease to an acceptable level, characterized by new, reduced bounds, the steady-state phase (3) commences. In this stage, bonding occurs.

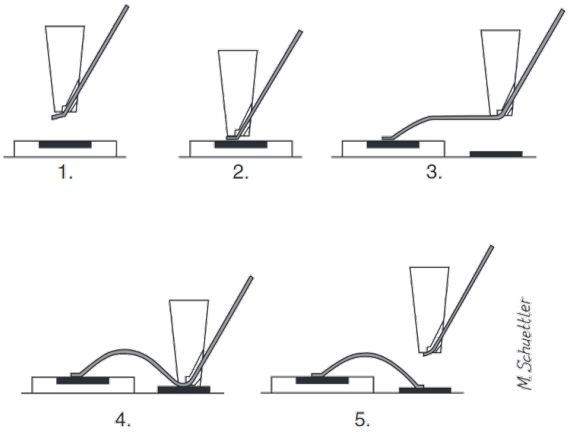

Figure 1.5: Illustration of a typical wire bonding cycle (reproduced with permission from [21])

The performance of a wire bonder is based on its precision, hence how accurate and repeatable the operation is and throughput, thus how fast the time of operation is. An increase in either will have a positive outcome on the overall competitiveness of the product on the market. An increase in precision will allow the device to be used with smaller microchips or bond more wires per squared centimeter. According to Moore's law, it is certain that in the future integrated circuits devices will decrease in scale [22], making this a necessary development for the future of semiconductor device fabrication. Moreover, the semiconductor industry is under constant pressure to increase the production of chips due to an ever-increasing demand that is predicted to last in the future [23]. A wire bonder's control system can affect both performance factors. An increase in the aggressiveness of the controller will decrease the time required to reach the settling region, whereas an increase in precision will allow smaller bounds to be defined for all regions. As stated in Section 1.1.2, using LTI control there is a strict trade-off between speed and precision. The goal is thus to use reset control to overcome these limitations. Additionally, another important characteristic of a wire bonder's control system is its robustness to plant uncertainties. Good robustness results in less down-time, which again trans-

lates to higher throughput.

In order to effectively compare different controllers, relevant time-domain performance metrics must be established. However, it is first necessary to define when the settling region starts and ends. For this thesis, the settling region will comprise the moment at which the tracking region ends, until the moment at which the controller output reaches and stays within a certain bound (steady-state bound). The precision of the controller will be studied through the root-mean-square of the error e_{RMS}. It is also important to study the maximum of the absolute value of the error e_{max} in order to understand the bounds that can be satisfied by the controller. The two errors are defined mathematically by

$$e_{RMS} = \sqrt{\frac{1}{n}\left(\sum_{i=1}^{n} e_i^2\right)}, \tag{1.6}$$

$$e_{max} = \max(|e_1|, |e_2| \ldots |e_n|), \tag{1.7}$$

where $n \in \mathbb{Z}^+$ is the total number of samples of the region of interest. The settling and steady-state regions will be looked at together when determining the error. The RMS error, will be thus defined as $e_{t_{RMS}}$ in the tracking phase and $e_{s_{RMS}}$ in the settling and steady-state phase. This metric will be defined similarly $e_{t_{max}}$ in the tracking region and $e_{s_{max}}$ in the settling and steady-state region. On the other hand, how fast the control system reacts to a change in reference can be investigated simply by measuring the settling time t_{set}, defined as the time spent in the settling region, given a reference such as the one depicted in Fig. 1.6. However, this metric is highly dependent on the value of the steady-state bound. Therefore, a more robust metric T_{set}, is defined as

$$T_{set} = \int_{b=b_{min}}^{b=b_{max}} t_{set}(b)\, dt, \tag{1.8}$$

with b_{min} the minimal value of the steady-state bound, b_{max} the maximal value of the steady-state bound and $t_{set}(b)$ the settling time for a given bound.

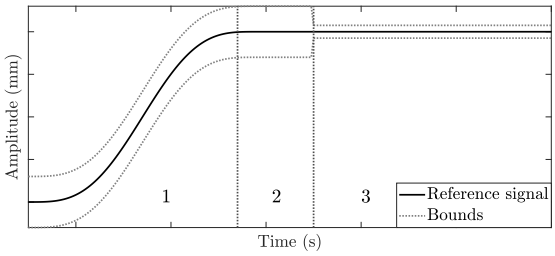

Figure 1.6: Typical shaped reference signal subdivided in a tracking region (1), a settling region (2) and a steady-state region (3).

Complex mechanical systems like wire bonders will often present intricate dynamic behaviour, such as friction, position dependency, cross-coupling etc. For this reason, it is also fundamental that the robustness of the control system is evaluated. Moreover, industrial machines are mass-produced, meaning that it will not be possible to tune the control system of each individual machine. Since different machines could present slight alterations, it is necessary that some robustness against parameter uncertainty is present.

1.3. THE AB383 WIRE BONDER AND ITS CONTROLLER

The AB383 wire bonder is a complex machine with multiple functionalities, however for control purposes the interest lies solely in its motion platform. The wire bonder has in fact a three degrees of freedom (DOF) motion platform, that allows its end-effector to translate in every translational direction. The motion stage is subdivided into an X-, a Y- and a Z-stage, which provide the respective translations guided by linear bearings. The X- and Y-translation are actuated by three-phase permanent magnet synchronous motors, whereas the Z-translation is actuated by a voice-coil actuator. Both the X- and Y-stages weigh several kilograms and can achieve a displacement of up to approximately 70 mm. The actuators can accelerate the stage in both directions to $> 200\ \mathrm{m/s^2}$. For the Z-translation a pivot mechanism is used instead. The resultant equivalent mass of the Z-stage is one order of magnitude smaller and the achieved acceleration is $> 1500\ \mathrm{m/s^2}$ [4].

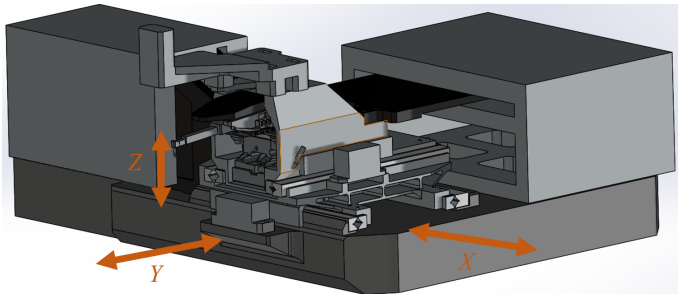

Figure 1.7: Drawing of the AB383 motion platform (reproduced with permission from [4]).

In order to better comprehend the dynamics of each stage they can be approximated as a double mass-spring-damper (MSD) system, as illustrated in Fig. 1.8b. For example for the X-stage, the first mass corresponds to the base frame which is connected to the ground, while the second mass is given by the motion platform itself. The frequency response function (FRF) of the transfer function from the actuator force acting between the X-stage and the base frame to the X-stage position is shown in Fig. 1.8a. It can be

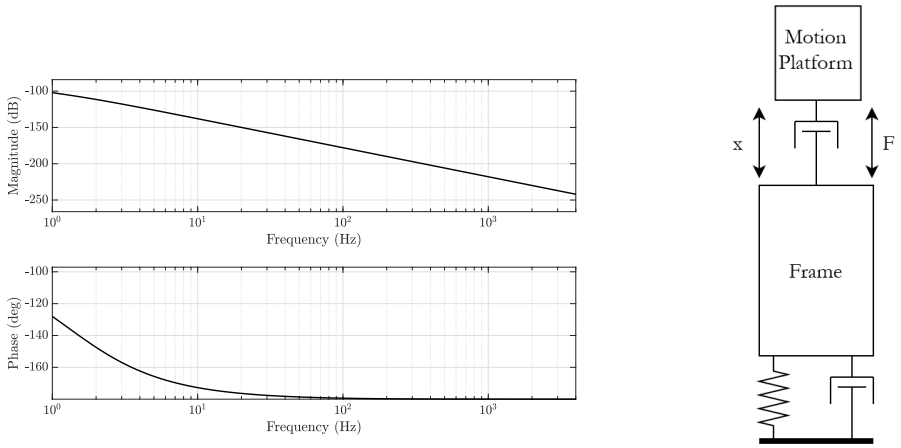

(a) (b)

Figure 1.8: (a) Frequency response function of X-stage MSD model approximation. (b) Diagram of approximated MSD system. F is the actuator force acting between the X-stage and the base frame and x is the encoder position.

distinguished between a low- and a mid-frequency behaviour. The former is dictated by the connection between the frame and the X-stage. At low frequencies the magnitude has a -1 slope, indicating that between the frame and the X-stage there is no stiffness but only damping. This simulates the guiding rail between the frame and the stage whose stiffness can be neglected. Nevertheless, viscous friction, acting like a damper, must be considered. In reality some Coulomb friction is also present in the system. This non-linear effect acts at very low frequencies introducing a steady-state error. In the mid-frequencies the slope becomes a constant -2, indicating a mass-line. In reality there exist a hidden resonance at $\approx$ 40 Hz, given by the connection between the X-stage and the base frame which does not appear in the frequency response function. This is given by the fact that the mass of the X-stage is negligible compared to the base frame.

The previous approximation gives no information on the high frequency behaviour. Moreover, it has been established that the three stages suffer from cross-coupling [4]. This is illustrated in Fig. 1.9, which shows the identified FRF between the current required from the actuators of each stage and the X-stage encoder position using a sampling frequency f_s = 8 kHz, which corresponds to the sampling frequency the controller of the AB383 uses during operation. The X-stage is actually the stage that suffers least from cross-coupling due to being the heaviest one [24]. Since the thesis will focus only on SISO systems, it is favourable to deal with the stage that suffers the least from cross-coupling. The main focus of the thesis will thus be on the X-stage. The dynamics of the stages is also position-dependent, meaning the FRF plots differ based on the end-effector position.

Fig. 1.9 shows the FRF at the center position, thus when all stages have no displacement.

It can be appreciated that in the low frequencies the behaviour resembles the double MSD system. A drift in phase is then to be seen. This is caused by the time-delay present in the system between the sensor readings and the actuator action. It can also be noted that cross-coupling has little effect in the low and mid-frequency region. The high frequency dynamics is also visible.

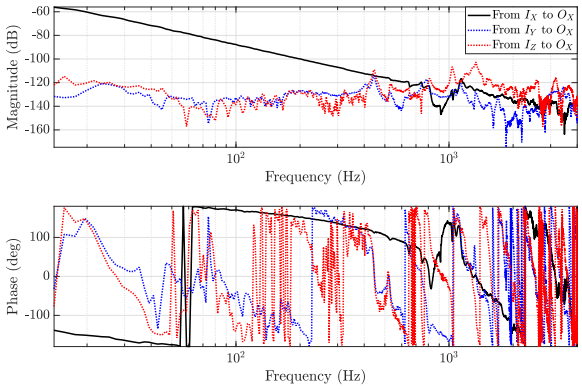

Figure 1.9: Identified FRF between X-, Y- and Z-stages actuator current and X-stage encoder position at the center position.

In [24] a Simscape Multibody [25] model that would accurately portray the mid-frequency dynamics of the wire bonder motion stage was constructed. The FRF of the X-stage linearized about the 0-position in continuous time and discretized at f_s with a 2.5 samples time delay, is shown in Fig. 1.10. It can be noticed how the time delay added to the model decreases the phase significantly in the frequency range of interest. Although the model approximates the cross-coupling between stages well, the high frequency range is inaccurate, since the Simulink model is based on a lumped-mass model and can't therefore accurately portray the flexible dynamics in the system's components. The low frequency dynamics are also inaccurate since Coulomb friction is not incorporated in the model. Furthermore, it should be noted that the actuator dynamics is also not present in the model.

The motion stages DOF are controlled separately approximating the X-,Y- and Z-stage as independent SISO systems. Hence, currently three SISO LTI control systems are employed to regulate the motion of the three stages. This means that each stage has to track a reference signal similar to the one depicted in Fig. 1.6 simultaneously. This decentralized control structure is not optimal in terms of control as it does not account for the

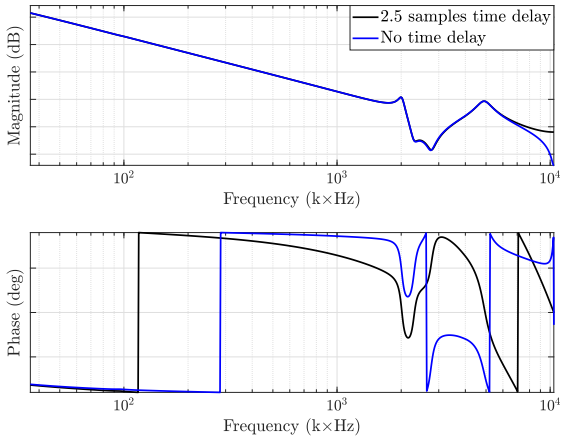

Figure 1.10: X-stage frequency response function of the Simscape Multibody model with and without time delay.

cross-coupling between the stages. Nevertheless, this control scheme allows to use SISO controllers which are easier to design, especially through loopshaping [2]. Currently, a controller structure as the one shown in Fig. 1.2 is employed for each stage.

The current LTI feedback controller C_{fb} of the X-stage has a PID-like structure, which gives a proportional static gain (P) that increases the magnitude without affecting the phase, a 'tamed' derivative action that provides a lead in phase (D), but also an increase in gain, and an integral action (I) that adds a -1 slope at low frequencies, while however also leading to a phase lag. Since in reality due to Coloumb friction at least one integrator is required to assure a zero steady-state error for the desired reference profile. The transfer function of a PID controller is given as

$$C_{fb}(s) = \underbrace{k_p}_{\text{P}} \underbrace{\left(1+\frac{\omega_i}{s}\right)}_{\text{I}} \underbrace{\left(\left(1+\frac{s}{\omega_d}\right)\Big/\left(1+\frac{s}{\omega_t}\right)\right)}_{\text{D}}, \tag{1.9}$$

with k_p the controller gain, ω_i the frequency at which the integral action (I) is stopped in order to limit the effect of the phase lag introduced it and $\omega_d < \omega_{BW}$ and $\omega_t > \omega_{BW}$ the frequencies the derivative action (D) acts between to achieve a phase lead in the cross-over region while limiting the increase in magnitude at low and high frequencies. Once the desired ω_{BW} has been selected, a set of rules of thumb can be used to design a first version of the PID controller that achieves $PM = 30°$. The parameters are selected as

follows, based on [26]:

$$\begin{aligned} \omega_i &= \frac{\omega_{BW}}{10} \\ \omega_d &= \frac{\omega_{BW}}{3} \\ \omega_t &= 3\omega_{BW} \\ k_p &= \left| \frac{1}{3G(j\omega_{BW})} \right| \end{aligned} \tag{1.10}$$

In addition to a PID controller, it might be beneficial to increase the suppression of the effects of noise and high frequency dynamics. In this case it is possible to add two different elements to $C_{fb}(s)$. A low-pass filter, with transfer function

$$\left(\frac{1}{s/\omega_c + 1} \right)^n, \tag{1.11}$$

with ω_c the low-pass filter corner frequency and $n \in \mathbb{Z}^+$ the filter order, decreases the magnitude slope by -n after ω_c, while introducing a phase lag of $-90n°$. On the other hand, a notch filter with transfer function

$$\frac{\left(\frac{s}{\omega_n}\right)^2 + \frac{s}{Q_w \omega_n} + 1}{\left(\frac{s}{\omega_n}\right)^2 + \frac{s}{Q_w Q_n \omega_n} + 1}, \tag{1.12}$$

with ω_n the notch frequency, $Q_w \in \mathbb{R}^+$ a weight related to the notch width (the larger Q_w, the narrower the notch) and $Q_n \in \mathbb{R}^+$ the notch height.

A certain degree of robustness is expected from the employed feedback controllers. For this reason the constraint $M_S < 6$ dB is placed to any controller in order for it to be implemented. The continuous time controller is then discretized at f_s using Tustin's approximation, which preserves the phase of the continuous time system better than any other approximation until close to the Nyquist frequency [27].

Although the focus of this thesis is on feedback control, it should be noted that every simulation and experiment will also include a feedforward controller to best represent the wire bonder's oporation. This is shown in Fig. 1.11, where two simulations were run using the Simscape Multibody model. In both cases a typical reference trajectory with amplitude $r_{max} = 4$ mm had to be followed given a PID controller designed using the rules of thumb specified in (1.10) with a bandwidth of 200 Hz. However, one of the control systems also utilizes feedforward, as designed in [24]. In both cases the steady-state error bounds were arbitrarily chosen as 0.5 mm for illustration purposes only. The maximal error amplitude over the three regions decreases by a factor of almost 100 when feedforward is employed. Moreover, it is possible to see that the shape of the error signal is vastly different between the case with and without feedforward. In fact, in the latter

case it is impossible to see the ≈ 40 Hz oscillations without having to zoom in. These are given by the natural frequency of the connection between the base frame and the ground. As explained beforehand, due to the difference in mass between the base frame and the X-stage this resonance is not visible in the FRF (Fig. 1.10). However, since the feedforward controller accounts for the dynamics of the X-stage, but not for the one of the base frame, it makes this resonance as the most influential disturbance in the system [24]. The feedback controller will therefore be utilized to suppress this disturbance. Figure 1.11 also shows how a constant disturbance, added at $t = 0$ to simulate the effect of Coulomb friction, which is not included in the Simscape model, is suppressed by the controller due to its integral action.

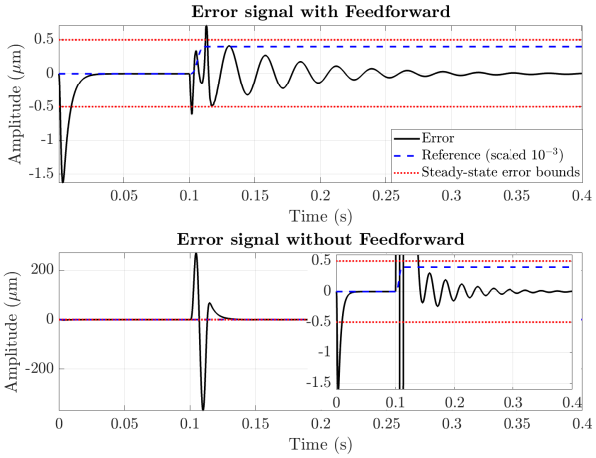

Figure 1.11: Error timeplots when using a PID-like LTI controller with and without feedforward. In both cases a constant disturbance of 0.1 N/m was added at $t = 0$ to simulate the effect of Coulomb friction.

2

Literature Review

Although since decades nonlinear control techniques have been in continuous development, 90% of the controllers used in industry are still based on the linear PID controller [3]. The slow adaption of nonlinear control in industry is given by the fact that the simple tools used in classic control theory are based on properties of linear systems (e.g. the principle of superposition) which in many cases are not valid for nonlinear control. This requires the understanding of new and often demanding mathematical principles [28] and does usually not allow stability or predictive performance analysis in the frequency domain [29]. For instance, most nonlinear methods do not offer a systematic way to design the controllers based on their frequency response (e.g.: model predictive control [30], adaptive control [31] and fuzzy control [32]). This makes the relation between the plant and the response complex and often unintuitive, thus usually not suitable for industrial applications. However, techniques such as variable gain control (VGC) [33], split-path nonlinear (SPAN) filters [34], hybrid integrator gain system (HIGS) [35] and reset control have been used to overcome LTI inherent limitations while also providing an approximation of their frequency domain response. In VGC, the gain of the controller is dependent on the input amplitude, allowing to have a steeper slope in the open-loop magnitude FRF at low and high frequencies respectively, due to the difference in amplitude between low and high frequency disturbances/noise. This allows to better suppress low frequencies disturbances and high frequency noise [33]. However, since the frequency response of such a filter is dependent also on the amplitude of the input [9], it is unsuitable for systems whose reference is unknown a priori like the wire bonder. SPAN filters allow to design a nonlinear controller in which phase lead is provided without affecting the magnitude, thus overcoming Bode's phase-gain relationship [34]. However, no frequency domain analysis tools were developed for such filters. In [4] frequency domain performance prediction and stability analysis of a HIGS used to control the AB383 wire bonder were performed successfully. The HIGS was then also implemented on the

AB383 validating an increase in performance. Nevertheless, literature on the HIGS is more scarce compared to reset control. Reset control offers therefore more design possibilities as well as better frequency domain predictive performance analysis methods (e.g.: close loop methods [8], [9]).

2.1. RESET CONTROL

In 1958 J.C. Clegg's seminal work presented the Clegg Integrator (CI), a nonlinear integrator whose first harmonic of the output could provide approximately the same magnitude frequency response as a linear integrator but with a phase of only approximately $-38°$ instead of $-90°$ [5]. In fact, in his paper Clegg presented a sinusoidal input describing function of the CI, which allows for an approximate frequency description of the magnitude and phase response of the system, based on it's first harmonic. Therefore, Clegg did not only introduce a controller that overcomes the fundamental limitations of LTI systems, but also a controller whose approximate frequency behaviour is known and can hence be utilized for loopshaping. Over the years the field of reset control has developed immensely. Not only in terms of applications, which saw reset controllers implemented in e.g. vibration suppression devices, HDDs, pH processes, heat exchangers, teleoperations, flexible mechanisms and many more [36], but nowadays there also exist many different structures of reset controllers based on different mathematical theories. The goal of this section is to examine these different structures to assess which one would suit industrial applications, like the control of the AB383 wire bonder, better.

2.1.1. STRUCTURE

A general description for a reset system $\mathscr{R}$, proposed for the first time in [37], is given as

$$\mathscr{R} = \begin{cases} \dot{x}_r = A_r x_r + B_r e & \text{if} \quad (x_r, e) \notin \mathscr{M} \\ x_r^+ = A_\rho x_r & \text{if} \quad (x_r, e) \in \mathscr{M} \\ u = C_r x_r + D_r e, & \end{cases} \tag{2.1}$$

assuming a SISO system, as depicted in Fig. 2.1. It can be noticed that the first and last lines describe a standard LTI continuous system in state-space, where $A_r \in \mathbb{R}^{n_r \times n_r}$, $B_r \in \mathbb{R}^{n_r \times 1}$, $C_r \in \mathbb{R}^{1 \times n_r}$ and $D_r \in \mathbb{R}$ are the base linear system (BLS) matrices. This description holds true whenever the state vector $x_r \in \mathbb{R}^{n_r \times 1}$ is not part of the reset surface $\mathscr{M}$. If, however, x_r is part of $\mathscr{M}$, the after-reset state at the reset time instant $x_r^+ = \lim_{y \to t+0} x_r(y)$ is governed by the reset matrix $A_\rho \in \mathbb{R}^{n_r \times n_r}$. The BLS transfer function can then easily be obtained as

$$R = C_r (sI - A_r)^{-1} B_r + D_r. \tag{2.2}$$

If we assume the plant to be strictly proper, which is always the case for motion systems,

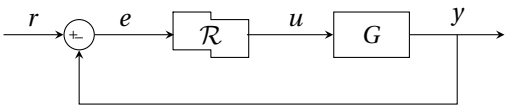

Figure 2.1: Unity feedback block diagram with reset controller.

the closed-loop system can be described as

$$\overline{\mathscr{R}} = \begin{cases} \dot{\hat{x}} = \overline{A}_r \hat{x} + \overline{B}_r r & \text{if} \quad \hat{x} \notin \overline{\mathscr{M}} \\ \hat{x}^+ = \overline{A}_\rho \hat{x} & \text{if} \quad \hat{x} \in \overline{\mathscr{M}} \\ y = \overline{C}_r \hat{x} \end{cases} \tag{2.3}$$

with

$$\overline{A}_r = \begin{bmatrix} A_r - B_r D_g C_r & -B_r C_g \\ B_r C_g & A_g \end{bmatrix}, \quad \overline{B}_r = \begin{bmatrix} B_r \\ 0 \end{bmatrix}$$
$$\overline{C}_r = \begin{bmatrix} D_g C_r & C_g \end{bmatrix}, \ \overline{A}_\rho = \begin{bmatrix} A_\rho & 0 \\ 0 & I \end{bmatrix}, \ \hat{x} = \begin{bmatrix} x_r \\ x_g \end{bmatrix}$$

where the subscript $_g$ indicates the states and matrices related to the plant G.

In [38] an impulsive description of reset control systems as well as a hybrid description are also shown. The latter one, introduced in [39] as

$$\mathscr{R} = \begin{cases} \dot{x}_r = A_r x_r + B_r e & \text{if} \quad x_r \in \mathscr{F} \\ x_r^+ = A_\rho x_r & \text{if} \quad x_r \in \mathscr{J} \\ u = C_r x_r + D_r e, \end{cases} \tag{2.4}$$

uses a flow set $\mathscr{F}$ to indicate when the BLS dynamics governs the system and a jump set $\mathscr{J}$ which enforces resetting, where $\mathscr{F}$ and $\mathscr{J}$ have to meet a number of conditions to make the representation valid [40]. For example, in the representation shown in (2.1) reset is only possible as long as some flow has occurred from the last reset, whereas this is not the case for the description shown in (2.4). Moreover, the sets $\mathscr{F}$ and $\mathscr{J}$ must be closed and have to overlap, whereas $\mathscr{M}$ and its complement are disjoint [40]. This allows for less strict stability conditions as will be seen in 2.1.3. The impulsive representation stems from the area of impulsive systems in applied mathematics. A typical representation is given by

$$\mathscr{R} = \begin{cases} \dot{x}_r = f(t, x_r) & \text{if} \quad h(t, x_r) \neq 0 \\ \Delta x_r = I_k(x_r) & \text{if} \quad h(t, x_r) = 0, \end{cases} \tag{2.5}$$

where $\Delta x = x^+ - x$ are the state jumps and $h(t,x)$ is the state- and time-dependent resetting condition [38]. This representation is not given in the standard state-space description making it unsuitable for controller design. Furthermore, only few papers deal with reset controllers as given in (2.5). The theory is hence still in its infancy, making it not

suitable for industrial applications.

The reset control system descriptions in (2.1) and (2.4) allow to categorize $\mathscr{R}$ based on three different aspects.

THE BLS MATRICES

It is clear that to design a reset controller it is still fundamental to properly tune a linear controller, as this will decide most of the response of the system. Different approaches to design an LTI controller exist, however due to its popularity in industry including the previously mentioned loopshaping. This method is currently employed at most companies, including ASMPT due to its simplicity in relating the frequency response of the close loop system to the tuning parameters. To make the design process as similar to reset control as possible, it was decided to only use loopshaping techniques to design the BLS for this thesis.

THE RESETTING CONDITION

There are many possible reset conditions that have been employed in literature. The most common condition is known as zero-crossing, defined for systems shown in (2.1). This reset condition states that reset occurs when $e = 0$. Formally, the reset surface is given as

$$\mathscr{M} := \{e = 0 \wedge (I - A_\rho)x_r \neq 0\}, \tag{2.6}$$

where the condition $(I - A_\rho)x_r \neq 0$, introduced in [37] assures that when the reset states are already zero, a redundant reset is avoided. The zero-crossing reset condition can be used to describe the typical CI introduced beforehand as

$$\mathscr{R} = \begin{cases} \dot{x}_r = e & \text{if} \quad e \notin \mathscr{M} \\ x_r^+ = A_\rho x_r & \text{if} \quad e \in \mathscr{M} \\ u = x_r. \end{cases} \tag{2.7}$$

In [8] the reset system architecture in Fig. 2.1 was expanded as illustrated in Fig. 2.2. In this case the zero-crossing law does not apply to e_r, but to $\hat{e}_r$, which is first shaped by the LTI shaping filter C_s. The architecture also allows to use a linear controller C_1 to shape the input to $\mathscr{R}$. The output of $\mathscr{R}$ also passes through a linear controller C_2 before reaching the plant.

In case reset occurs when, instead of crossing the 0-line, e crosses a scalar $\delta \in \mathbb{R}^+$ from above or $-\delta$ from below, the reset condition is known as a reset band [38]. Formally the reset surface is then

$$\mathscr{M} := \{(e = \delta \wedge \dot{e} < 0) \vee (e = -\delta \wedge \dot{e} > 0)\}. \tag{2.8}$$

Using a reset band can increase robustness [41] and lower the quantization induced error [42]. They can also provide additional phase lead, thus improve performance over zero-crossing systems. This is especially relevant for systems with time-delay [43]. Due to

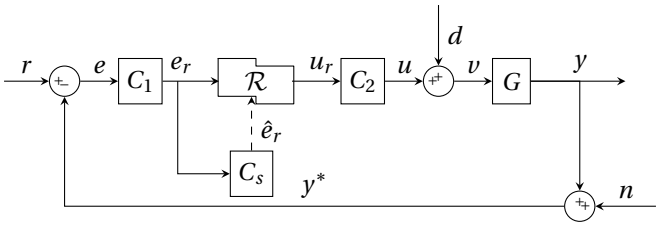

Figure 2.2: Expanded reset control feedback system architecture. Adapted from [8].

the fact that δ should be tuned according to the reference, it is usually favoured to use a variable reset band. In [36] the reset surface for a variable reset band controller tuned for a system with time delay τ is given as

$$\mathcal{M} := \{\tau \dot{e} + e = 0\}. \tag{2.9}$$

Using the definition of $\mathscr{R}$ given in (2.4), it is possible to use a $\mathscr{F}$ and $\mathscr{J}$ such that they define different sectors in the (e-u) plane. The most common definition of $\mathscr{F}$ and $\mathscr{J}$ is

$$\begin{aligned} \mathscr{F} &:= \{eu \geq 0\}, \\ \mathscr{J} &:= \{eu \leq 0\}, \end{aligned} \tag{2.10}$$

which enforces resetting whenever the sign of the output and input differs [39]. In [44], the $\mathscr{F}$ sector was made smaller for stability reasons, as will be explained in Section 2.1.3. Formally $\mathscr{F}$ and $\mathscr{J}$ are then given as

$$\begin{aligned} \mathscr{F} &:= \{eu \geq \frac{1}{\alpha} u^2\}, \\ \mathscr{J} &:= \{eu \leq \frac{1}{\alpha} u^2\}. \end{aligned} \tag{2.11}$$

Another reset condition can be achieved by predetermining the reset time instances. This has been done for example in [45] through the minimisation of a cost function. Determining the reset times a priori requires however knowledge of the reference signal and is thus not suitable for many industrial applications, including the control of the AB383 wire bonder, and will therefore not be considered further.

Sometimes it is beneficial to not allow reset before a certain time has passed before the previous reset. Time regularization poses a constraint on the reset instances such that

$$t_{k+1} = t_k + \delta_t, \tag{2.12}$$

where $t_k \in \mathbb{R}^+$ is a reset instance, $t_{k+1} \in \mathbb{R}^+$ is the subsequent reset instance and $\delta_t \in \mathbb{R}^+$ is the time between the two instances. As will be seen in Section 2.1.3, using time regularization allows to use different stability analysis methods. Time regularization has also been used to reduce performance degradation due to quantization [46].

THE RESET MATRIX

In order to avoid coupling between resetting states, the reset matrix can be chosen as a diagonal matrix $A_\rho = \text{diag}(\gamma_1, \gamma_2 \dots \gamma_{n_r})$, with $|\gamma_i| \leq 1$, $\gamma \in \mathbb{R}$ to avoid amplification instead of resetting, which would cause instability [8]. In case $\gamma_i = 0$, the corresponding state is said to be fully reset. On the contrary, a value of $\gamma_i = 1$ in A_ρ would mean that resetting has no effect on the corresponding state. If $1 > \gamma_i, \gamma_i \neq 0$, the state is only partially reset. This is best illustrated in Fig. 2.3, where the output of the CI described by (2.7) with three different values of γ is plotted. It can be seen that as γ approaches 1, the response approaches the sine wave that is obtained from the BLS. Based on the properties of A_ρ, it can be differentiated between:

- Full reset: all $\gamma_i = 0$,
- Partial state reset: at least one $\gamma_i = 1$,
- Partial reset: at least one $\gamma_i \neq \{0, 1\}$.

In case of partial state reset, the reset matrix can thus be defined as

$$A_\rho = \begin{bmatrix} I_{\tilde{n}_r \times \tilde{n}_r} & 0 \\ 0 & \hat{A}_{\rho, \hat{n}_r \times \hat{n}_r} \end{bmatrix}, \tag{2.13}$$

where $\tilde{n}_r \in \mathbb{Z}^+$ is the number of non-resetting states, $\hat{n}_r \in \mathbb{Z}^+$ is the number of resetting states ($\tilde{n}_r + \hat{n}_r = n_r$) and $\hat{A}_\rho$ is a diagonal matrix $\hat{A}_\rho = \text{diag}(\gamma_1, \gamma_2 \dots \gamma_{\hat{n}_r})$, with $|\gamma_i| \geq 1$, $\gamma \neq 1$. In order to maximise design DoF, it is beneficial to choose reset systems that allow partial state and partial reset.

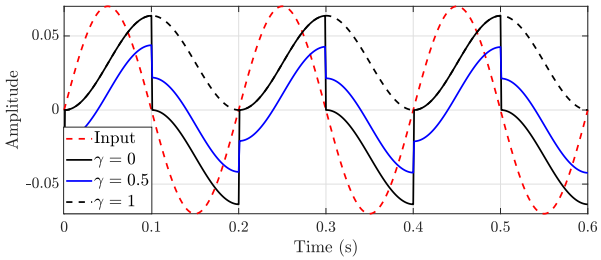

Figure 2.3: Output to a 5 Hz sinusoidal input with amplitude 1 of a CI with $\gamma = 0$, $\gamma = 0.5$ and $\gamma = 1$ respectively.

2.1.2. PREDICTIVE PERFORMANCE

The time response of an LTI system to a sinusoidal or polynomial input can be decomposed in a transient and a steady-state part. These can both be calculated analytically. Additionally, there also exist rules of thumb to relate transient response performance parameters such as overshoot, rise time and settling time to the LTI system parameters

[47]. However, when designing a controller through loopshaping the relation between the LTI system and its steady-state response is fundamental. As shown in Fig. 2.4, when a sinusoidal input acts on an LTI system, the magnitude and phase of the output are solely dependent on the input frequency ω. Additionally, the output frequency remains ω. This straightforward relationship can be used to determine closed-loop stability (for open-loop stable systems), robustness, steady-state performance and also to qualitatively predict transient behaviour, as illustrated in Section 2.2.

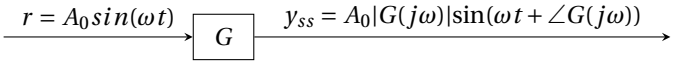

Figure 2.4: Relation between sinusoidal input r and steady-state output y_{ss} for LTI systems.

The goal is to derive a similar relationship for reset systems such that loopshaping is possible. Through the minimization of a cost function, a nonlinear system can be estimated as an LTI system, the so called base linear approximation [48]. Usually white noise is inputted into the nonlinear system and a linear system is fitted based on its time domain response, allowing to use linear techniques for the controller design. However, nonlinear systems behave differently than linear ones and may suffer from nonlinear effects that cannot be accurately represented in such an approximation. Common nonlinear effects are [49]:

- Gain compression and expansion: Magnitude and phase can be dependent on both input frequency as well as amplitude.
- Desensititsation: Magnitude can be dependent on possible interfering signals at frequencies other than the main input frequency.
- Intermodulation: Since the principle of superposition does not hold for nonlinear systems, frequencies combine nonlinearly.
- Harmonic generation: The output signal can consist of not only ω but also higher order harmonics at multiples of ω.

Different nonlinear frequency domain analysis tools are capable of capturing the various effects. Nonlinear Bode plots are an expansion of Bode plots that give the relationship between the magnitude and phase for both input frequency and amplitude [50]. Usually in reset systems magnitude and phase are only dependent on the input frequency [51], making this technique unnecessary. On the other hand, desensitisation, intermodulation and harmonic generation do affect reset systems. Volterra based approaches allow to capure all nonlinear effects with good accuracy [49]. On the other hand, the derivation of frequency domain characteristics using this method is often complex and to the best of the author's knowledge, an analytical method for reset controllers has not been studied in literature as of the time of writing. Morever, the interpretation of such characteristics is also complicated, which makes them unsuitable for controller design techniques such as loopshaping. The most commonly used predictive performance method

for reset controllers is also the one that most closely resembles LTI FRFs, the sinusoidal input describing function (SIDF) method [52]. A SIDF gives quasi-linear approximation of the first harmonic of the output signal when a nonlinear system is subject to a sinusoidal input signal. It is defined as the quotient between the Fourier transform of the first harmonic of the output and the Fourier transform of the input, where the input is a sinusoidal of a certain frequency [53]. Information on desensitisasion, intermodulation and harmonic generation is omitted in SIDFs. However, FRFs are generated by inputting only one signal at one particular frequency at the time. This means that the nonlinear effects of desensitisasion and intermodulation would not appear on FRF plots. Nevertheless, harmonic generation does affect reset systems and must be taken into account in order to gain better insight on the system's predictive performance. The subsequently developed HOSIDFs provide additional information on the generation of higher order harmonics. In fact, in [54] nonlinear systems are modelled as virtual harmonic generators. When a single harmonic is inputted infinite higher order harmonics are present in the output, each with their own gain and phase. These can then be added together to construct the resulting output signal. Numerical methods such as the Matlab system identification toolbox [55] could give an idea of the FRF of a reset system. However, in order to effectively make use of loopshaping it is necessary to have a more precise method. Unfortunately, not every reset control structure offers the possibility to derive the HOSIDFs analytically. In [9] the equation for the n^{th} HOSIDF for the reset system (2.1) with a resetting condition described by (2.6) was derived first. In the expanded reset system architecture in Fig. 2.2, a shaping filter C_s is used to determine the reset condition. Assuming C_s is LTI and introduces a phase lag $\varphi \in \mathbb{R}$, the reset instances will occur at $t_k = \frac{k\pi+\varphi}{\omega}$, with $\omega \in \mathbb{R}$ the excitation frequency and $k \in \mathbb{Z}^+$ the instance. The equation for the n^{th} HOSIDF with C_s was derived in [56] as

$$H_n(j\omega) = \begin{cases} C_r(A_r - j\omega I)^{-1}\Theta_\varphi(\omega) + C_r(j\omega I - A_r)^{-1}B_r + D_r & \text{for} \quad n = 1 \\ C_r(A_r - j\omega nI)^{-1}\Theta_\varphi(\omega) & \text{for odd} \quad n \geq 2 \\ 0 & \text{for even} \quad n \geq 2 \end{cases} \tag{2.14}$$

with

$$\begin{aligned} \Theta_\varphi(\omega) &= \frac{-2j\omega e^{j\varphi}}{\pi}\Omega(\omega)(\omega I\cos(\varphi) - A_r\sin(\varphi))\Lambda^{-1}(\omega)B, \\ \Omega(\omega) &= \Delta(\omega) - \Delta(\omega)\Delta_\rho^{-1}(\omega)A_\rho\Delta(\omega), \\ \Delta(\omega) &= I + e^{\frac{\pi}{j\omega}A_r}, \\ \Delta_\rho(\omega) &= I + A_\rho e^{\frac{\pi}{\omega}A_r}, \\ \Lambda(\omega) &= \omega^2 I + A_r^2. \end{aligned}$$

Although this holds true only for pure sinusoidal inputs [37], leading to potential prediction inaccuracies between HOSIDFs and the corresponding time response to a non-sinusoidal input signal, these equations have been proven reliable enough for designing controllers through loopshaping for various applications [7]. Furthermore, the solution

to a sinusoid must be globally asymptotically stable. This can be verified by

$$\left|\lambda(A_\rho e^{A_r \delta})\right| < 1 \quad \forall \delta \in \mathbb{R}^+, \tag{2.15}$$

where $\lambda(M)$ is the set of eigenvalues of a matrix M. In literature oftentimes reset control systems are implemented by preceding $\mathscr{R}$ by a linear controller. Moreover, to compute the open-loop HOSIDFs, the plant has to be taken into consideration as well.

The necessity of including higher order harmonic information is best illustrated through an example, adapted from [9]. Figure 2.5 shows the output to a 5 Hz sinusoidal input with amplitude 1 obtained by a CI as well as its SIDF. It is apparent that the jumps in the actual output cannot be captured by the SIDF. By adding the contribution of the first 13 higher order harmonics the response can be approximated much better. If all infinite higher order harmonics were to be added, the result would be identical.

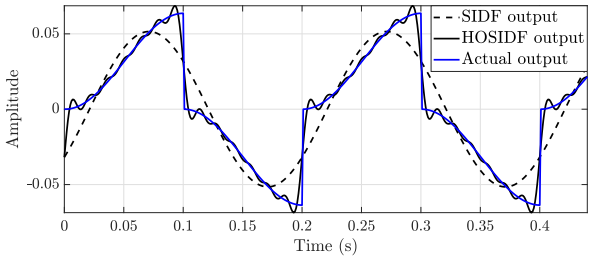

Figure 2.5: Output to a 5 Hz sinusoidal input with amplitude 1 of a CI, its SIDF and a combination of the first 13 HOSIDFs.

The importance of accounting for HOSIDFs can be shown in the frequency domain as well, through an example from [9]. Assuming a system like the one in Fig. 2.1 with $\mathscr{R}$ a typical CI and

$$G(s) = \frac{100}{s^2 + 0.25s + (20\pi)^2}, \tag{2.16}$$

representing a MSD system with low damping and a natural frequency of 10 Hz, the open-loop HOSIDFs FRF from e to y can plotted as shown in Fig. 2.6. It is evident that the higher order harmonics provide additional undesired peaks in the FRF which would have a remarkable effect on the performance of the system. For example they could excite resonances of the plant. The location of the peaks can be determined by intuition if the plant excitation frequency is known. Knowing that harmonic generation creates higher order harmonics at multiples of the input frequency ω, the third harmonic would excite the plant at $\omega/3 = 3.3$ Hz, the fifth harmonic at $\omega/5 = 2$ Hz and so on. Even harmonics are omitted because they have a magnitude of 0 for most reset systems. Damped systems would not show such peaks but it has been studied that the SIDF is even more unreliable than undamped systems at the bandwidth frequency [9]. On the contrary,

plants with integrators, low frequency poles or in general low-pass filter behaviour suffer less from higher order harmonics, as the n^{th} HOSIDF is filtered out before the first harmonic since it excites the low-pass filter corner frequency ω_c first, at ω_c/n [9]. Generally, the goal when loopshaping with HOSIDFs is to keep all higher order harmonics low, such that they do not have major impact in the response, and thus performance can be accurately predicted from the SIDF. Higher order harmonics get lower in magnitude with increasing order, therefore it is not necessary to plot all higher order harmonics. Since their shape is also alike, merely shifted to the left, plotting only the first higher order harmonic normally suffices to understand their open loop frequency domain behaviour.

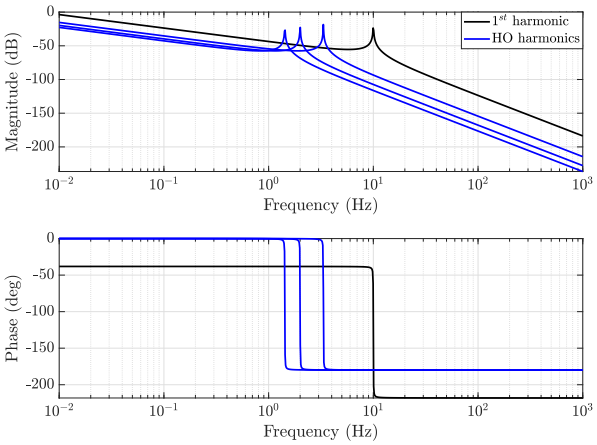

Figure 2.6: FRF of the HOSIDFs of a typical CI in series with G as given by (2.16).

Albeit the nonlinear effects of desensistisation and intermodulation cannot be captured by HOSIDF, these are a convenient, if not necessary, tool for controller synthesis through loopshaping.

The HOSIDFs can be easily augmented in case LTI systems are present in series before or after the reset controller, by considering $\mathscr{R}$ as a harmonic generator, as pictured in

Fig. 2.7, where

$$\begin{aligned} e &= A_0 \sin(\omega t), \\ e_r &= A_0 |C_1(j\omega)| \sin(\omega + \angle C_1(j\omega)), \\ h_n &= A_0 |C_1(j\omega)||H_n(j\omega)| \sin(n\omega + \angle C_1(j\omega) + \angle H_n(j\omega)), \\ u_n &= A_0 |C_1(j\omega)||H_n(j\omega)||C_2(jn\omega)| \sin(n\omega + \angle C_1(j\omega) + \angle H_n(j\omega) + \angle C_2(jn\omega)), \\ u &= \sum_{n=1}^{\infty} u_n. \end{aligned} \tag{2.17}$$

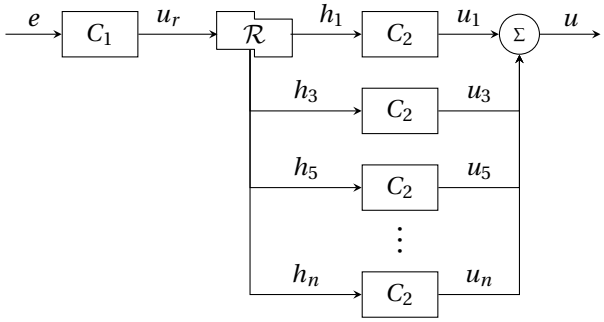

Figure 2.7: Representation of HOSIDFs for reset controllers in series with a linear controllers C_1 and C_2.

In [38] the SIDF for reset systems with a fixed reset band was derived. In this case the SIDF is dependent both on the input frequency ω and amplitude A_0. A general method to obtain the SIDF for systems with a variable band reset condition has not been proposed yet. It is thus not possible to derive the HOSIDFs for reset systems with reset band. As can be noticed all HOSIDFs equations so far have all been utilizing the reset description (2.1). In fact, HOSIDFs for the representation (2.4) have not been proposed to the best of the author's knowledge.

The effectiveness of loopshaping comes from the fact that it is possible to easily relate the open-loop and the closed-loop through the sensitivity equations (1.1). In [9] it was however shown that simply utilizing (1.1) with H_1 or a combination of H_1-H_n instead of C provides a highly inaccurate approximation of the closed-loop HOSIDFs. This is given by the fact that the nonlinear effects influence the reset instances in close loop. In [8] pseudosensitivities $S_\infty(\omega)$ were proposed as a way to combine the information on closed-loop higher order harmonics into an analogue of a sensitivity function for reset systems, thus helpful for loopshaping. Although the principle of superposition does not hold, it was established that even for non-sinusoidal inputs, the pseudosensitivity functions can provide a reliable quantitative performance prediction to effectively de-

sign reset controllers [8]. The pseudosensitivity magnitude is defined as

$$|S_\infty(\omega)| = \max(e_{ss}(\omega, t))/a_r, \tag{2.18}$$

where $e_{ss}(\omega, t)$ is the steady-state error of the reset system excited by a reference input $a_r \sin(\omega t)$. The simplest possible way to obtain $S_\infty(\omega)$ is through simulation. However, not only it is computationally expensive, as it requires a simulation for each frequency, it is also difficult to relate open-loop and closed-loop characteristics, due to the black-box nature of the method. Furthermore, a parametric description of the plant is necessary to compute the simulations. Therefore, a less accurate analytical methods, able to relate open- and closed-loop from FRF data, was established in [9]. Two assumptions are required for the validity of this method. Firstly, the reset system must be input-to-state convergent. This assumption can be expected to hold when the reset system meets the H_β-condition (Section 2.1.3) [8]. Additionally, it must be assumed that only the first harmonic of the error results in resets and hence the creation of higher-order harmonics in the output. This does not always hold, as higher order harmonics in the error have an effect on the reset instance, although not as strong as the first harmonic. Nevertheless, this still leads to a more accurate solution than just using (1.1) with the SIDF to compute the closed-loop HOSIDFs [9]. The fact that higher order error harmonics do not affect the reset instances can be represented as a virtual harmonic separator. The first error harmonic is inputted into the reset system $\mathscr{R}$, whereas the higher order harmonics are passed to the BLS R, as shown in Fig. 2.8.

Mathematically, the error is thus defined as

$$e_{ss} = \sum_{n=1}^{\infty} |S_n(j\omega)| \sin(n\omega t + \angle S_n(j\omega)), \tag{2.19}$$

with

$$S_n(j\omega) = \begin{cases} S_1(j\omega) & \text{for} \quad n = 1 \\ -\dfrac{L_n(j\omega)}{1 + L_{BLS}(j\omega)} \left(\left| S_1(j\omega) \right| e^{jn\angle S_1(j\omega)} \right) & \text{for odd} \quad n \geq 2 \\ 0 & \text{for even} \quad n \geq 2, \end{cases} \tag{2.20}$$

and

$$\begin{aligned} S_1(j\omega) &= \frac{1}{1 + L_1(j\omega)}, \\ L_n(j\omega) &= C_1(j\omega) H_n(j\omega) C_2(jn\omega) G(jn\omega), \\ L_{BLS}(j\omega) &= C_1(j\omega) R(j\omega) C_2(jn\omega) G(jn\omega), \end{aligned}$$

The pseudosensitivity can then be computed using (2.18). Overall, the approximate method is less computationally expensive and allows being used with FRF data, thus providing better usability. On the other hand, in case the required assumptions do not

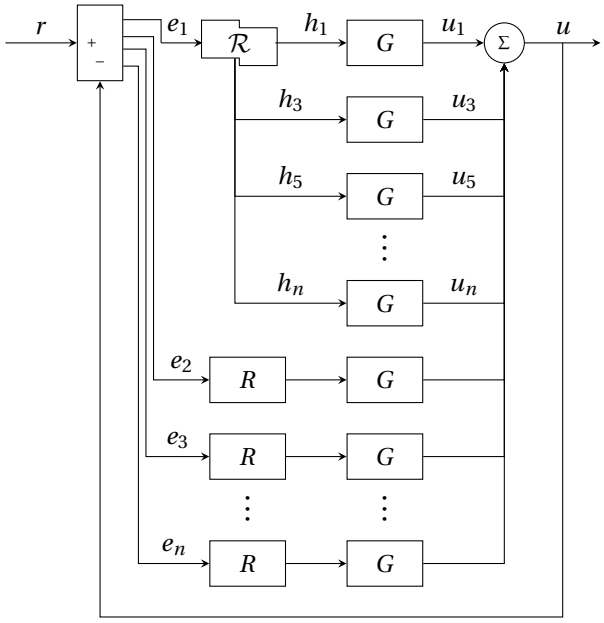

Figure 2.8: Representation of closed-loop HOSIDFs. Adapted from [9].

hold, it cannot be assured that the results would be accurate. Moreover, (2.19) shows that the greater the number of HOSIDFs n that are accounted for in the sum, the more accurate the results. However, as for the the open loop method, when using FRF data for the plant, information on the n^{th} HOSIDF can be provided only up to frequencies $\omega < \omega_{max}/n$, with ω_{max} being the highest frequency for which FRF data is available, which makes the accuracy of the method frequency dependent: the higher the frequency, the less HOSIDFs are taken into account. Nevertheless, it is difficult to evaluate which method would provide the most advantage when designing a controller. To the best of the author's knowledge, no comparison between the two method when designing a controller for an industrial setting is present in literature. For this reason, it is beneficial to utilize both methods until its clear if an increase in usability makes up the loss in accuracy.

In [57] reset systems are modelled as *'linear systems with a state-dependent timed impulse train input'*. Using such a description, it was shown that it is possible to accurately compute the open- and closed-loop HOSIDFs of a reset system analytically when the reset instances and the corresponding reset states are known. This method is still in its infancy and more research is required to quickly convert between a state-space impulsive description and the description proposed in [57]. However in the future this method could become a viable option to obtain accurate closed-loop HOSIDFs analytically.

For linear systems, frequency domain parameters can be analytically related to not only steady-state but also qualitatevely to transient characteristics [2]. This relationship has not been studied analytically in reset systems. However, numerical results that confirm that an increase in phase margin of the SIDF leads to a decrease in overshoot and settling time and an increase in bandwidth of the SIDF leads to a shorter rise time, are demonstrated in [11]. Of course, due to the nonlinearity of reset systems other aspects must also be taken into consideration when studying the transient behaviour, such as the effect of higher order harmonics [11].

Overall, HOSIDFs have proven to be the most popular frequency domain analysis tool for reset controllers due to their similarity to linear Bode plots. Although not all nonlinear effects are captured, they are often a necessary tool for loopshaping a reliable controller. Therefore, reset control structures which do not allow an analytical way to derive the HOSIDFs or restrict the HOSIDFs to be either amplitude dependent or available for only particular systems, pose a great constraint to the controller synthesis process. For this reason, controllers that do allow an analytical way to determine the HOSIDFs, such as the one described by (2.1), with $\mathscr{M}$ given by (2.6) used in the architecture shown in Fig. 2.2, will be prioritized for this thesis.

2.1.3. STABILITY

Although HOSIDFs provide a great tool for controller design purposes regarding predicive performance, one essential property of FRF of linear systems, namely that they can be used to evaluate linear frequency domain stability criteria such as Bode's criterion or the Nyquist criterion, does not hold for nonlinear systems. Frequency domain stability criteria allow to guarantee stability based on measurements of the FRF, such that it is not required to derive a parametric approximation of the plant, which is time expensive and introduces uncertainty. In linear systems various robustness analysis methods can be employed to ensure that the uncertainty does not affect stability results. Suitable robustness methods for nonlinear systems are not always available. Moreover, it was proven that reset controllers can destabilize stable BLS [38]. As the difficulty in finding stability analysis methods that are relatively simple to evaluate and perhaps can be proven even without parametric plant description are one of the most significant drawbacks of nonlinear control methods, it is important to study the literature to find a suitable stability method for reset control systems. Before considering stability, it should be noticed that while in LTI systems the response is existent and unique by definition, this is not the case in nonlinear systems. Ill-posed nonlinear systems can show different behaviours such as deadlock, beating or Zenoness. Deadlock occurs when x_r does not have a possible solution, whereas beating appears when the after-reset state is still contained in the reset surface [38]. Both can be avoided by choosing the resetting condition correctly. All resetting conditions proposed in Section 2.1.1 achieve this. On the other hand, Zenoness, defined as the presence of infinite reset actions in a finite time, can be avoided through time-regularization. In digital systems an interval at least equal to the sampling period

is present between any reset instance. One can thus define $\delta_t \geq 1/f_s$ in (2.12). Since the wire bonder has a digital control system, well-posedness will be assumed for each stability method presented next.

When J.C. Clegg first developed the CI, closed-loop stability of a system containing such a reset element, was not yet considered. In [58] and other of his works, Horowitz uses a SIDF to approximate closed-loop stability of simple reset elements based on the Bode's stability condition. This method is unreliable, especially for non-autonomous systems (i.e. systems with external inputs), as explained by Horowitz itself. The first formal closed-loop stability proof in reset control, was presented only two decades later in [59]. It is based on the resetting instances and is valid for a reset system containing a CI shown in (2.7). However, it assumes the systems is autonomous and the plant is of order lower than two. In a subsequent work the bounded-input bounded-output (BIBO) stability of a reset controller described by (2.1), with $n_r = \hat{n}_r = 1$, $A_\rho = 0$ and $\mathscr{M}$ given by (2.6) was proven under the β positive real condition [60]. This was then generalized in [37] through the H_β-condition, which allows $n_r = \hat{n}_r \in \mathbb{Z}^+$. Such a reset system was proven to be quadratically stable if and only if the H_β-condition is satisfied. In fact, the H_β-condition is a necessary and sufficient condition for the existence of a quadratic Lyapunov function [37]. However, the H_β-condition is not a necessary condition for stability, meaning reset systems which do not satisfy the H_β-condition could still be stable. The presence of stable systems which do not satisfy this condition was investigated in [61], which defines the H_β-condition as rather conservative. The H_β-condition imposes a strictly positive real (SPR) constraint on the BLS, thus requiring $\overline{A}$ to be Hurwitz. It is then satisfied if, assuming $C_s = 1$,

$$H_\beta(s) = C_0(sI - \overline{A})^{-1}B_0, \tag{2.21}$$

with

$$B_0 = \begin{bmatrix} I_{n_r \times n_r} \end{bmatrix}, \quad C_0 = \begin{bmatrix} \varrho & \beta C \end{bmatrix},$$

is SPR, with $(\overline{A}, B_0)$ controllable and $(\overline{A}, C_0)$ observable and

$$A_\rho^T \varrho A_\rho - \varrho \leq 0,$$

where $\varrho = \varrho^T > 0$, $\varrho \in \mathbb{R}^{n_r \times n_r}$, $\beta \in \mathbb{R}^{n_r \times 1}$. The existence of a solution to (2.21) can thus be found by solving linear matrix inequalities (LMIs). A system that satisfies the H_β-condition and whose states that reset do not depend on the states that are not reset, is fully stable. Full stability is defined in [37] as uniform bounded-input bounded-state (UBIBS) stability [37] and global asymptotic stability (GAS). The H_β-condition was subsequently expanded in [62] to also include reset systems with partial state reset. In [8] the H_β-condition was again expanded to systems with $C_s \neq 1$ by setting $C_0 = \begin{bmatrix} \varrho & \beta C_e \end{bmatrix}$ instead.

The conservativeness of the H_β-condition is given by the fact that it requires a quadratic

Lyapunov function that decreases along the entire state-space [63]. Using the reset system description in (2.4), it is possible to instead subdivide the state-space into sectors and thus consider piecewise quadratic Lyapunov functions instead. This was demonstrated in [39], [40], [40], [64] which proved that beyond UBIBS stability, it is also possible to achieve a more robust $\mathscr{L}_2$-stability, which can be defined as a nonlinear $\mathscr{H}_\infty$ measure of input-output robustness [65]. Other similar stability methods were developed in [66], [67], [68], [44], [69]. The latter method is based on a discrete time implementation of the reset condition, thus fitting for digital control systems. It was later proven that even reset systems described by (2.1), with $\mathscr{M}$ given by (2.6) and $A_\rho = 0$, can achieve $\mathscr{L}_2$-stability. In [70] the conditions for $\mathscr{L}_2$ reference-output and disturbance-output stability were stated. For the former it is sufficient that the system has $n_r = \hat{n}_r$ and the H_β-condition is satisfied. For $\mathscr{L}_2$ disturbance-output an additional H_γ-condition must be satisfied. In this case the system can also have partial state resetting [70].

The least conservative stability methods for reset controllers are based on passivity. All stability analysis methods studied beforehand require a stable finite order BLS. Time delay could for example not be taken into account. In [71] and [72] two different methods suitable for stable systems with time delay are presented. In case the BLS is unstable, or in case the reset is triggered by predetermined reset instances, passitivity approaches based on the reset instances have been utilized [73], [72]. Generally, the trade off for less conservativeness is that a more complex set of LMIs have to been solved. Moreover, often stability resulting from passitivity methods does not guarantee UBIBS stability, and is thus not favorable for systems with inputs, such as the ones used in industrial applications [38].

Most stability analysis techniques mentioned so far require solving LMIs. In case the plant is of high order, which is the case for complex industrial machines such as the AB383 wire bonder, these become complex and computationally expensive [8]. Furthermore, with LMI-based methods it is difficult to relate the result from the numerical computation to the controller parameter, often making the controller design procedure lengthy. Additionally, LMIs necessitate a state space description of the plant, which requires approximating the plant parameters, introducing uncertainty. This uncertainty, which plays an especially important role in industry, as different machines will have slightly different parameters, must be accounted for by selecting an appropriate robustness analysis method. However, studies on robustness of reset systems are still scarce. In [38] and [51] two alternative methods were proposed, both of which are however not suitable for systems with inputs. For these reasons, three different stability methods which do not require to solve any LMIs, do not require a parametric plant description and give a qualitative notion on the robustness of the system, are provided next. The first one, presented in [74], [75], [76] uses a circle criterion-like argument to guarantee pre-input-to-state stability (pre-ISS). Pre-ISS is stronger condition than UBIBS, in fact UBIBS is implied in pre-ISS [77]. The method requires $\mathscr{R}$ to be given by the representa-

tion in (2.4) with $\mathscr{F}$ and $\mathscr{J}$ as shown in (2.11). Pre-ISS can then be guaranteed if

$$T_{nR}(s) = \frac{G(s)C_{fb}(s)}{1+G(s)C_{fb}(s)}$$

is Hurwitz and the following condition holds:

$$\frac{1}{\alpha} + \mathrm{Re}\left(\lim_{\omega\to\infty} T_{nR}(j\omega)\right) > 0,$$
$$\frac{1}{\alpha} + \mathrm{Re}\left(T_{nR}(j\omega)\right) > 0 \quad \forall\omega \in \mathbb{R}.$$

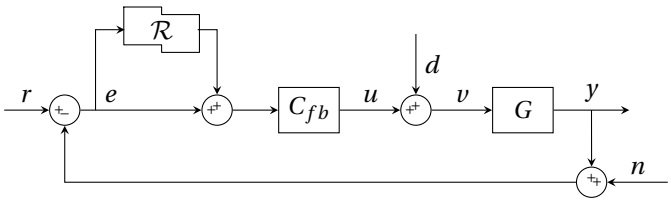

Figure 2.9: Controller structure for circle-like stability criterion adapted from [74]

A different approach to stability was introduced in [10] and expanded in [8], and can be utilized for some system described by (2.1), with $\mathscr{M}$ given by (2.6) and $n_r \geq \hat{n}_r$. This method can be utilized also for systems with the architecture portrayed in Fig. 2.2. It is necessary that the BLS is stable, with no pole-zero cancellations and that $\mathscr{R}$ has the structure of a CI, a PCI, a FORE, a SORE or a SOSRE[1]. The method relies on a frequency domain condition to prove that the H_β-condition holds. Assuming $C_s(0) > 0$ the condition is defined as

$$\left(-\frac{\pi}{2} < \theta_1 < \pi\right) \wedge \left(-\frac{\pi}{2} < \theta_2 < \pi\right) \wedge (\theta_2 - \theta_1 < \pi), \tag{2.22}$$

where

$$\theta_1 = \min_{\omega\in\mathbb{R}^+} \angle\overrightarrow{\mathscr{N}}(\omega), \quad \theta_2 = \max_{\omega\in\mathbb{R}^+} \angle\overrightarrow{\mathscr{N}}(\omega),$$

with

$$\overrightarrow{\mathscr{N}}(\omega) = \begin{bmatrix}\mathscr{N}_x(\omega)\\ \mathscr{N}_y(\omega)\end{bmatrix} = \begin{bmatrix}\mathrm{Re}(L_{BLS}(j\omega)C_s(j\omega)(1+L^*_{BLS}(j\omega)))\\ \mathrm{Re}((1+L^*_{BLS}(j\omega))R(j\omega))\end{bmatrix},$$

being the so called nyquist stability vector (NSV), where L^*_{BLS} is the complex conjugate of L_{BLS}. The condition can be computed using the measured FRF data of the BLS, thus not requiring a parametric plant description or solving LMIs. Furthermore one could argue that the distance between the resulting phase of $\overrightarrow{\mathscr{N}}(\omega)$ and the bounds can give

[1] These systems are defined in Section 2.1.4

a qualitative idea on the robustness of the system. However, to the best of the author's knowledge, this assessment of robustness was never studied in literature. Furthermore, it should be noted that, in case $\mathscr{R}$ is a SORE, the method requires solving additional optimization problems, making it more computationally demanding and complex. It is clear that this stability method poses strict constraints on the structure of $\mathscr{R}$. However, studies in recent years using controllers with architectures that satisfy these constraints have shown promising results, especially in the field of motion control [8]. A third frequency domain stability method valid for FORE systems described by (2.1) with $\mathscr{M}$ given by (2.6) and $A_\rho = 0$ is given in [37], [78]. Again this method allows to solve for the H_β condition using frequency domain conditions. In fact, in case $\mathscr{R}$ satisfies the aforementioned conditions, (2.21) can be instead computed as

$$H_\beta = R(j\omega)S(j\omega) + \beta T(j\omega). \tag{2.23}$$

However, since this method requires to find a suitable β, it is difficult to verify (2.23) holds. Moreover, the newer NSV method also allows to study the stability of FORE systems, making this method obsolete.

Overall, many different stability methods exist in literature. UBIBS stability of systems described by (2.1) with $\mathscr{M}$ given by (2.6) can be guaranteed making use of the classical H_β-condition (2.21), as long as the BLS is stable. This method requires solving LMIs that are usually easier to evaluate compared to other methods, but is rather conservative [51]. If $\mathscr{M}$ is instead described by (2.8) or (2.9) a passitivity based method must be employed. These can also be utilized for unstable BLS. However, they are often not suitable for systems with inputs. Systems described by (2.4) offer different, less conservative stability methods, which often also give a more robust $\mathscr{L}_2$-stability definition. In some cases systems described by (2.1) can also be guaranteed $\mathscr{L}_2$-stability. However, only two methods offer the desired characteristics of not requiring a parametric plant description, not requiring solving LMIs and providing a qualitative assessment of robustness. Reset systems described by (2.4), with resetting condition given by (2.11), offer the circle-like stability condition to be utilized. However, the systems in question do not allow analytical derivation of HOSIDFs, making loopshaping not possible. Using the architecture shown in Fig. 2.2, with $\mathscr{R}$ a CI, PCI, FORE, SORE or SOSRE, as defined in Section 2.1.4, and with $\mathscr{M}$ given by (2.6), the NSV stability method can be used, although in case $\mathscr{R}$ is a SORE, the NSV method is more complex. Additionally, the qualitative assessment of robustness that can be performed using this approach was never studied before. Nevertheless these reset elements allow the analytical derivation of HOSIDFs.

2.1.4. SUITABLE RESET CONTROLLERS

The previous two subsections demonstrated that of the vast amount of reset control structures present in literature, only a fraction allows both the analytical derivation of HOSIDFs and a suitable stability analysis. These two characteristics have however great benefits in the controller design process and reset controllers which possess them should

therefore be prioritized. For this reason, the following section will present controllers present in literature that allow both. All reset elements mentioned in the following section can fit within the architecture shown in Fig. 2.2.

TRADITIONAL CI

The CI shown in (2.7) is the most basic reset element. When it was first introduced in 1958 in [5], it was assumed that $A_\rho = 0$. However, since then it has been generalized to allow $A_\rho = \gamma$, just like all other control structures presented subsequently [9]. As shown from the FRF of the SIDF in Fig. 2.3, a CI reduces the phase lag of a linear integrator from $-90°$ to $\approx -38°$, while only slightly affecting the magnitude response. However, in case the BLS leads to a steady-state error, a CI will introduce a limit-cycle behaviour. This due to the fact that resetting causes the stored energy from the integral action, required to avoid a steady-state error, to be eliminated [9].

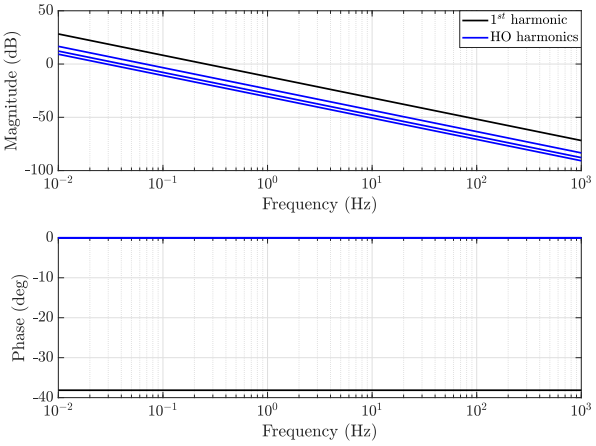

Figure 2.10: FRF of the SIDF and HOSIDFs of a typical CI.

PCI

A CI can be transformed into a PCI if a zero is introduced in the BLS at the corner frequency ω_r. The state-space matrices then become

$$A_r = 0, B_r = \omega_r, C_r = 1, D_r = 1, A_\rho = \gamma. \tag{2.24}$$

As shown in Fig. 2.11, the system behaves as a CI at $\omega << \omega_r$ and as a static gain at $\omega >> \omega_r$. Due to the same low frequency response, the issues affecting the CI's steady-state error are also present in the PCI.

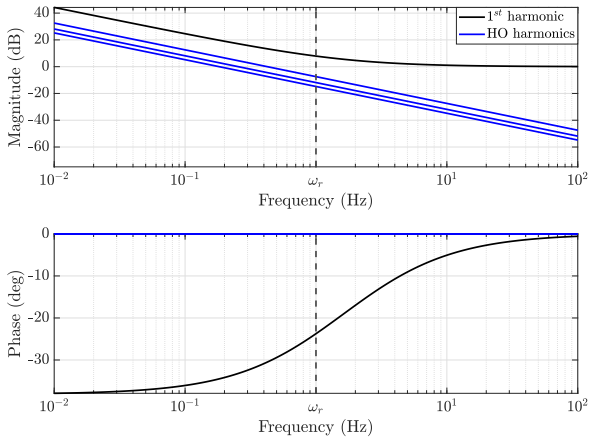

Figure 2.11: FRF of the SIDF and HOSIDFs of a PCI with $\omega_r = 2\pi$ rad/s.

PI+CI

The PI+CI was introduced in [79] as a simple-to-tune alternative to the traditional PCI that would overcome its limit cycle issues. Its structure is shown in Fig. 2.12, where $\mathscr{R}$ is a traditional CI controller, $k_p \in \mathbb{R}$ is the proportional gain, $\tau_i \in \mathbb{R}$ is the integral time and $p_r \in [0,1]$ is the reset ratio. Is is noticeable that the PI+CI adds a linear PI controller in parallel to a standard CI controller. The reset ratio imposes the relative weight of the CI over the PI. When $p_r = 0$, the controller is a PI and when $p_r = 1$, the controller is a PCI [80]. The state-space matrices can be obtained as

$$\begin{aligned} A_r &= \begin{bmatrix} 0 & 0 \\ 0 & 0 \end{bmatrix}, B_r = \begin{bmatrix} 1 \\ 1 \end{bmatrix}, A_\rho = \begin{bmatrix} 1 & 0 \\ 0 & 0 \end{bmatrix}, \\ C_r &= \frac{k_p}{\tau_i} \begin{bmatrix} 1 - p_r & p_r \end{bmatrix}, D_r = kp. \end{aligned} \tag{2.25}$$

Although in [81] and [36] it is stated that for the PI+CI the H_β-condition cannot be utilized, due to the fact that the resulting $\overline{A}$ is not Hurwitz, this is given by the fact that the description in (2.25) is a non-minimal realization of the system. By simply assuming the BLS to be a first order system and hence utilizing only the first state of the PI+CI system, stability can be guaranteed through the H_β-condition, in the same way as for a PCI. In fact, in [81] it is stated that for the PI+CI system, although the original H_β-condition cannot be used, stability of the BLS and satisfaction of the H_β-condition can be used to guarantee stability for practical purposes. This allows to similarly also use the NSV stability method.

The PI+CI tuning rules suggest to tune a BLS with high overshoot, which will be reduced

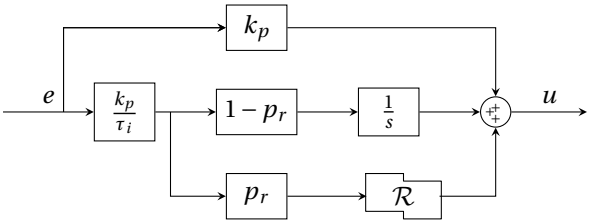

Figure 2.12: Block diagram representation of PI+CI controller.

by the PCI. The parallel PCI is therefore used as an alternative to the derivative action, since it reduces phase lag, however without sacrificing response speed. This allows to design controllers with higher bandwidths than achievable through an LTI PI controller. Nevertheless, the phase lag of a PI+CI will always be greater than that of a standard PCI as long as $p_r > 0$. This signifies there is a trade-off between between the nonlinearity of the PCI and the linear integral action, which makes this controller architecture suboptimal. This is best illustrated in Fig. 2.13.

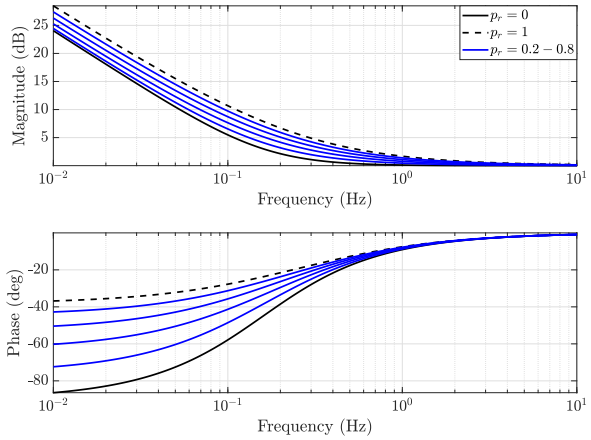

Figure 2.13: FRF of the SIDF of a PI+CI with $\tau_i = 1$, $k_p = 1$ and various values of p_r

FORE

Resetting low-pass filters of order $n_r = 1$ are known as first order reset elements (FOREs). After they were first introduced in [82], they have been studied thoroughly in literature. In [9] a FORE with partial reset was classified as a generalized FORE (GFORE). It should be noticed that the term GFORE was utilized as well in [83] and [84] to describe two different first order reset controller, both described by (2.4). The state-space matrices of

the FORE from [85] are given as

$$A_r = -\omega_r,\ B_r = \omega_r,\ C_r = 1,\ D_r = 0,\ A_\rho = \gamma. \tag{2.26}$$

FOREs are the building blocks of many reset controllers and can hence be utilized in different applications. On their own they have a low-pass filter behaviour, as portrayed in Fig. 2.14, acting as a static gain of 1 at low frequencies, and as a CI at frequencies greater than ω_r.

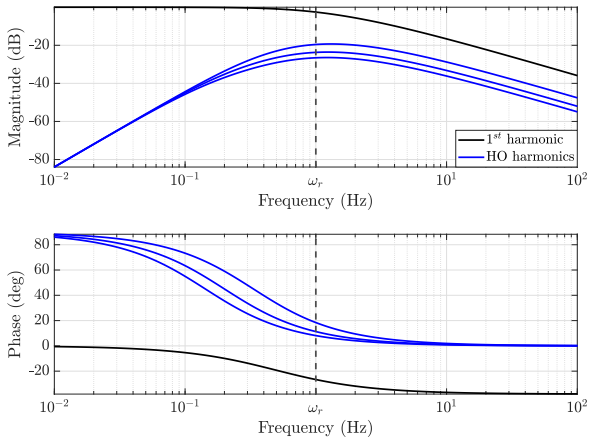

Figure 2.14: FRF of the SIDF and HOSIDFs of a FORE with $\omega_r = 2\pi$ rad/s and $A_\rho = 0$

SORE

Resetting low pass filters of order $n_r = 2$ are known as second order reset elements (SOREs). This definition was first used in [86], but as for the FORE, different structures have been associated with the given name. Within this report, the term SORE will be used to describe a reset controller with state-space matrices

$$\begin{aligned} &A_r = \begin{bmatrix} 0 & 1 \\ -\omega_r^2 & -2b\omega_r \end{bmatrix},\ B_r = \begin{bmatrix} 0 \\ \omega_r^2 \end{bmatrix},\ A_\rho = \begin{bmatrix} \gamma_1 & 0 \\ 0 & \gamma_2 \end{bmatrix}, \\ &C_r = \begin{bmatrix} 1 & 0 \end{bmatrix},\ D_r = 0, \end{aligned} \tag{2.27}$$

As can be seen from Fig. 2.15, a SORE has a similar behaviour to a linear second order low pass filter, however the phase does not go below 52° for $\gamma_1 = \gamma_2 = 0$. With b, a new tuning parameter is introduces, which regulates the damping of the system. The closer to 0, the more the system will be underdamped, thus showing a faster roll-off in the phase. However, contrarily to linear LTI low pass filters, the damping barely affects the magnitude response, which does not show major peaks even in case of very low values

of b. This can be advantageous in terms of control, since resonance peaks in the magnitude after the bandwidth frequency can lower the precision in closed-loop. This leads to a less strict trade-off between phase lag in frequencies lower than ω_r and increase in magnitude compared to LTI filters making undamped reset filters more attractive.

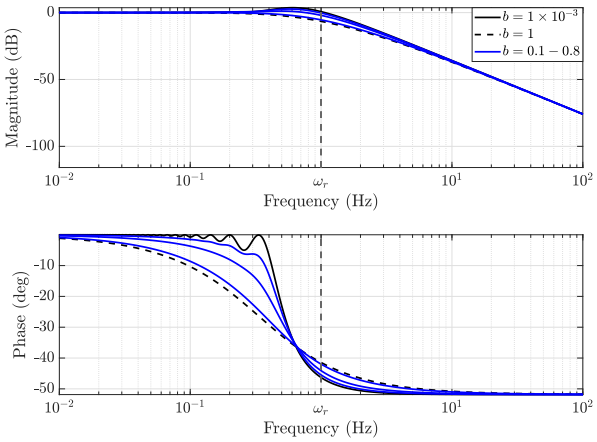

Figure 2.15: Frequency response function of the SIDF of a SORE with $\omega_r = 2\pi$ rad/s, $A_\rho = 0_{2\times 2}$ and different values of b.

SOSRE

A SORE which has only one resetting state is defined as a second order single resetting element (SOSRE). Its state-space matrices are equal to (2.27), however with $A_\rho = \text{diag}(\gamma, 1)$ instead. The resulting HOSIDF show that the magnitude behaviour of the first harmonic remains almost unchanged, whereas the third harmonic, and thus all higher order harmonics, have a greater roll-off slope as well as a notch filter behaviour at ω_r (Fig. 2.16).

RESET PID

The FORE has been utilized in [85] to construct a reset version of the classic PID controller. This is done by replacing

$$\left(1 + \frac{s}{\omega_t}\right)$$

with a FORE in (1.9). As depicted in Fig. 2.17, a 'reset PID' can achieve the same low frequency behaviour as an LTI PID, while also increasing the bandwidth without loss in phase margin.

Nevertheless, this element has become obsolete since another reset controller based on

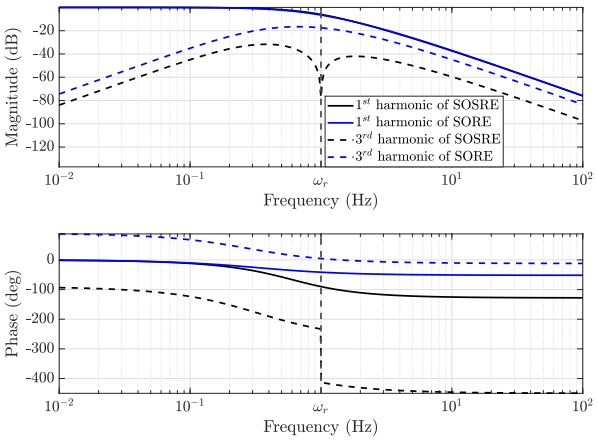

Figure 2.16: FRF of the SIDF and 3^{rd} HOSIDF of a SORE with $\omega_r = 2\pi$ rad/s, $A_\rho = 0_{2\times 2}$ and $b = 1$ and a SOSRE with $\omega_r = 2\pi$ rad/s, $A_\rho = \text{diag}(0, 1)$ and $b = 1$.

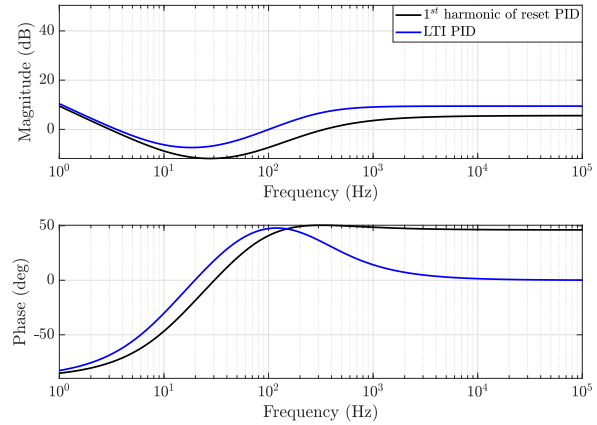

Figure 2.17: Frequency response function of the SIDF of a 'reset PID' and an LTI PID with the same low frequency behaviour.

a resetting low pass filter, the CgLp, has made its appearance in literature. Combined with a PID, a CgLp allows for easier tuning and more design freedom, while having the same working principle of reducing the phase lag introduced by the integral action of a PID.

CgLp

The CgLp reset element was developed only recently in [7], although a similar approach was already introduced in [87] and [88]. However, due to its characteristics it is highly suited for motion systems and has thus appeared in literature various times since [13], [89], [90], [91]. A CgLp can in fact create a band of frequencies in which phase lead occurs with only a minimal effect on the magnitude. Its characteristic makes it thus multipurpose, as the phase lead can be utilized in different ways. Depending on the desired effect, a CgLp can be for example used to increase the bandwidth and low frequency gain, while keeping the same phase margin as a linear controller, or to increase the phase margin and decrease the slope at low frequencies while keeping the same bandwidth as a linear controller. It consists of a FORE or a SORE in series with a first order lead filter F_l or a second order skewed-notch filter F_{sn} respectively, where the two filters are defined as

$$F_l = \frac{\frac{s}{\omega_d}+1}{\frac{s}{\omega_t}+1}, F_{sn} = \frac{(\frac{s}{\omega_d})^2 + \frac{2sb_F}{\omega_d}+1}{(\frac{s}{\omega_t})^2 + \frac{2s}{\omega_t}+1}, \tag{2.28}$$

with $\omega_d \in \mathbb{R}$ being the corner frequency at which phase lead is provided and $\omega_t > \omega_d \in \mathbb{R}$ the corner frequency at which phase lag is provided by the linear filters and $b_F \in \mathbb{R}$ a parameter related to the value of the anti-resonance peak at ω_d. One can quickly assess that in case $A_\rho = 1$ and the FORE/SORE acts fully linear, choosing $\omega_r = \omega_d$ and $\omega_t >> \omega_d$ would essentially cancel out the low filter behaviour of the FORE/SORE and act as a constant gain of 1 with 0° phase until $\approx \omega_t$. One can thus appreciate that if the FORE/SORE has $A_\rho < 1$, it's phase lag decreases while the magnitude behaviour only slightly changes, thus providing a phase lead, while the gain is still 1, when in series with F_l/F_{sn}. Nevertheless, the magnitude behaviour does slightly change, especially it's corner frequency. Therefore, the FORE/SORE is usually adjusted such that $\omega_r = \omega_d/\alpha$, where $\alpha \geq 1 \in \mathbb{R}$ is a tuning parameter used to calibrate the constant gain region of the CgLp [13] to account for the change in corner frequency. Figure 2.18 shows that CgLps create a region of phase lead in the range $[\omega_d, \omega_t]$ nearly without affecting the gain. In case of SORE CgLp, the phase advantage is significantly greater than the one obtained by a FORE CgLp.

As stated before, only using the SIDFs to approximate the FRF is often unprecise. This becomes evident when the third harmonic of a FORE and SORE CgLp are plotted as well (Fig. 2.18). It can be noticed that the FORE has a much more satisfactory behaviour, with higher order harmonics having a lower magnitude than the first harmonic. This is not the case for the SORE CgLp, where in the range $[\omega_d, \omega_t]$, the third harmonic reaches a greater magnitude compared to the first harmonic. This could lead to different issues in closed-loop and must thus be avoided. In [92] a CgLp constructed using a SOSRE was demonstrated to achieve only a slightly worse magnitude and phase behaviour as a FORE CgLp, while also producing smaller HOSIDFs, as portrayed in Fig. 2.19. In fact, a SOSRE CgLp provides a tunable notch filter behaviour in the higher order harmonics. By tuning α, it is possible to position the notch filter at the desired frequency, e.g. at a frequency that would assure a resonance of the plant is not excited by higher order har-

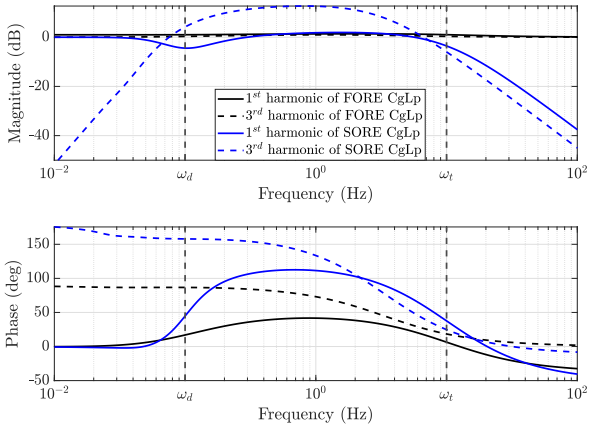

Figure 2.18: FRF of the SIDF and 3^{rd} HOSIDF of a FORE CgLp with $\alpha = 1.2$, $\omega_d = 0.1$ rad/s, $\omega_t = 10$ rad/s, $A_\rho = 0$ and of a SORE CgLp with $\alpha = 1.2$, $\beta = 0.5$, $\omega_d = 0.1$ rad/s, $\omega_t = 10$ rad/s and $A_\rho = 0_{2\times 2}$.

monics.

It was shown in [93], that the sequence of the linear filters and reset controller affects the prevalence of higher order harmonics. This can be explained from (2.17). The magnitude of the n^{th} HOSIDF is determined by $|C_1(j\omega)|$ and $|C_2(jn\omega)|$. The LTI filters F_l and F_{sn} have both a positive magnitude at frequencies $\omega > \omega_d$. To assure the HOSIDFs are low in this range it is therefore advantageous to place them after $\mathscr{R}$. This is however not necessarily true if a lag element is used in combination with the CgLp. In that case, the combination that minimises the HOSIDF magnitude is dependent on the FRF characteristics of the lag element. For example, in [93] the CgLp is used in combination with an LTI PI. The resultant best performing sequence of a FORE CgLp-PI was achieved when $\mathscr{R}$ was preceded by F_l and the PI was placed last. However, it is clear that a lead will amplify noise in the range $\omega > \omega_d$. Noise can affect reset systems even more than their LTI counterparts, since it can influence the resetting instances. In [93] and [91] it was discovered that when the signal-to-noise ratio (SNR) overcame 1%, the suggested sequence would perform worse than when F_l followed $\mathscr{R}$.

CONTINUOUS RESET ARCHITECTURE

One of the potential implementation issues that is introduced by reset control, is given by the jumps in the output, given by discontinuity of the signal. These jumps in u demand the actuator to have an infinite rate of change of current, which is physically not possible and can thus lead to saturation. Using the continuous reset (CR) architecture, it was proven that the output is instead continuous, overcoming this limitation, while virtually not affecting the SIDF [11]. This is achieved by choosing C_1 and C_2 in Fig. 2.2 as

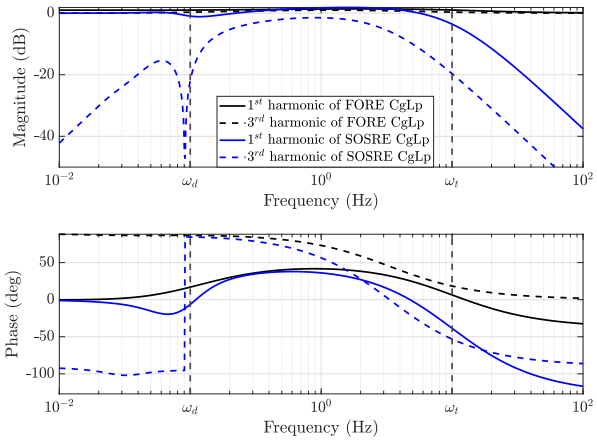

Figure 2.19: FRF of the SIDF and 3^{rd} HOSIDF of a FORE CgLp with $\alpha = 1.2$, $\omega_d = 0.1$ rad/s, $\omega_t = 10$ rad/s, $A_\rho = 0$ and of a SOSRE CgLp with $\alpha = 1.2$, $\beta = 0.5$, $\omega_d = 0.1$ rad/s, $\omega_t = 10$ rad/s and $A_\rho = \text{diag}(0,1)$.

F_l and

$$F_l^* = \frac{1}{\frac{s}{\omega_d}+1}, \tag{2.29}$$

respectively. The SIDF is not affected up to ω_t since the contribution of the zero in F_l is cancelled out by the pole in F_l^*. On the other hand, F_l^* acts as a low pass filter for the HOSIDFs, as can be verified from (2.17). The smoothing effect is however not given only by the lowered HOSIDFs. The lead F_l anticipates the reset instances which in closed loop are now not only based on the error but on a linear combination between the error and it's derivative. The change in reset instances signifies that the transient behaviour changes as well as the steady-state one. Using the CR architecture it was shown that it is possible to lower overshoot, while not affecting settling time [11].

SHAPING FILTERS

The effect of shaping filters, defined by C_s in Fig. 2.2, on the performance of reset systems has not been studied extensively, as they have only been introduced recently [8]. In [12] it was shown how using a shaping filter it is possible to band-pass the nonlinearity of a reset controller with $n_r = 1$, i.e. the reset controller can be tuned such that it acts linear in a certain range of frequencies. This can be achieved by assuring C_s introduces a certain phase lag $-\angle C_s(\omega) = \varphi(\omega)$ between e_r and $\hat{e}_r$. The necessary value of $\varphi(\omega)$ required to assure a fully liner behaviour is dependent, apart from ω, on the parameters of $\mathscr{R}$. These can be found by setting $H_n(j\omega) = 0$ for a certain ω for $n \geq 2$ in (2.14). In fact, when the HOSIDFs are 0, the system behaves like the BLS. This however means that the gain advantage and the phase advantage given by reset control are also lost. The

variable φ affects the SIDF as well as the HOSIDFs, potentially increasing the phase advantage provided by a reset controller. For this reason, they have been utilized to shape the phase of a CgLp in order to approximate complex-order controllers [56], something that was already performed for a reset system containing a CgLp witout a shaping filter [94]. Although approximating complex-order controllers is outside the scope of this thesis, it can be appreciated that C_s introduces a new design DoF which could potentially result beneficial and should thus be explored accordingly.

In this section the basics of reset control were explored. After looking at the structure, predictive performance and stability analysis methods for reset controllers, the conclusion was drawn that only a restricted number of systems allow both analytical description of the HOSIDFs and a suitable stability analysis method that does not require solving complex LMIs and provides a qualitative assessment of robustness. Nevertheless, different configurations of both linear and reset elements provide various design DoF. Some of these configurations were presented in this section. Using a CI or a PCI without a linear integrator could introduce a steady-state error and can thus not be deemed reliable enough. The PI+CI solution solves this issue at the expense of the nonlinearity that makes reset systems attractive in the first place. For this reason, it is more beneficial to utilize CI, PCI, FORE, SORE and SOSRE based systems used to in combination with linear controllers that include one integrator. Since the overarching goal is to make the implementation of reset controllers as straightforward as possible, it is beneficial for these reset elements to be utilized to improve the performance of a PID-like LTI controller, as the one already utilized by ASM PT. Given the phase lag introduced in the plant by the time delay, using a CI would require a very strong derivative action to achieve $PM = 30°$ with a PID-like controller, reducing disturbance suppression in the mid-frequency range. Instead, a PCI-PID can be utilized for this purpose, taking advantage of the increased tracking performance and error suppression at low frequencies. A CgLp-PID controller will also be designed. SORE-CgLp controllers require a more computationally demanding stability proof and result in greater HOSIDFs, making them disadvantageous compared to FORE-CgLp and SOSRE-CgLp controllers. Out of the two, FORE systems are far more established in literature and offer a simpler, lower order, controller structure. Moreover, the HOSIDFs notch behaviour of the SOSRE-CgLp controllers can be achieved with any reset element utilizing a shaping filter, which actually allows a more tunable trade-off between the magnitude of HOSIDFs and the gain and phase advantage from reset [12]. Therefore, a FORE-CgLp system will prioritized, while also studying the effect of linear controllers C_1 and C_2 and C_s.

2.2. PAST IMPLEMENTATION OF RESET CONTROL ON THE AB383 WIRE BONDER

In [4] the implementation of two different reset controllers to lower the RMS error in the tracking and settling/steady-state region of the AB383 wire bonder, was studied. The results were only partially successful, as some open issues prevented the controllers from being adopted on the machine and replace their linear counterpart. In order to avoid the same issues from occurring again, in this section the implementation of reset control in [4] will be studied.

Figure 2.9 shows the feedback control system employed in [4] to regulate the motion of the AB383 wire bonder's X-stage, where C_{fb} was chosen as a lead-lag compensator, tuned using some rules of thumb stated in [4]. The first controller that was utilized as $\mathscr{R}$ was a CI, given by the representation (2.1) with state space matrices $A_r = 0$, $B_r = \omega_r$, $C_r = 0$, $D_r = 0$, $A_\rho = 0$ and $\mathscr{M}$ given by (2.6). The equivalent series representation of the system is thus a PID controller as given by (1.9) whose integral action (I) is replaced by the CI. The linear part of the controller, as well as the corner frequency of the CI, was kept identical to the LTI PID controller. The reset controller achieved a substantial RMS error reduction in both the tracking and settling/steady-state region, even though the CI suffers from the limit-cycle behaviour that prevents it from being able to achieve a zero steady-state error Section 2.1.4. The HOSIDFs of the control systems were obtained using (2.14). The H_β-condition was then computed using (2.21). However, no feasible solution to the LMIs could be found. In order to be able to utilize a less conservative stability method, the same controller was also described using the representation in (2.4), with $\mathscr{J}$ and $\mathscr{F}$ as given by (2.10). Based on the new representation of the CI, the stability method from [69] was successfully utilized to guarantee $\mathscr{L}_2$-stability. The time domain response of the two configurations was proven to be the same, thus it was argued that intuitively the same HOSIDFs can be utilized. This statement was however not proven and can thus not be considered generalizable for other reset structures. Furthermore, no closed-loop frequency domain performance analysis method was utilized to investigate the control system. As mentioned in Section 2.1.3, the utilized stability analysis method is also based on solving LMI's and does not provide any indication on robustness. In fact, no suitable robustness analysis method could be found. Moreover, the stability result relied on the identified plant model, which contains parametric uncertainty [4].

To allow the use of a frequency domain stability method instead, a sector-bounded CI was designed next. The sets $\mathscr{F}$ and $\mathscr{J}$ were defined as given by (2.11), with α the greatest possible value such that the system is still stable and allowing A_ρ to be a nonzero value. The circle criterion-like stability method from [74] could thus be employed, allowing to analyse stability without necessitating a parametric plant description. Moreover, the graphical result from the circle criterion-like stability analysis allowed to give a qualitative measure of robustness, which proved the reset controller would be reli-

able enough for implementation. Using this method, stability could be guaranteed for a higher bandwidth system, which could achieve an even greater reduction in RMS errors. Nevertheless, it was discovered that a lower α, decreases the performance, due to the introduction of more severe premature resets [4]. Therefore, this type of sector-bounded systems are not ideal, as the higher α, therefore the greater $\mathscr{F}$, the greater the increase in performance. Additionally, an analytical method to derive the HOSIDF is not available for this type of system. This makes it impossible to use loopshaping to effectively tune the controller.

The most critical limitations of the reset controllers explored in [4] can be summarized as follows:

- The schemes are based on replacing the integral action of the controller with a CI, thus not allowing to achieve a zero steady-state error.
- Neither scheme allows both an open-loop frequency domain predictive performance analysis and a frequency domain stability analysis method.
- No closed-loop predictive performance analysis method was utilized, thus not allowing loopshaping techniques to be employed.

3

CgLp-PID

The objective of a CgLp is to provide a phase advantage at ω_{BW}, while keeping the SIDF's gain close to 1 up to the low-pass filter behaviour. It is thus necessary to account for the shift in corner frequency given by lowering $\gamma < 1$, to assure the FORE and the numerator of F_l cancel out. It is therefore often suggested to tune $\omega_d = \alpha\omega_r$, where $\alpha > 1$ is the ratio between the corner frequency of the FORE BLS and the FORE itself [7]. However, this method only applies if $\omega_t >> \omega_d$. The parameter ω_t can instead be accounted for when finding ω_r through the optimization problem

$$\mathbb{P}: \begin{cases} \min\limits_{\omega_r} & \left| \max\limits_{\forall\omega} |H_1 F_l| - \min\limits_{\omega<\omega_{BW}} |H_1 F_l| \right| \\ \text{subj. to} & \angle(H_1(\omega_{BW})F_l(\omega_{BW})) \geq \theta_d, \end{cases} \tag{3.1}$$

where $\theta_d \in \mathbb{R}^+$ is the desired phase advantage. Since the problem is convex, given a certain ω_d, ω_t and γ, there exist only one ω_r which minimizes the change in gain of the CgLp until the low-pass filter behaviour, while providing the desired amount of phase advantage at ω_{BW}.

For a CgLp, the HOSIDFs are low at low frequencies and increase up to shortly after ω_r. The CgLp has therefore a high degree of nonlinearity in the range $\omega > \omega_r$. It is hence desired to keep ω_r and thus ω_d as high as possible. However, increasing ω_d will lead to a smaller phase advantage at ω_{BW}. To show this, three CgLp elements were tuned. They all have the same ω_t and $\gamma = 0$, but each has a different ω_d. The parameter ω_r was derived by solving the optimization problem (3.1). The SIDF and third HOSIDF of three CgLp elements can be seen in Fig. 3.1, which also shows how the phase difference between F_l and the corresponding CgLp SIDF at ω_{BW} is $\approx 30°$ for all CgLp. In fact, it was found empirically that when using (3.1) to find ω_r, this relationship holds true independently on the parameters ω_d and ω_t.

In [13] it was discovered that the combination of ω_d and γ that results in the lowest HOSIDFs at low frequencies maximises low frequency disturbance suppression. In general, it is usually proposed to choose $\omega_t = [5\omega_{BW}, 10\omega_{BW}]$ [13], [7]. Based on the findings in [13], [7] and the optimization problem (3.1), a tuning procedure for a CgLp to be used in combination with a low phase margin LTI PID controller is proposed. A CgLp-PID reset controller is then constructed by selecting $C_1 = 1$, $C_s = 1$, $\mathscr{R}$ as a FORE and C_2 including both the low phase margin LTI PID controller and F_l. This order was selected to assure resetting occurs when the error crosses the zero-line (i.e. $\hat{e}_r = e$). Subsequently the proposed tuning procedure is shown.

Tuning Procedure 3.0.1 (CgLp)

1. *Tune an LTI controller such that the system has the desired open-loop gain with cross-over frequency ω_{BW} and phase margin $PM < 30°$.*
2. *Choose $\theta_d = 30° - PM$, $\gamma = 0$ and $\omega_t = 7\omega_{BW}$ as an initial guess.*
3. *Find the parameter of ω_d with which $\angle F_l(\omega_{BW}) = \theta_d + 30°$ to assure that with the CgLp the SIDF of system has a phase margin of $30°$ at ω_{BW}.*
4. *Solve the optimization problem (3.1), obtaining ω_r.*
5. *In case the peak of the pseudosensitivity magnitude can be increased further (i.e. it is lower than the acceptable level, e.g. 6 dB), the combination of γ and ω_r that results in the lowest HOSIDFs at low frequencies must be found empirically: Decrease/increase γ while simultaneously increasing/decreasing ω_r, making sure the open-loop HOSIDFs at low frequencies have decreased. Return to step 4.*

With this tuning procedure a CgLp which lowers the magnitude peak of pseudosensitivity compared to the peak of sensitivity of the same system controlled solely by the LTI PID controller can be found. The procedure is iterative, as no analytical relationship to determine the magnitude peak of pseudosensitivity was ever derived. Two CgLp controllers, CgLp_{10} and CgLp_{15} providing $\theta_d = 10°$ and $\theta_d = 15°$ respectively are designed using the above procedure for a plant resembling a highly damped non-collocated 2-DoF MSD system

$$G_a = \frac{ds + k}{m_1 m_2 s^4 + d(m_1 + m_2)s^3 + k(m_1 + m_2)s^2}, \tag{3.2}$$

with parameters given in Table 3.1. Although difficult to see due to the high damping, G_a has a resonance at 1 kHz. This structure approximates many industrial stages, including the ASMPT wire bonder (Fig. 1.9). An LTI controller with the structure shown in (1.9), and with parameters also given in Table 3.1 was tuned for G_a to achieve $\omega_{BW} = 200$ Hz. It has a weak D-action that does not provide enough phase to keep $M_S < 6$ dB, thus making it not implementable by ASMPT Section 1.3. Figure 3.2 shows that the tuned CgLp-PID

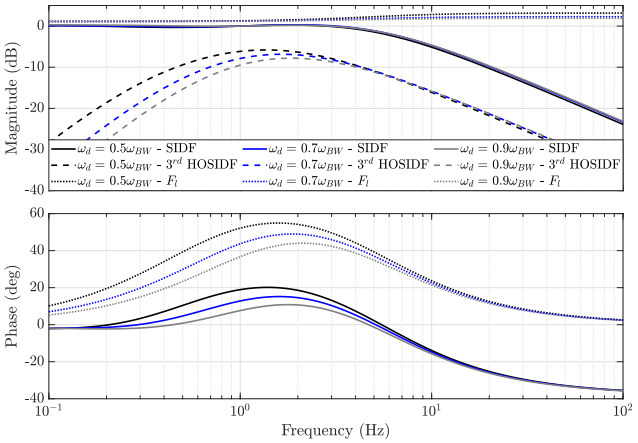

Figure 3.1: FRF of the SIDF, 3^{rd} HOSIDF and corresponding F_l of a FORE CgLp for different ω_d with ω_r resulting from (3.1), $\omega_t = 5\omega_{BW}$ and $\gamma = 0$. The gain of the CgLp was adjusted for $\omega_{BW} = 1$ Hz.

Table 3.1: Parameters of G_a, PID$_a$, CgLp$_{10}$ and CgLp$_{15}$.

G_a	m_1	m_2	k	d
	100	100	1.97×10^9	60.6×10^4
PID$_a$	k_P	ω_I	ω_D	ω_T
	1.68×10^8	20 Hz	111.11 Hz	360 Hz
CgLp$_{10}$	ω_r	ω_d	ω_t	γ
	152.3 Hz	198 Hz	2000 Hz	0
CgLp$_{15}$	ω_r	ω_d	ω_t	γ
	125.38 Hz	163 Hz	2000 Hz	0

controllers provide 10° and 15° respectively with only negligible effects on the gain of the SIDF.

The resultants pseudosensitivities computed through the approximate method are portrayed in Fig. 3.3. The effect of the CgLp is apparent from the lower magnitude peak of the resultant pseudosensitivities. The magnitude peak of the LTI system without CgLp is of 7.4 dB. Although not equivalent in terms of robustness, it was deemed necessary to set an equivalent constraint to $M_S < 6$ dB on the peak of the pseudosensitivity to prevent large amplification of the reference. When implementing the CgLp$_{10}$, the peak decreases to 4.2 dB, while with the CgLp$_{10}$ it decreases to 3.7 dB. This brings the control system within the 6 dB peak of pseudosensitivity requirement by an extensive margin, allowing for the phase margin of the LTI part of the system to be reduced further. A slight increase of the magnitude in the range [40, 100] Hz compared to the LTI system shows that although low, HOSIDFs have already an effect on performance.

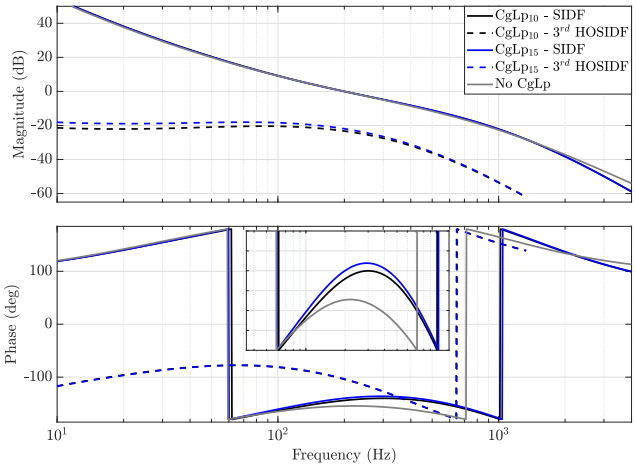

Figure 3.2: FRF of the SIDF and 3^{rd} HOSIDF of the open-loop system with G_a as the plant, PID$_a$ as the LTI controller and without CgLp, with CgLp$_{10}$ and with CgLp$_{15}$ respectively.

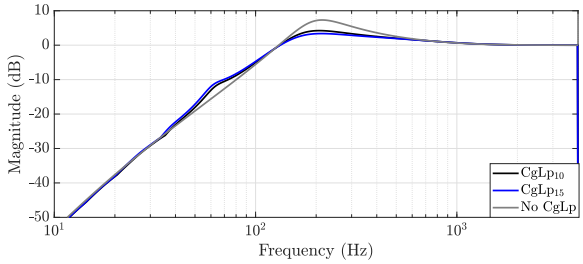

Figure 3.3: Pseudosensitivities magnitude computed through the approximate method of the closed-loop system with G_a as the plant, PID$_a$ as the LTI controller and without CgLp, with CgLp$_{10}$ and with CgLp$_{15}$ respectively.

To the best of the author's knowledge, in literature the CgLp controllers were designed only for particular types of systems with either highly damped resonance peaks, as the highly damped 2 DoF MSD system, or resonances at frequencies much greater or lower than the bandwidth frequency. In reality however, industrial stages, including the one of the ASMPT wire bonder, are often not as damped (Fig. 1.9). The effect of these high frequency resonances on stability will be studied next. A second, less damped plant G_b was constructed, with the same structure as G_a, but with $d = 4.6 \times 10^4$. In order to suppress

the resonance of G_b a notch filter acting at 1 kHz, given as

$$F_{n_1} = \frac{2.53 \times 10^{-08} s^2 + 1.59 \times 10^{-3} s + 1}{2.53 \times 10^{-08} s^2 + 3.56 \times 10^{-3} s + 1}, \tag{3.3}$$

was also tuned. The phase of the NSV as well as $\theta_2 - \theta_1$ for the control system with G_a, G_b and $G_b F_{n_1}$ as the plant respectively, is portrayed in Fig. 3.4. While for the system with G_a the NSV phase and $\theta_2 - \theta_1$ for both CgLp are within the bounds, the opposite is true for the system with G_b, due to the spike of the NSV phase at the resonance frequency. The H_β-condition is hence not satisfied and stability cannot be guaranteed (Section 2.1.3). In case of the system with $G_b F_{n_1}$, the bounds are not overcome for $\theta_2 - \theta_1$ when CgLp_{10} is utilized, while the opposite is true when CgLp_{15} is used. This is given by the higher value of ω_r for the system employing CgLp_{15}, leading to higher HOSIDFs at the resonance frequency. An even stronger notch filter would be required to satisfy the H_β-condition. On the other hand, although the system employing CgLp_{10} does satisfy the H_β-condition, it is not beneficial to implement it. Due to the relative proximity between ω_{BW} and the resonance frequency, the notch filter has an effect on the phase margin, reducing it by more than $-10°$. To guarantee stability it is hence required to use a notch filter that lowers the phase margin more than the respective CgLp provides phase advantage. The whole purpose of increasing the phase margin is therefore negated by the notch filter, causing the CgLp to be ineffective.

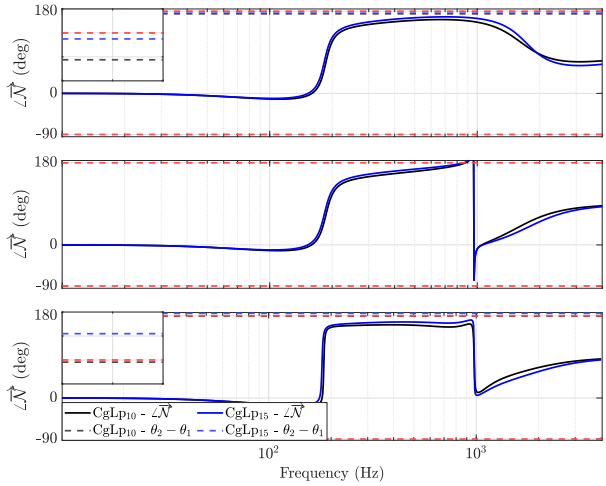

Figure 3.4: NSV plots of the closed-loop system with plant G_a (top), G_b (middle), and $G_b F_{n_1}$ (bottom), PID_a as the LTI controller and CgLp_{10} or CgLp_{15} respectively.

By definition a CgLp element has high HOSIDFs at high frequencies and low HOSIDFs at low frequencies. If a motion system has a resonance peak at high frequency, the reso-

nance is excited by the HOSIDFs, which could lead to complications when proving stability. The lower ω_r, the higher the HOSIDFs, thus the greater the NSV phase peak caused by the resonance. When the resonance peak is too large, it is not possible to simply increase ω_r, a notch filter must be implemented as well. Such a filter provides however also a phase lag, lowering the phase margin, especially if ω_{BW} is relatively close to the resonance frequency. In order to make the CgLp have any beneficial effect it is necessary for it to provide a greater phase advantage than the phase lag introduced by the notch filter. This is however not always possible. Although γ also affects the presence of HOSIDFs, the NSV phase is independent from it (Section 2.1.3). In some instances it might hence be possible to lower γ in order to obtain enough phase advantage without affecting stability. However, decreasing $\gamma < 0$ exponentially increases HOSIDFs, thus leading to an overall worse performance [13]. In case of high frequency resonance peaks of high amplitude or relatively close to ω_{BW}, a CgLp element could be unsuitable. This appeared to be the case for the ASMPT wire bonder's motion stage, for which no beneficial CgLp could be designed.

4

PCI-PID

The following chapter will iinclude the most significant findings of this work in a standalone paper format, in which no confidential information will be disclosed. This will allow the distribution of the findings. The introductory sections will include background theory already presented in Section 1.2, Section 1.3 and Section 2.1.

Increasing the tracking performance of an industrial motion stage with reset control

Daniel Caporale*

***Abstract*—Promising findings in recent literature suggest that with reset control, a nonlinear control technique, it is possible to overcome inherent limitations of Linear Time-Invariant (LTI) control. However, current literature on reset controllers aimed for industrial applications, especially regarding precision motion control, is lacking. In this work the Proportional Clegg Integrator (PCI), a resetting PI element, is studied with the aim of increasing the tracking performance of an industrial motion stage. In fact a PCI has an increased open-loop gain and decreased phase lag compared to an equivalent PI element. Two frequency domain methods, namely open-loop Higher Order Sinusoidal Input Describing Functions (HOSIDFs) and pseudosensitivities computed through analytically derived (approximate) closed-loop HOSIDFs, were effectively applied to predict steady-state performance. This allowed the use of loopshaping techniques similar to LTI control for the design of reset controllers, allowing to present frequency-based tuning guidelines for all proposed structures. Experimental results, validated on an ASM Pacific Technology wire bonding machine, confirmed that disturbances can be suppressed more effectively by adopting a PCI-PID controller compared to a LTI PI-PID. However, being nonlinear, the PCI introduces unwanted higher order harmonics that can reduce performance. The series Continuous Reset (CR) architecture was recently introduced in literature to lower the higher order harmonics, thus increasing performance. Experimental results show that although capable of suppressing higher order harmonics, different issues can prevent an optimal performance when implemented digitally. A novel parallel CR architecture, which overcomes the issues of the series CR architecture, is thus presented. With this structure, a significant decrease in the root mean square of the settling error compared to an equivalent LTI controller could be achieved.**

I. Introduction

Linear Time-Invariant (LTI) control is indisputably the most popular choice for motion control strategies, with the overwhelming majority of industry relying on it [1]. The success of LTI control can be attributed to the simplicity it offers regarding the controller design process. It allows for the use of classical control theory, which offers frequency domain tools to predict performance, as well as determine stability and robustness of feedback systems. Often these tools are utilized in industry to shape the open- and closed-loop transfer functions to obtain the desired controller characteristics, what is often referred to as loopshaping [2]. Nevertheless, LTI control suffers from inherent limitations, such as the 'waterbed effect' [3] and 'Bode's gain-phase relationship' [4]. Therefore, employing such controllers creates a trade-off between e.g., rise time, tracking precision, noise suppression and robustness. Improving one characteristic requires to worsen at least one of the other characteristics as a consequence. For this reason, for the last few decades nonlinear control has been given great consideration in literature. Nevertheless, adoption in industry is still scarce [1]. This is given by the fact that for most techniques it is not possible to get a reliable indication on the performance or stability/robustness of the system in the frequency domain, thus preventing the use of loopshaping techniques.

Reset control appeared for the first time in literature more than 60 years ago [5]. However, it is only four decades later that the field has been given enough attention to be considered a potentially reliable alternative to linear control [6]. Recent literature demonstrated that frequency domain predictive performance and stability analysis methods exist for some particular reset control structures [7]. This makes it is possible to design and analyze these particular nonlinear controllers in a similar way as linear controllers, while overcoming the inherent limitations of their linear counterparts. The majority of literature works are focused however on the 'Constant in gain-lead in phase' (CgLp) element [8]. This structure has high versatility, as it can be used in combination with any LTI controller, increasing its robustness without loss in performance. However, being a nonlinear technique, reset controllers introduce unwanted higher order harmonic in the response. Recently, it was proven that the performance of a CgLp element can be potentially further improved when used in a series Continuous Reset (CR) structure, capable of reducing the nonlinearity of the reset element over broad frequency band [9].

However, literature on synthesis and implementation of reset controllers in industrial applications is lacking. The potential issues of CR in a digital implementation were for example never studied. Additionally, it is known that noise can affect the performance of a CgLp [10], however its effects on the CR architecture are also still unknown. Furthermore, a significant drawback affects the CgLp. When used to control plants that have resonance peaks at frequencies higher than the bandwidth, it is very difficult to guarantee their stability [11]. This is particularly significant in industry, where many motion stages have the structure of a non-collocated mass-spring-damper system with high frequency resonances.

A different structure, known as the Proportional Clegg Integrator (PCI) [12] allows a larger low frequency open-loop gain compared to an equivalent LTI Proportional integrator

*Daniel Caporale is a MSc student in Mechanical Engineering at the Faculty of Mechanical, Maritime and Materials Engineering (3mE), Delft University of Technology.

(PI) system, for the same phase margin. This leads to increased disturbance suppression when paired with an LTI PID, thus potentially increasing the tracking performance of the system. Although having a simpler structure than the CgLp, the PCI has been studied in literature for such purpose only once. In [13], a PCI-PID system was compared to a PI-PID system for reference tracking, with the former one not being able to outperform its linear counterpart. However, since then new predictive performance analysis tools were developed, as well as the aforementioned CR architecture, allowing for new design possibilities.

The aim of this paper is thus to study the viability of PCI-PID controller, within the CR framework, for increasing the tracking performance of an industrial motion stage. State-of-the-art frequency domain analysis tools are used to analyze the controllers. Tuning guidelines based on loopshaping principles are proposed for a simple PCI-PID, as well as a series CR PCI-PID and a novel parallel CR PCI-PID structure. Furthermore, it is made sure that the controllers are easily implementable digitally. The findings are validated experimentally on the motion stage of an industrial wire bonder, a machine which creates interconnections between chips and their packaging.

The next section (Section II) presents the ASMPT wire bonder, used as the experimental setup. The following section (Section III) includes the necessary background theory in terms of reset control. In the subsequent section (Section IV) the PCI-PID structure will be analysed using methods presented in Section III. Relevant tuning guidelines are also proposed. In Section V the advantages and drawbacks of the series CR architecture are presented. A novel parallel CR structure, capable of overcoming the drawbacks of the series CR architecture, is presented in Section VI, along with tuning guidelines. In Section VII, the reset controller is implemented digitally on the wire bonder's stage and experimental results are shown. Finally, the relevant contributions and suggestions for future work are given in Section VIII.

II. Wire bonder model

To experimentally validate the results obtained in this work, a wire-bonding machine (Fig. 1) produced by ASM Pacific Technology (ASMPT) is utilized. A wire bonder is a complex machine with multiple functionalities, however for control purposes the interest lies solely in its motion platform. The wire bonder has in fact a three degrees of freedom (DoF) motion platform, that allows its end-effector to translate in every translational direction. The motion stage is subdivided into an X-, a Y- and a Z-stage. The former two provide the respective translations guided by linear bearings, whereas the Z-stage utilizes a pivot mechanism. The three stages suffer from cross-coupling, high frequency dynamics and a transport time delay [14]. This is illustrated in Fig. 2, which shows the identified FRF between the current required from the actuators of the X- and Y-stage respectively, and the X-stage encoder position. Due to confidentiality, the X-axis has been scaled by

Fig. 1: Picture of the wire bonder whose stage was utilized in this work (reproduced with permission from [14]).

an arbitrary constant k. The dynamics of the stages is also position-dependent, meaning the FRF plots differ based on the end-effector position. Fig. 2 shows the FRF at the center position, thus when all stages have no displacement.

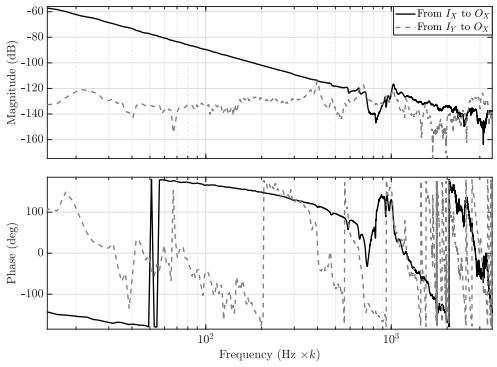

Fig. 2: Identified FRF between X-, Y- and Z-stages actuator current and X-stage encoder position at the center position.

The motion stages DoF are controlled separately approximating the X-,Y- and Z-stage as independent SISO systems. Currently a SISO LTI feedback and feedforward control systems is hence employed to regulate the motion of each of the three stages. Although feedforward control is capable of substantially reducing the transient error, it does not account for the dynamics of the base frame that connects the stage to the ground. The base frame resonance mode acts therefore as a disturbance creating undesired oscillations in the settling phase [15] that have to be suppressed by feedback control. Many controllers utilized currently by ASMPT have a structure of a

PID controller, defined in terms of a transfer function as

$$C_{PID}(s) = \underbrace{k_P}_{\text{P}} \underbrace{\left(1+\frac{\omega_I}{s}\right)}_{\text{I}} \underbrace{\left(\left(1+\frac{s}{\omega_D}\right)\Big/\left(1+\frac{s}{\omega_T}\right)\right)}_{\text{D}}, \tag{1}$$

with $k_P \in \mathbb{R}$ and ω_I, ω_D, $\omega_T \in \mathbb{R}^+$ in rad/s. PID controllers are the most widespread option for feedback control. In order to simplify the implementation of reset control it is thus beneficial to design reset controllers that can be utilized in combination with PID controllers, increasing their settling performance.

III. Preliminaries

Over the years the field of reset control has developed significantly. Not only in terms of applications [16], but nowadays there also exist many different structures of reset controllers. However, frequency domain tools for predictive performance and stability analysis that allow loopshaping techniques to be employed have been developed only for a certain class of reset controllers. This paper will only address these.

A. Definition of reset element

In this paper the definition from [17], given as

$$\mathcal{R} = \begin{cases} \dot{x}_r = A_r x_r(t) + B_r e_r(t), & \text{if} \quad (x_r(t), e_r(t)) \notin \mathcal{M} \\ x_r^+(t) = A_\rho x_r(t), & \text{if} \quad (x_r(t), e_r(t)) \in \mathcal{M} \\ u_r(t) = C_r x_r(t) + D_r e_r(t), \end{cases} \tag{2}$$

is used to describe a SISO reset system $\mathcal{R}$. The first and last lines of (2) describe a standard LTI system in state-space, where $A_r \in \mathbb{R}^{n_r \times n_r}$, $B_r \in \mathbb{R}^{n_r \times 1}$, $C_r \in \mathbb{R}^{1 \times n_r}$ and $D_r \in \mathbb{R}$ are the Base Linear System (BLS) matrices, $x_r(t) \in \mathbb{R}^{n_r \times 1}$ is the reset element's state vector, $e_r(t) \in \mathbb{R}$ is its input, $u_r(t) \in \mathbb{R}$ is its output and $t \in \mathbb{R}^+$ indicates time. For the sake of brevity, the dependency on t will be omitted henceforward. The LTI system description holds true whenever x_r is not part of the reset surface $\mathcal{M}$, defined as

$$\mathcal{M} := \{e_r = 0 \wedge (I - A_\rho) x_r \neq 0\}, \tag{3}$$

If, however, x_r is part of $\mathcal{M}$, the after-reset state at the reset time instant $x_r^+ = \lim_{y \to t+0} x_r(y)$ is determined by the reset matrix $A_\rho = \text{diag}(\gamma_1, \ldots, \gamma_{n_r})$, with $|\gamma_i| \leq 1$. If $A_\rho = I^{n_r \times n_r}$, resets do not affect the system, which thus behaves like its BLS, defined as

$$R = C_r(sI - A_r)^{-1} B_r + D_r, \tag{4}$$

with $s \in \mathbb{C}$ being the Laplace variable.

B. Control system architecture

In [7] the closed-loop reset system architecture depicted in Fig. 3 was presented. C_1, C_2 are single-input single-output (SISO) LTI filters, G is the plant, $r \in \mathbb{R}$ is the reference, $u \in \mathbb{R}$ is defined as the controller output, $d \in \mathbb{R}$ is the disturbance, $n \in \mathbb{R}$ is the sensor noise, $y \in \mathbb{R}$ is the true output, $y^* = y + n$ is the measured output, $e = r - y^*$ is the error and $v = u + d$ is the plant input.

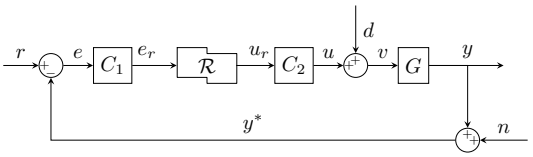

Fig. 3: Expanded reset control feedback system architecture. Adapted from [7].

The LTI part of the closed-loop system $\overline{\mathcal{L}}$ can be described by [7]

$$\overline{\mathcal{L}} = \begin{cases} \dot{\zeta} = A\zeta + B_{e_r} e_r + Bw \\ y = C\zeta, \\ e_r = C_{e_r}\zeta + D_{e_r} r, \end{cases} \tag{5}$$

where $\zeta \in \mathbb{R}^{n_p}$ is the vector of the states of all linear filters and the plant and $w = [r, d, n]^T$. The overall closed-loop system can then be described by [7]

$$\overline{\mathcal{R}} = \begin{cases} \dot{x} = \overline{A}x + \overline{B}w, & \text{if} \quad (x_r, e_r) \notin \mathcal{M} \\ x^+ = \overline{A}_\rho x, & \text{if} \quad (x_r, e_r) \in \mathcal{M} \\ y = \overline{C}x, \end{cases} \tag{6}$$

where

$$x = \begin{bmatrix} x_r \\ \zeta \end{bmatrix}, \quad \overline{A} = \begin{bmatrix} A_r & B_r C_{e_r} \\ B_{e_r} C_r & A + B_{e_r} D_r C_{e_r} \end{bmatrix},$$
$$\overline{B} = \begin{bmatrix} 0^{n_r \times 2} \\ B \end{bmatrix} + \begin{bmatrix} B_r D_{e_r} & 0^{n_r \times 1} \\ B_{e_r} D_r D_{e_r} & 0^{n_p \times 1} \end{bmatrix}, \quad \overline{C} = \begin{bmatrix} 0^{1 \times n_r} & C \end{bmatrix},$$
$$\overline{A}_\rho = \begin{bmatrix} A_\rho & 0^{n_r \times n_p} \\ 0^{n_p \times n_r} & I^{n_p \times n_p} \end{bmatrix}.$$

C. PCI

Different structures of $\mathcal{R}$ fit the definition in (2), however this paper focuses on the PCI, with state-space matrices given by

$$A_r = 0,\ B_r = \omega_r,\ C_r = 1,\ D_r = 1,\ A_\rho = \gamma, \tag{7}$$

where $\omega_r \in \mathbb{R}^+$ in rad/s represents the element's BLS corner frequency.

D. Stability

A sufficient condition for Uniform Bounded-Input Bounded-State (UBIBS) stability of a closed-loop reset system with a stable BLS was introduced in [17] and expanded in [18] as the H_β-condition (Theorem III.1).

Theorem III.1. *[17], [18] A closed-loop reset system* (6) *with a stable BLS is UBIBS stable if there exists a* $\varrho = \varrho^T > 0$, $\varrho \in \mathbb{R}^{n_r \times n_r}$, *and a* $\beta \in \mathbb{R}^{n_r \times 1}$ *such that*

$$H_\beta(s) = C_0(sI - \overline{A})^{-1} B_0,$$

with

$$B_0 = \begin{bmatrix} I_{n_r \times n_r} \end{bmatrix}, \quad C_0 = \begin{bmatrix} \varrho & \beta C \end{bmatrix},$$

is strictly positive real (SPR), with $(\overline{A}, B_0)$ *controllable,* $(\overline{A}, C_0)$ *observable and*

$$A_\rho^T \varrho A_\rho - \varrho \leq 0.$$

Proving whether Theorem III.1 holds necessitates solving complex Linear Matrix Inequalities (LMIs) using a parametric plant description. This would require approximating the parameters of the motion stage, which is time consuming and leads to model inaccuracies. Moreover, it is difficult to relate the result from the LMIs to the parameters of the reset element itself. Finally, it is complex to deduce information on the robustness of the system from the solution of the LMIs. In order to at least partially overcome these limitations, an equivalent frequency domain condition, based on the so-called Nyquist Stability Vector (NSV), can be utilized to prove that the H_β-condition holds instead [7] if $\mathcal{R}$ is a PCI (Theorem III.2).

Theorem III.2. *[7] Given $\mathcal{R}$ as in* (2) *is a PCI, the BLS is stable, no pole-zero cancellations occur and the open-loop system has at least one pole at the origin, the H_β-condition is satisfied if and only if*

$$\left(-\frac{\pi}{2} < \theta_1 < \pi\right) \wedge \left(-\frac{\pi}{2} < \theta_2 < \pi\right) \wedge (\theta_2 - \theta_1 < \pi),$$

where

$$\theta_1 = \min_{\omega \in \mathbb{R}^+} \angle \overrightarrow{\mathcal{N}}(\omega), \quad \theta_2 = \max_{\omega \in \mathbb{R}^+} \angle \overrightarrow{\mathcal{N}}(\omega),$$

with frequency $\omega \in \mathbb{R}$ and NSV

$$\overrightarrow{\mathcal{N}}(\omega) = \begin{bmatrix} \mathrm{Re}(L_{BLS}(s)(1 + L_{BLS}(s)^*)) \\ \mathrm{Re}((1 + L_{BLS}(s)^*)R(s)) \end{bmatrix},$$

where $\omega \in \mathbb{R}$ represents a frequency.

$$L_{BLS}(s) = C_1(s)R(s)C_2(s)G(s)$$

and $L_{BLS}(s)^*$ is the complex conjugate of $L_{BLS}(s)$.

Theorem III.2 thus requires the NSV phase to be within certain bounds over all frequencies. Although never studied in literature, one could argue that the distance between the resulting phase of $\overrightarrow{\mathcal{N}}(\omega)$ and the bounds can give a qualitative idea on the robustness of the system. Moreover, one can easily assess stability given the variation of some parameters. An analog to the phase and gain margin can for example be assessed by evaluating stability after increasing/decreasing the open-loop phase and gain respectively. Furthermore, the shape of the NSV can be plotted against frequency. This allows to determine at which frequency the bound is crossed and can give an indication on how the control system can be tuned in order for the H_β-condition to be satisfied. Finally, the NSV can be computed using the measured Frequency Response Functions (FRFs) data of the plant, thus not requiring a parametric plant description or solving LMIs. This avoids incurring in model inaccuracies and simultaneously allows to speed up the analysis process, making it an essential tool for industrial implementation.

E. Predictive performance

The steady-state input-output relationship of LTI systems in the frequency domain allows to analytically compute FRFs, necessary for the use of loopshaping techniques in the controller design process. A quasi-linear approximation of a nonlinear system, equivalent to the Bode plot of an LTI system, can be determined by the Sinusoidal Input Describing Function (SIDF) method [19]. A SIDF is defined as the quotient between the Fourier transform of the first harmonic of the output and the Fourier transform of the input, where the input is a sinusoidal of a certain frequency [20]. Being nonlinear, reset control systems suffer from the effect of harmonic generation. This denotes that the output signal, given an input sinusoid of a certain frequency, consists of not only the excitation frequency but also higher order harmonics at multiples of the excitation frequency [21]. The Higher Order Sinusoidal Input Describing Functions (HOSIDFs) introduced in [22], provide information on the generation of the higher order harmonics. Theorem III.3 can be utilized to analytically obtain the HOSIDFs for a reset element.

Theorem III.3. *[23] For a reset element $\mathcal{R}$ as in* (2)*, with input e_r a sinusoidal signal of frequency ω, the equation for the SIDF (H_1) and n^{th} HOSIDF (H_n, $n \in \mathbb{R}$, $n > 1$) then is*

$$H_n(j\omega) = \begin{cases} C_r(j\omega I - A_r)^{-1}(I + j\Theta_D(\omega))B_r + D_r \\ \qquad \text{for} \qquad n = 1 \\ C_r(j\omega n I - A_r)^{-1} j\Theta_D(\omega) B_r + D_r \\ \qquad \text{for odd} \quad n \geq 2 \\ 0 \quad \text{for even} \quad n \geq 2 \end{cases} \tag{8}$$

with $j = \sqrt{-1}$ and

$$\begin{aligned} \Theta_D(\omega) &= \frac{-2\omega^2}{\pi} \Delta(\omega)[\Gamma_\rho(\omega) - \Lambda^{-1}(\omega)], \\ \Lambda(\omega) &= \omega^2 I + A_r^2, \\ \Delta(\omega) &= I + e^{\frac{\pi}{\omega} A_r}, \\ \Delta_\rho(\omega) &= I + A_\rho e^{\frac{\pi}{\omega} A_r}, \\ \Gamma_\rho(\omega) &= \Delta_\rho^{-1}(\omega) A_\rho \Delta(\omega) \Lambda^{-1}(\omega), \end{aligned}$$

It should be noted that usually the magnitude of the FRF of the n^{th} HOSIDF of a reset element follows the same shape of its SIDF, with a lower gain and shifted to the left with a factor ω/n. This is depicted in Fig. 4, where an arbitrary mass-spring-damper (MSD) system with resonance 10 Hz is positioned in series with a CI, a PCI with $\omega_r = \infty$. For this reason it is usually only necessary to analyse the first non-zero HOSIDF (i.e. the third harmonic) in order to comprehend the behaviour of all HOSIDFs.

Generally, the goal when loopshaping with HOSIDFs is to keep the magnitude of all higher order harmonics low, such that they do not have major impact in the response, and thus performance can be accurately predicted from the SIDF, making the controller design procedure similar to LTI controllers. The phase of the higher order harmonics does also contribute to the resulting response. However, if the magnitude of the HOSIDFs is low, the effect of the phase is negligible. Therefore, the phase is not utilized in any of the analysis methods employed in this work and can therefore be neglected in the analysis process. Theorem III.3 allows to compute HOSIDFs only for continuous time reset controllers. When digitally implementing the reset controller, the BLS

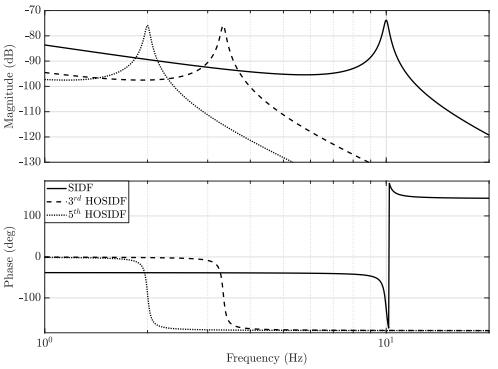

Fig. 4: FRF of the SIDF, 3^{rd} HOSIDF and 5^{th} HOSIDF of a CI in series with an arbitrary MSD system.

will have to be discretized. It will therefore be assumed that in the frequency range of interest the sampling period is small enough to assure the difference in the HOSIDFs is negligible. When computing the open-loop HOSIDFs using FRF data for the plant, information on the n^{th} HOSIDF can be provided only up to frequencies $\omega < \omega_{max}/n$, with ω_{max} being the highest frequency for which FRF data is available. The HOSIDFs can be easily augmented in case LTI systems are present in series before or after the reset controller, as depicted in Fig. 3. The resulting steady-state output signal given an input sinusoid $e_r = A_0 \sin(\omega t)$ can be computed as an infinite sum of sinusoids

$$\begin{aligned} u \quad &= \sum_{n=1}^{\infty} A_0 |C_1(j\omega)||H_n(j\omega)||C_2(nj\omega)| \sin(n\omega t \\ &\quad + \angle C_1(j\omega) + \angle H_n(j\omega) + \angle C_2(nj\omega)). \end{aligned} \tag{9}$$

The effectiveness of loopshaping in case of LTI systems comes from the fact that it is possible to easily relate the open-loop and the closed-loop through the sensitivity equations. In [24] it was however shown that even when low, HOSIDFs are usually not negligible in closed-loop and simply utilizing the SIDF provides a highly inaccurate approximation of the closed-loop FRF. In [25] the so-called pseudosensitivity $S_\infty(\omega)$ was proposed, with magnitude defined as

$$|S_\infty(\omega)| = \max_{0<t<2\pi/\omega} (e_{ss}(\omega, t))/A_r, \tag{10}$$

where $e_{ss}(\omega, t)$ is the steady-state error of closed-loop reset system excited by a reference input $A_r \sin(\omega t)$, with $A_r \in \mathbb{R}^+$. It allows to combine the information on closed-loop higher order harmonics into an analogue of a sensitivity function for reset systems, thus helpful for loopshaping. Although the principle of superposition does not hold, it was established that even for non-sinusoidal inputs, the pseudosensitivity functions can provide a reliable quantitative performance prediction to effectively design reset controllers [26]. Obtaining $S_\infty(\omega)$ through simulation is computationally expensive, as it requires a simulation for each frequency, and also difficult to relate open-loop and closed-loop characteristics, due to the black-box nature of the method. Furthermore, a parametric description of the plant is necessary to compute the simulations. Therefore, a less accurate analytical methods, able to relate open- and closed-loop HOSIDFs, given some assumptions, was established in [24] and is given in Theorem III.4.

Theorem III.4. *[24] Given a closed-loop reset system with input $r = \sin(\omega t)$, the steady-state error can be approximated by*

$$e_{ss}(t) = \sum_{n=1}^{\infty} |S_n(j\omega)| \sin(n\omega t + \angle S_n(j\omega)), \tag{11}$$

with

$$S_n(j\omega) = \begin{cases} S_1(j\omega) & \text{for} \quad n = 1 \\ -\dfrac{L_n(j\omega)}{1 + L_{BLS}(j\omega)} \left(|S_1(j\omega)|\, e^{jn\angle S_1(j\omega)} \right) & \\ \qquad\qquad \text{for odd} \;\; n \geq 2 & \\ 0 \qquad\qquad \text{for even} \; n \geq 2 & \end{cases} \tag{12}$$

and

$$\begin{aligned} S_1(j\omega) &= \frac{1}{1 + L_1(j\omega)}, \\ L_n(j\omega) &= C_1(j\omega) H_n(j\omega) C_2(jn\omega) G(jn\omega), \end{aligned}$$

as long as the following assumptions hold true:

1) *The system is input-to-state convergent*
2) *The resets are a result of only the first harmonic of e_r.*

The first assumption, on input-to-state convergence, can be expected to hold when the reset system satisfies the H_β-condition [25]. The second assumption, specifying that only the first harmonic of e_r results in resets and hence the creation of higher-order harmonics in the output, is does not always hold. In fact, higher order harmonics in the error have an effect on the reset instants, although usually not as strong as the first harmonic. Moreover, (11) shows that the greater the number of HOSIDFs that are accounted for in the sum, the more accurate the result. However, as for the the open-loop method, when using FRF data for the plant, information on the n^{th} HOSIDF can be provided only up to frequencies $\omega < \omega_{max}/n$. This makes the accuracy of the method frequency dependent: the higher the frequency, the less HOSIDFs are taken into account, therefore the more inaccurate the result. Nevertheless, this still leads to a more accurate solution than just using the SIDF to compute the closed-loop HOSIDFs. In fact, the method was deemed accurate enough for controller design synthesis of a precision positioning stage [24]. Furthermore, as aforementioned, the goal will be to tune the reset control system with low HOSIDFs compared to the first harmonic. These will be more likely to reset as a result of the first harmonic, thus making the approximate closed-loop HOSIDFs more accurate.

A certain degree of robustness is expected from the employed feedback controllers. For this reason a constraint on the peak of the sensitivity transfer function < 6 dB is placed by ASMPT to any LTI controller in order for it to be implemented. Although not equivalent in terms of robustness, it was deemed necessary to set the same constraint on

the peak of the pseudosensitivity (10) for a reset control system to prevent large amplification of the reference. A pseudosensitivity can be viewed as a 'worst-case-scenario' closed-loop sensitivity in terms of performance, as only information on the maximum amplitude is regarded. This conservative approach makes sure that the reset controller does not amplify excessively signals of certain frequencies in closed-loop.

In case of an LTI closed loop system, it is possible to qualitatively relate transient response performance parameters such as overshoot, rise time and settling time to frequency domain parameters [27]. To the best of the author's knowledge, proof of such a relationship for a reset control system has not been studied. Nevertheless, due to the fact that reset systems behave linearly during most of the response, a similar relationship can be expected. Evidence of this was found empirically in [9], where an increase in phase margin resulted in a smaller overshoot and faster settling time, equal or improved compared to an equivalent LTI system.

IV. PCI-PID

A PCI (7) is a resetting integrator with corner frequency ω_r. The nonlinearity affects therefore mostly the low frequencies in the range $\omega < \omega_r$, where the resetting leads to a smaller phase lag compared to a linear integrator and a constant positive offset in magnitude. Nevertheless, contrary to a PI, a PCI cannot be utilized to suppress steady-state errors. This is due to the fact that resetting causes the stored energy from the integral action, required to avoid a steady-state error, to be eliminated, introducing a limit-cycle behaviour [28]. For this reason it is not beneficial to replace the 'PI-part' of the linear PID controller (1) with a PCI. On the contrary, the use of a PCI in addition to an LTI PID could improve performance.

It is usual for industrial motion stages to be controlled with cutting-edge feedforward controllers which are capable of tracking a predetermined reference. Feedback control is then needed mostly to increase tracking precision by suppressing disturbances, as is the case for the ASMPT wire bonder. For improved tracking precision, it is necessary to increase the open-loop gain at low frequencies. Due to Bode's gain-phase relationship, this affects the phase margin of the system and thus its stability and robustness. With reset control this limitation can be overcome, allowing a larger low frequency open-loop gain compared to an LTI system, for the same phase margin. It should be however noted that although in reduced extent compared to a PI, a PCI also introduces phase lag. Therefore, a system controlled by a PCI-PID controller has an increased magnitude peak of pseudosensitivity compared to the peak of sensitivity of the same system controlled solely by the PID controller. This must be accounted for, by assuring the LTI controller has a high phase margin. A PCI-PID is then constructed by selecting $C_1 = 1$, $\mathcal{R}$ as a PCI and C_2 as a high phase margin LTI PID controller.

Overall, although a PCI element is less versatile compared to a CgLp, it could still prove to be beneficial in industry. Since PCI-PID systems have smaller HOSIDFs at high frequencies compared to CgLp-PID systems, the effect of high frequency resonances on the NSV is usually irrelevant. The satisfaction of the H_β-condition for PCI-PID systems is therefore mostly straightforward for plants such as the X-stage of the ASMPT wire bonder. In fact, the only parameter affecting the NSV is ω_r, which can simply be decreased to lower the HOSIDFs. Finally, PCI-PID systems are less prone to result in inaccurate approximate closed-loop HOSIDF computed through Theorem III.4 compared to CgLp-PID systems. The method decreases in accuracy with higher HOSIDFs magnitude and higher frequency. As CgLp-PID systems have high HOSIDFs at high frequencies, this can lead to greater imprecision compared to the PCI-PID systems.

As it only has two parameters, ω_r and γ, tuning a PCI-PID is relatively straightforward. By increasing ω_r, the magnitude and phase behaviour of the SIDF and HOSIDFs can be shifted to the right. This will lead to a higher gain at frequencies lower than the bandwidth, but also higher HOSIDFs and a lower phase margin. A similar effect is given by γ. Decreasing the parameter leads to a smaller phase lag and greater gain at the cost of increased HOSIDFs. As depicted in Fig. 5, it is thus possible to achieve the same phase lag for different combinations of γ and ω_r. In order to find the combination that achieves the greatest increase in magnitude of the SIDF in a certain frequency region [ω_a, ω_b], the following optimization problem is proposed

$$\mathbb{P}: \begin{cases} \max\limits_{\omega_r,\,\gamma} & \int_{\omega_a}^{\omega_b} |H_1(\omega)|\, d\omega \\ \text{subj. to} & \angle H_1(\omega_{BW}) \geq \varphi_d, \\ & \min\limits_{\omega_a<\omega<\omega_b} (|H_1(\omega)| - |H_3(\omega)|) \geq h_d, \end{cases} \tag{13}$$

where $\omega_{BW} \in \mathbb{R}^+$ is the open-loop cross-over frequency, $\theta_d \in \mathbb{R}^-$ is the phase lag of the PCI at ω_{BW} and $h_d \in \mathbb{R}^+$ is the desired minimal difference between the SIDF and the third HOSIDF in the region [ω_a, ω_b]. The optimization problem is subject to two constraints. The first constraint assures that the proposed combination does not decrease the phase margin more than the acceptable value φ_d. The second constraint guarantees that the HOSIDFs are lowered by a factor of h_d. In order to effectively utilize (13) to design a PCI-PID, the following tuning procedure is suggested:

Tuning Procedure (PCI-PID)**.**

1) *Tune an LTI controller such that the open-loop system has the desired cross-over frequency ω_{BW} and phase margin $PM > 30°$.*
2) *Choose the region [ω_a, ω_b] in which it is desired to increase the open-loop gain compared to the LTI system.*
3) *As an initial guess, choose $\varphi_d = -(PM - 30°)$, to constrain the SIDF to have a phase margin of $30°$ and $h_d = 20$ dB to constrain the third HOSIDF to have a maximal magnitude of less than 10% of the SIDF in the region [ω_a, ω_b].*

4) *Solve the optimization problem* (13).
5) *Plot the magnitude of the pseudosensitivity of the closed-loop system.*
6) *In case the pseudosensitivity in the region [ω_a, ω_b] does not show the desired level of suppression (i.e. the gain is higher than desired), increase h_d, to lower the HOSIDFs. Return to step 4.*
7) *In case the peak of the pseudosensitivity magnitude can be increased further (i.e. it is lower than the acceptable level, e.g. 6 dB), decrease φ_d. Return to step 4.*

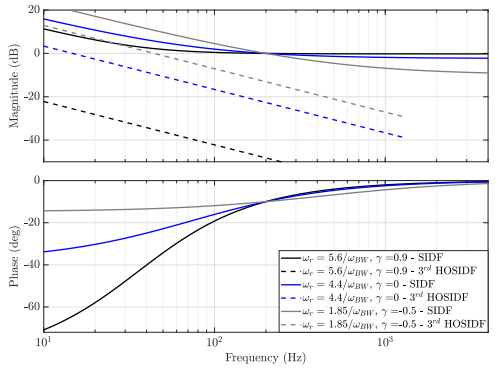

Fig. 5: FRF of the SIDF and 3^{rd} HOSIDF of three PCI elements with different combinations of ω_r and γ resulting in a phase lag of 10° at 200 Hz. The gain was adjusted to keep the crossover frequency as 200 Hz.

V. Series CR PCI-PID

It is clear how the HOSIDFs pose a constraint on the tuning of a PCI element. It would therefore be beneficial to to lower the HOSIDFs without affecting the SIDF. It was shown in [10], that switching C_1 and C_2 results in the same SIDF but in different HOSIDFs. This can be explained from (9). The magnitude of the n^{th} HOSIDF is determined by $|C_1(j\omega)|$ and $|C_2(jn\omega)|$. Therefore, in case a lead-lag element such as a PID controller is used in combination with a reset controller, placing the lead part of the controller in C_1 and the lag part in C_2 would minimize the HOSIDFs.

Based on the same principle, the series continuous reset (CR) architecture was developed [9]. A n_l^{th} order lead filter F_l can be defined as

$$F_l = \left(\frac{\frac{s}{\omega_d}+1}{\frac{s}{\omega_t}+1}\right)^{n_l}, \quad \omega_d < \omega_t, \tag{14}$$

with ω_d, $\omega_t \in \mathbb{R}^+$ in rad/s and $n_l \in \mathbb{Z}^+$. By keeping the PID in C_2, but also adding F_l and F_l^{-1} to C_1 and C_2 respectively, it is possible to tune the region in which HOSIDFs are lowered, and by how much they are lowered, without affecting the SIDF or the NSV. This allows for greater design freedom compared to changing the sequence without any drawback and is thus preferred. To determine the range in which HOSIDFs have the most significant effect, and which HOSIDF has the greatest effect, the power spectral density of the error signal when utilizing a PCI-PID without CR can be analyzed. In case feedforward control is employed, most of the power should be caused by either external disturbances or resonances not modelled in the feedforward. If these disturbances/resonances are present at frequencies ω_{dis}, the n^{th} HOSIDF will excite these, causing undesired higher order harmonics of frequencies $n\omega_{dis}$. It can be evaluated from (8), that by choosing $\omega_d = \omega_{dis}$ and $\omega_t = n\omega_{dis}$, $|F_l(j\omega)||F_l^{-1}(jn\omega)|$ has a minimum at ω_{dis}, whose value $H_\varsigma(\omega_{dis}) = |F_l(j\omega_{dis})||F_l^{-1}(jn\omega_{dis})|$ represents the suppression of the n^{th} HOSIDF. The lead filter order n_l can then be increased, increasing the suppression by a factor $n_l H_\varsigma(\omega_{dis})$.

Next, the effect of CR will be visualized through an example. A PCI-PID was tuned for a plant resembling a highly damped non-collocated 2-DoF MSD system

$$G_1 = \frac{ds+k}{m_1m_2s^4 + d(m_1+m_2)s^3 + k(m_1+m_2)s^2}, \tag{15}$$

with parameters given in Table I, using the aforementioned tuning procedure. The transfer function parameters of the respective LTI PID controller PID_1 and of the PCI are given in Table I. The open-loop block diagram is pictured in Fig. 6. PID_1 was tuned such that it has $\approx 40°$ phase margin at $\omega_{BW} = 200$ Hz, allowing the PCI to have 10° phase lag at 200 Hz. Two different F_l & F_l^{-1} pairs were tuned allowing to utilize two CR architectures, CR_1 and CR_2 respectively, with parameters also given in Table I. The two F_l & F_l^{-1} pairs have the same ω_d and ω_t, but while $n_l = 1$ for CR_1, $n_l = 2$ for CR_2. The two F_l & F_l^{-1} pairs were tuned assuming a disturbance $d = \sin(\omega_{dis}t)$, where $\omega_{dis} = 50$ Hz, is acting on the system, thus assuring $H_\varsigma(\omega_{dis}) \ll 0$. In fact for CR_1, $H_\varsigma(\omega_{dis}) = -6.02$ dB and for CR_2, $H_\varsigma(\omega_{dis}) = -12.04$ dB. The resultant open-loop FRF are plotted in Fig. 7. It can be appreciated how in the range [ω_d, ω_t] the HOSIDFs are lowered with increasing $H_\varsigma(\omega_{dis})$, whereas the SIDF remains unchanged.

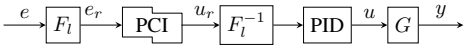

Fig. 6: Series CR PCI-PID block diagram.

TABLE I: Transfer functions of PCI, PID_1 and of F_l used for CR_1 and CR_2.

G_1	m_1	m_2	k	d
	100	100	1.97×10^9	$d = 4.6 \times 10^4$
PID_1	k_P	ω_I	ω_D	ω_T
	8.204×10^7	20 Hz	76.92 Hz	520 Hz
PCI	ω_r	γ		
	60 Hz	0		
CR_1	ω_d	ω_t	n_l	
	50 Hz	50×3 Hz	1	
CR_2	ω_d	ω_t	n_l	
	50 Hz	50×3 Hz	2	

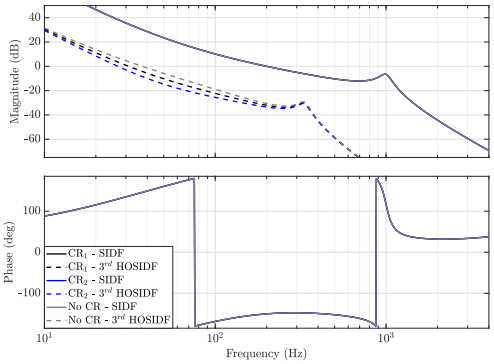

Fig. 7: FRF of the SIDF and 3^{rd} HOSIDF of the open-loop system with G_1 as the plant, PID_1 as the LTI controller, PCI as $\mathcal{R}$ and without CR architecture, with CR_1 or CR_2 respectively.

A Simulink [29] simulation was then performed with inputs $r = 0$, $n = 0$, $d = \sin(\omega_{dis}t)$, where $\omega_{dis} = 50$ Hz. The resulting closed-loop error is given in Fig. 8. The cumulative power spectral density (CPSD) of the PCI-PID system without CR shows that the power spectra has peaks at 150 Hz and 250 Hz, 3 and 5 times the disturbance frequency respectively. These higher order harmonics are resultants of the excitation of the 50 Hz disturbance frequency by the third and fifth HOSIDF respectively. The increase in performance resulting from the lower HOSIDFs at ω_{dis} introduced by the series CR architecture, is clearly to be seen. While the peak at 50 Hz in the CPSD remains almost identical, evidence that the SIDF does not change, the peaks at 150 Hz and 250 Hz decrease with increasing $H_\varsigma(\omega_{dis})$.

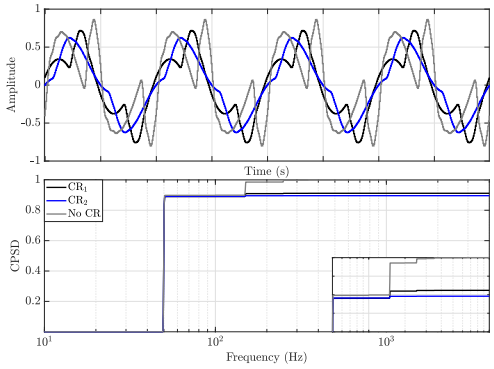

Fig. 8: Normalized closed loop error signal resulting from a Simulink simulation of a system with G_1 as the plant, PID_1 as the LTI controller, PCI as $\mathcal{R}$ and without CR architecture, with CR_1 or with CR_2 respectively. The inputs to the system are $r = 0$, $n = 0$, $d = \sin(\omega_{dis}t)$, where $\omega_{dis} = 50$ Hz.

Nevertheless, the CR architecture does not only affect the HOSIDFs, but also transient performance. In [9] it was demonstrated that having C_1 as a first order lead filter results in the reset instants being affected not only by e_r, but also by $\dot{e}_r$. A change in reset instants can affect the transient behaviour, potentially allowing to lower the overshoot of a CgLp-PID system [9]. However, due to the presence of feedforward control, affecting the transient behaviour is of less interest and beyond the scope of this work.

A. *Effect of noise*

The change in reset instants will affect transient behaviour, but also steady-state performance in case noise is present in the system. To compute the open-loop SIDF and HOSIDFs it is assumed that the input is a sinusoid, which allows to predetermine the reset instants t_k. When noise is present in the system, the reset instants could differ. The greater the power of the noise, the higher the chance for one of these undesired resets. A lead element such as F_l increases the magnitude of the output signal in a certain frequency range. The power of the noise present in the error signal e_r at ω is therefore increased with increasing $H_\varsigma(\omega_{dis})$ hence causing the SIDF and HOSIDFs to be more unreliable. This is visualized in Fig. 9, where the simulation shown in Fig. 8 is repeated with n being white noise. It can be seen that an increase in $H_\varsigma(\omega_{dis})$ still results in lower excitation of higher order harmonics, however in this case the three signals have a different suppression of the disturbance frequency itself, confirming that the SIDF is less reliable in the presence of noise.

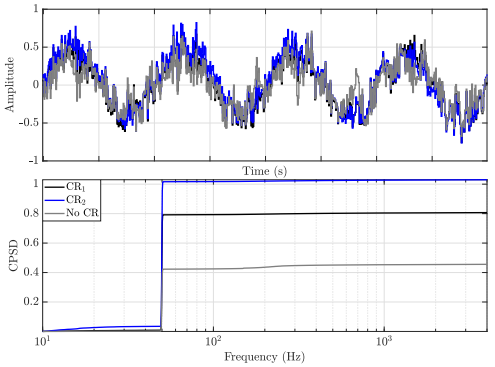

Fig. 9: Normalized closed loop error signal resulting from a Simulink simulation of a system with G_1 as the plant, PID_1 as the LTI controller, PCI as $\mathcal{R}$ and without CR architecture, with CR_1 or CR_2 respectively. The inputs to the system are $r = 0$, n is white noise with power 1×10^{-5} V^2/Hz, $d = \sin(\omega_{dis}t)$, where $\omega_{dis} = 50$ Hz.

B. *Effect of aliasing*

Even without considering noise, the CR architecture has an additional limitation when considering its discrete implementation. As derived from (8), when inputting a signal of a certain frequency into a reset element, the output signal will not only contain that frequency but also odd integer multiples. A sampled system requires signals to have

≈ 0 power content for frequencies higher than the Nyquist frequency (ω_N) to avoid aliasing, which introduces fictitious low frequency content. This is usually not a problem in reset control as the higher the order of the HOSIDFs, the lower its amplitude. Moreover, usually open-loop FRFs are designed to have a steep negative slope at high frequencies or anti-aliasing low-pass filters to suppress noise. Nevertheless, when in closed-loop, if the fictitious frequency content is not within the range $\omega \ll \omega_d$, F_l will cause its amplification, thus changing the reset instants. This is especially relevant when the input frequency is high enough such that already low HOSDIFs generate power content at frequencies greater than ω_N.

The magnitude plots of the pseudosensitivities given in Fig. 10, computed after discretising all LTI parts of the system at 10 kHz, show a contrasting behaviour between low and high frequencies. At low frequencies an increase in $H_{\varsigma}(\omega_{dis})$ corresponds to a lower magnitude, thus an increase in disturbance suppression, caused by the suppression of the HOSIDFs. Contrarily, at high frequencies, the amplification of the fictitious frequency content caused by aliasing leads to undesired peaks in the magnitude of the pseudosensitivity.

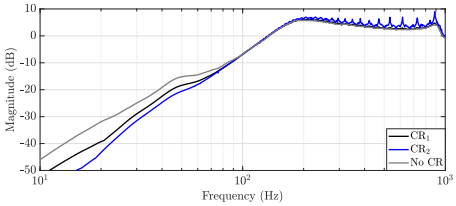

Fig. 10: Pseudosensitivities magnitudes computed through the approximate method (Theorem III.4) of the closed-loop system with G_1 as the plant, PID_1 as the LTI controller, PCI as $\mathcal{R}$ and without CR architecture, with CR_1 or CR_2 respectively, discretized at 10 kHz.

Greater insight is given by plotting the closed-loop error signal of the discrete time system resulting from a sinusoid with the same frequency as one of the spikes in the pseudosensitivity magnitude plot for a PCI-PID without CR. Arbitrarily a sinusoid of 290 Hz was chosen. The error signal was computed analytically using the approximate method (Theorem III.4), which gives the possibility to sample the error signal at any frequency, independently on the sampling frequency of the system itself. As portrayed in Fig. 11, the signal sampled at 10 kHz, the same frequency as the system, shows power content in frequencies lower than the excitation frequency. As given by (8), this is not expected, meaning this power content is fictitious, resulting from aliasing. In fact, the same closed-loop error sampled at a ten times higher sampling rate does not show any power in frequencies lower than the excitation frequency, neglecting numerical artefacts from computation. Instead, spikes at odd multiples of the excitation frequency, representing the HOSIDFs can be seen, as expected.

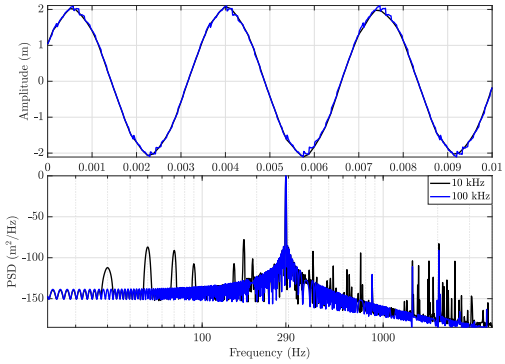

Fig. 11: Steady state time plot (only two periods shown) and power spectral density of the error signal of the closed-loop system with G_1 as the plant, PID_1 as the LTI controller, PCI as $\mathcal{R}$ and without CR architecture, discretized at 10 kHz. The inputs to the system are $r = 0$, $n = 0$, $d = \sin(290 \times 2\pi t)$. The error signal was sampled at two different sampling frequencies.

VI. Parallel CR PCI-PID

It was shown that with the CR architecture HOSIDFs can be successfully reduced in a frequency range, without affecting the SIDF. Nevertheless, the architecture suffers from limitations, caused by the effect of amplifying the error signal through F_l. To avoid this, a novel parallel CR architecture, is proposed. The block diagram of the structure is depicted in Fig. 12, with $\mathcal{R}$ a PCI and with F_l^{-1} placed in C_2. This allows to still utilize the lag element F_l^{-1} to lower HOSIDFs, while also avoiding to affect reset instants by removing C_1. For a fully LTI system (i.e. $\mathcal{R} = R$), it is possible to find that by choosing $C_{par} = R(F_l - 1)$ the system is equivalent to the series CR architecture. However, when resetting is introduced, it would be necessary to instead use $C_{par} = \mathcal{R}(F_l - 1)$. This would require having two separate reset controllers (one in $\mathcal{R}$ and one in C_{par} in Fig. 12). However, the theory presented in Section III does not allow for two separate reset controllers in the same loop. Therefore, in case $\mathcal{R}$ is a PCI, an approximation with

$$C_{par} = \text{PI}_{par}(F_l - 1), \quad \text{PI}_{par} = 1 + \frac{s}{\omega_{i_{par}}}, \tag{16}$$

with $\omega_{i_{par}} = \omega_r$ can be utilized instead.

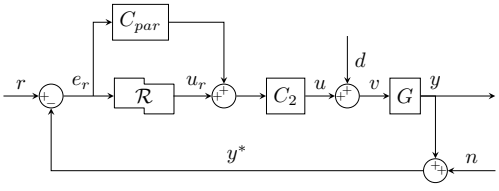

Fig. 12: Modified expanded reset control feedback system architecture that allows C_{par} to be in parallel of $\mathcal{R}$ instead of C_1 preceding it in series.

When $\mathcal{R} \neq R$, the open-loop SIDF is not identical contrarily

to the standard CR architecture. This is confirmed in Fig. 13, where the PCI in the series CR_2 is compared to a parallel CR architecture with the same parameters. It is shown that at low and high frequencies the SIDF behaviour of the parallel architecture asymptotically reaches the series architecture. However, in the mid-frequency range the parallel architecture has a smaller gain and lower phase. Furthermore, the HOSIDFs are also different between the two structures, with the parallel architecture having significantly lower HOSIDFs in the frequency range $\omega > \omega_d$. The reason is given by the fact that in a series CR architecture the HOSIDFs gain is dependent on $|C_1|$, whereas in a parallel CR architecture it is not dependent on $|C_{par}|$, as it contributes only to the first harmonic. In fact, for a parallel CR system such as the one shown in Fig. 12, (9) becomes

$$\begin{aligned} u = \; & |C_{par}(j\omega)|\sin(\omega t + \angle C_{par}(j\omega)) + \\ & \sum_{n=1}^{\infty} |H_n(j\omega)||C_2(jn\omega)|\sin(n\omega t \\ & + \angle H_n(j\omega) + \angle C_2(jn\omega)). \end{aligned} \tag{17}$$

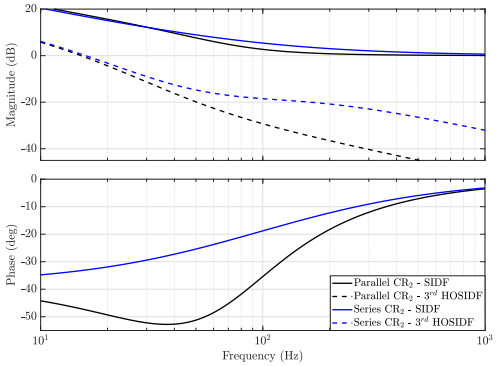

Fig. 13: FRF of the SIDF and 3^{rd} HOSIDF of the PCI in the series CR_2 architecture and a parallel CR_2 architecture with $PI_{par} = R$.

Instead of simply utilizing $\omega_{i_{par}} = \omega_r$, $\omega_{i_{par}}$ can be tuned. As shown in Fig. 14, the lower $\omega_{i_{par}}$, the greater the phase advantage gained by the system at ω_{BW}. The trade-off is given by a slightly lower gain in the mid-frequency range. On the other hand, the HOSIDFs are independent from C_{par} and hence from $\omega_{i_{par}}$. It is therefore possible to lower $\omega_{i_{par}}$ in order to increase the phase advantage while only marginally lowering the gain in the mid-frequency region.

Since the HOSIDFs in the parallel CR architecture are significantly lower than the series CR architecture in the range $\omega > \omega_d$, it allows for γ to be lowered while still maintaining lower HOSIDFs in the range of interest compared to a PCI-PID without CR. The effect of γ on the parallel CR architecture is portrayed in Fig. 15. The HOSIDFs increase over the entire frequency range, while the SIDF increases in the low- and mid-frequency range. The proposed tuning procedure for a parallel CR PCI-PID is thus as follows:

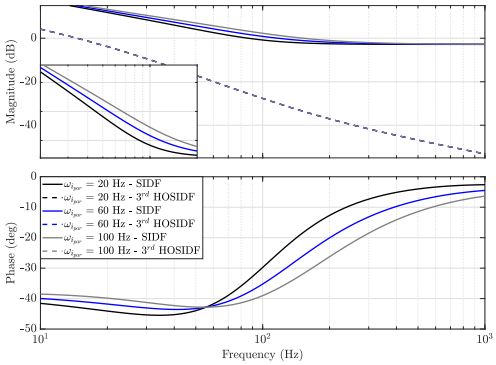

Fig. 14: FRF of the SIDF and 3^{rd} HOSIDF of the PCI in the parallel CR_2 architecture for different values of $\omega_{i_{par}}$.

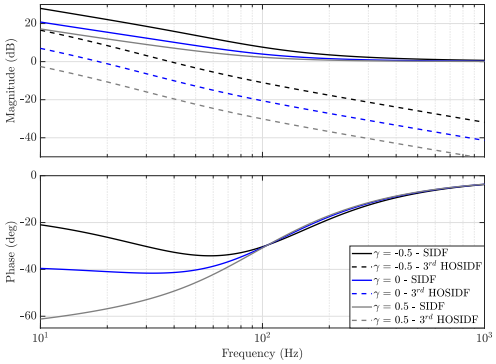

Fig. 15: FRF of the SIDF and 3^{rd} HOSIDF of the PCI in the parallel CR_2 architecture for different values of γ.

Tuning Procedure (Parallel CR PCI-PID)**.**

1) *Tune a series CR PCI-PID first.*
2) *Choose* $\omega_{i_{par}} = \omega_r$ *as an initial guess and compute* C_{par} (16).
3) *Transform the series CR PCI-PID into a parallel CR PCI-PID, by removing* C_1 *and adding* C_{par} *in parallel of* $\mathcal{R}$.
4) *Lower* γ *until the difference between the SIDF and the HOSIDFs over the entire frequency range of interest* (ω_{dis}) *is the same or greater than with the series CR architecture.*
5) *Lower* $\omega_{i_{par}}$ *until the phase at* ω_{BW} *is the same as with the series CR architecture.*
6) *Adjust the gain to set the cross-over frequency at* ω_{BW}.
7) *In case the peak of the pseudosensitivity magnitude must be decreased further (i.e. it is higher than the acceptable level, e.g., 6 dB), return to step 5, however aiming at obtaining a higher phase at* ω_{BW}.

8) *In case the peak of the pseudosensitivity magnitude can be increased further (i.e. it is lower than the acceptable level, e.g., 6 dB), return to step 5, however aiming at obtaining a lower phase at ω_{BW}.*

The tuning procedure was performed to convert the series CR_2 PCI-PID controller into a parallel CR controller. The gain was adjusted to keep the cross-over frequency as 200 Hz. The resulting $\omega_{i_{par}} = 30$ Hz and $\gamma = -0.3$ were found. The controllers' FRF are pictured in Fig. 16. An LTI PI system with the same phase at the cross-over frequency as the two CR PCI system is also shown. For the same phase margin and a greater difference between SIDF and 3^{rd} HOSIDF in the range $\omega > 50$ Hz, the parallel achieves a greater SIDF gain in the low-frequency range. However, in the range SIDF [70, 200] Hz, the series CR architecture provides a greater gain. Furthermore at higher frequencies the series CR PCI has a steeper SIDF slope and thus provides greater noise and disturbance suppression. Nevertheless, in both cases the parallel CR structure still outperforms the LTI PI structure. Additionally, all implementation issues of the series CR architecture occurring due to its effect on the reset instants are overcome, making this architecture more suitable for industry.

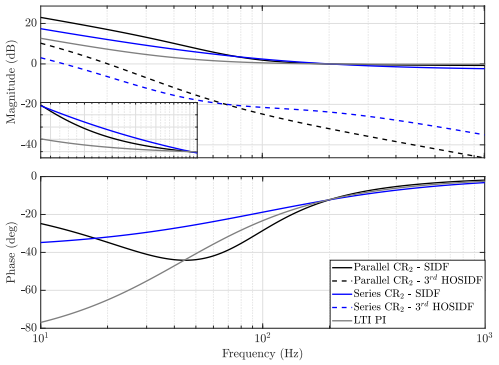

Fig. 16: FRF of the SIDF and 3^{rd} HOSIDF of the PCI in the series CR_2 architecture, a parallel CR_2 architecture with $\omega_{i_{par}} = 30$ Hz and $\gamma = -0.3$ as well as an LTI PI element with equivalent phase lag at 200 Hz.

In order to make use of the analysis methods presented in Section III, the parallel CR architecture must be able to be represented using (2). It is possible to describe a the system as given in Fig. 12 by augmenting $\mathcal{R}$ and A_ρ as

$$\begin{aligned} A_r &= \begin{bmatrix} \hat{A}_r & 0 \\ 0 & A_{C_{par}} \end{bmatrix}, & B_r &= \begin{bmatrix} \hat{B}_r \\ B_{C_{par}} \end{bmatrix} \\ C_r &= \begin{bmatrix} \hat{C}_r & C_{C_{par}} \end{bmatrix}, & D_r &= \begin{bmatrix} \hat{D}_r + D_{C_{par}} \end{bmatrix} \\ A_\rho &= \begin{bmatrix} \gamma & 0 \\ 0 & I^{n_{C_{par}} \times n_{C_{par}}} \end{bmatrix}, & C_1 &= 1, \end{aligned} \tag{18}$$

with $\hat{A}_r, \hat{B}_r, \hat{C}_r, \hat{D}_r$ the state-space matrices of the resetting part of $\mathcal{R}$ (e.g. a PCI) and $n_{C_{par}} \in \mathbb{Z}^+$ the number of states of C_{par}. Using this definition all theorems presented in Section III hold, apart from Theorem III.2. No frequency domain condition can be utilized to prove stability. It is therefore necessary to rely on the classical H_β-condition (Theorem III.1).

VII. Experimental implementation and results

In the previous two sections different reset control structures were presented and analyzed based on computational method and simulations. The following section will present how these structures were implemented digitally to perform experiments using the previously described experimental setup (Section III). The results of these experiments are then exhibited. The block diagram that describes the closed-loop system is portrayed in Fig. 17. It can be noticed that a feedforward controller C_{ff} is present in the system. The system in Fig. 17 has both a C_1 and a C_{par} block. It is clear that when the series CR architecture is employed, it is assumed that $C_{par} = 0$, whereas when the parallel CR architecture is employed one can assume $C_1 = 1$.

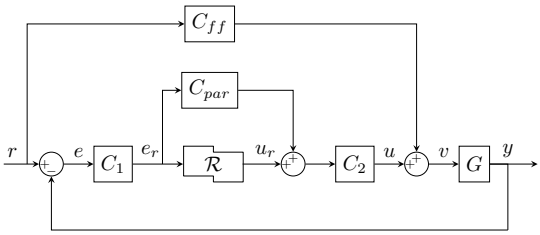

Fig. 17: Block diagram representation of the experimental setup.

A. Implementing a reset controller

So far it was assumed that the reset controller acts in the continuous time domain. However, in reality a discrete time reset controller is implemented in the physical system. In order to describe the dynamics of a discrete time reset controller, (2) was modified to

$$\mathcal{R} = \begin{cases} x_{r_{k+1}} = \tilde{A}_r x_{r_k} + \tilde{B}_r e_{r_k}, & \text{if} \quad (x_{r_k}, e_{r_k}) \notin \mathcal{M} \\ x_{r_{k+1}} = \tilde{A}_r A_\rho x_{r_k} + \tilde{B}_r e_{r_k}, & \text{if} \quad (x_{r_k}, e_{r_k}) \in \mathcal{M} \\ u_{r_k} = \tilde{C}_r x_{r_k} + \tilde{D}_r e_{r_k}, \end{cases} \tag{19}$$

with

$$\mathcal{M} := \{e_{r_k} e_{r_{k-1}} < 0 \wedge (t_k - t_{k-1} \geq t_s)\},$$

where $t_s = 1/f_s$ indicates the sampling period and $\tilde{A}_r$, $\tilde{B}_r$, $\tilde{C}_r$, $\tilde{D}_r$ are the state-space matrices of the discretized BLS. It can be noticed that the second line of (19) differs compared to (2). This is given by the fact that although it is not possible to exactly implement x_r^+ in discrete time, a good approximation is provided by $x_r^+ = x_{r_k} = A_\rho x_{r_k}$. This term can then be substituted in the first equation of Equation (19) to determine $x_{r_{k+1}}$ when reset occurs. Resetting is thus based on the condition that e_r in the current instant changes sign compared to the previous instant. Furthermore, a constrain is posed on the fact that after a reset at least $t = t_s$ must have passed before the next reset. This condition does not have to be

enforced during implementation, as it always holds true since samples are always t_s apart. The condition is beneficial as it avoids the occurrence of Zenoness, a cause of ill-posedness, defined as the presence of infinite reset actions in a finite time.

B. Experimental Results

An LTI PI-PID controller was tuned first, assuring the peak of sensitivity is $\approx$ 6 dB. The same PID was paired with a PCI, tuned using the procedure given in Section IV, resulting in a PCI-PID system. Two series CR architectures were tuned next. Both with the same ω_d and ω_t, however one with $n_l = 1$ (CR_1) and one with $n_l = 2$ (CR_2). Both were then converted to parallel CR architecture using the procedure in Section VI, resulting in parallel CR_1 and parallel CR_2 respectively. The parameters are not revealed due to confidentiality. The (scaled) open-loop FRF plots are portrayed in Fig. 18, whereas the respective magnitude plots of the pseudosensitivities are plotted in Fig. 19. It can be appreciated that for the same peak of sensitivity, all reset systems have greater open-loop gain and a lower magnitude of the pseudosensitivity at low frequencies compared to the LTI system. Moreover, as expected, the parallel CR systems have a larger open-loop magnitude compared to the respective series CR systems with the same F_l. It is also observed that systems with the CR_2 architectures have lower open-loop HOSIDFs compared to the respective CR_1 architecture systems. Nevertheless, in a certain range before ω_{BW}, the magnitude of pseudosensitivities of the two systems controlled by parallel CR PCI-PID controllers are higher in magnitude compared to the system controlled by the respective series CR PCI-PID controllers. This is a trade-off of the parallel CR architecture already mentioned in Section VI. The waterbed

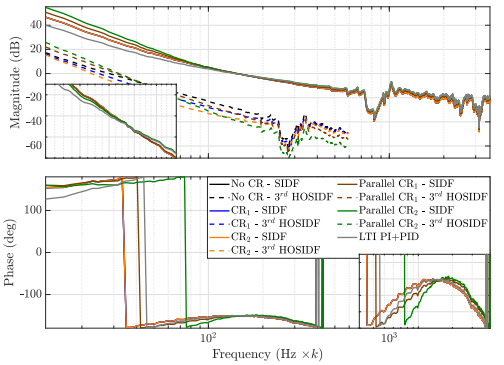

Fig. 18: FRF of the SIDF and 3^{rd} HOSIDF of the open-loop system with the FRF data of the ASMPT wire bonder at the center position as the plant and different reset control structures.

effect can be described mathematically by the Bode sensitivity integral, which can be simplified as

$$\int_0^\infty \ln(S)d\omega \geq 0. \tag{20}$$

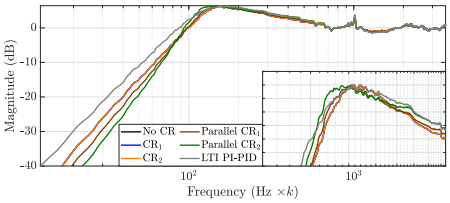

Fig. 19: Pseudosensitivities magnitudes of the closed-loop system with the FRF data of the ASMPT wire bonder at the center position as the plant and different reset control structures.

The area underneath the 0 dB line in a sensitivity plot, which should be minimized to increase tracking performance, can thus not be greater than the one above. Due to the waterbed effect, an improvement in one range of frequencies comes at cost of worse performance at other frequencies. For the same plant, every minimum phase LTI controller will result in the same $\int_0^\infty \ln(S)d\omega$ value. From Fig. 20, it can be seen how this constraint is overcome with reset control. All reset controllers achieve in fact a better value for the Bode sensitivity integral compared to the LTI system.

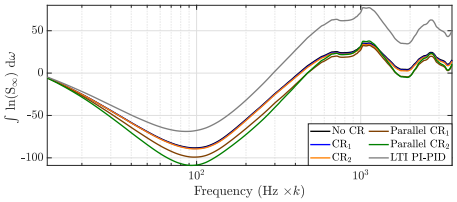

Fig. 20: Bode sensitivity integral using the FRF data of the ASMPT wire bonder at the center position as the plant and different reset control structures. For the LTI system S is utilized instead of S_∞

The NSV plots of the PCI-PID system without CR, which are also valid for the series CR systems since this architecture has no effect on the NSV, are depicted in Fig. 21. The bounds given in Theorem III.2 are not overcome, thus the system is UBIBS stable. It was found numerically that the bounds are still not overcome if a phase lag of $< 33.8°$ or a gain increase of < 9.7 dB is added to the system. This gives a qualitative indication of the robust stability of the system. For the parallel CR configuration, the NSV method cannot be utilized. The classical H_β-condition (Theorem III.1) can instead be utilized to guarantee stability after augmenting the system as given in (18). In order to do that, a parametric plant description is necessary. Additionally, no qualitative indication on the robustness of the system can be obtained.

The (scaled) resulting error signals and their cumulative power spectral density, for a typical reference input trajectory, are portrayed in Fig. 22. The final root-mean-square of the steady-state part of the error e_{RMS}, normalized with respect to the e_{RMS} resulting from the LTI PCI-PID system, is shown in Table II. The PCI-PID system without CR has a greater e_{RMS} than the fully LTI system due to the prevalence of

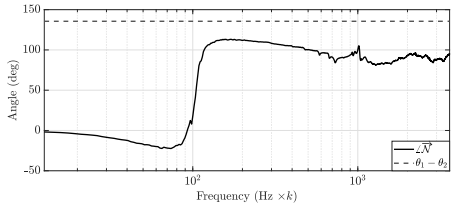

Fig. 21: NSV angle and $\theta_1 - \theta_2$ (Theorem III.2) of the PCI-PID system.

HOSIDFs. This is accounted for partially using the series CR_1 architecture which shows significantly lower power in the higher frequencies. However, the series CR_2 architecture results in greatly increased power of the first harmonic. This shows that the noise present in the system is amplified by this architecture, to the point where performance deteriorates. Finally, the highest suppression of the first harmonic is achieved by the parallel CR structures, which also result in the lowest excitation of higher-order harmonics. The parallel CR_2 architectures reduces the steady-state RMS error by more than 30% compared to the LTI system. This is however also due to the fact that in the range in which their pseudosensitivities are larger compared to the series CR structures, the disturbance is less significant.

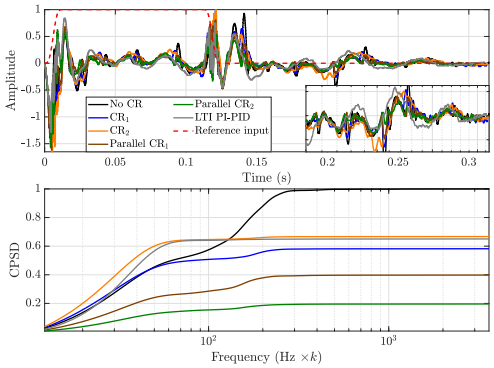

Fig. 22: Normalized error signal and cumulative power spectral density obtained from experiments for a typical reference trajectory (plotted scaled).

TABLE II: SCALED e_{RMS} FROM EXPERIMENT.

	No CR	CR_1	CR_2	p. CR_1	p. CR_2	LTI
e_{RMS}	1.1763	0.9847	1.0491	0.8708	0.6839	1

VIII. CONCLUSION

Reset control has gained significant attention in literature as a potential alternative to LTI control. It offers increased performance and at the same time simple controller design methods comparable to LTI control. In this work, various findings recently proposed in literature were combined to verify if and how a PCI reset controller can be utilized to increase tracking performance of a standard industrial motion stage, such as the one of an ASMPT wire bonder. Open- and closed-loop HOSIDFs were successfully put at use as a predictive performance frequency domain tool. It was demonstrated how, by reducing the magnitude of HOSIDFs, it is possible to treat reset control systems in a very similar fashion as LTI controllers, allowing loopshaping techniques to be used for design. It was thus possible to relatively easily design reset controllers that were utilized in combination with PID controllers, to improve closed-loop performance.

Three different structures based on the PCI were suggested. A PCI can increase open-loop gain at low frequencies even more than an equivalent PI, thus increasing suppression of low frequency disturbances. Furthermore it has a lower phase lag compared to an equivalent LTI PI element. Nevertheless, the low frequency HOSIDFs can cause performance degradation in case of low frequency disturbances. Two different CR architectures were thus explored to reduce the HOSIDFs. The first structure, namely a series CR architecture, involves adding a lead element F_l before the reset element $\mathcal{R}$ while simultaneously adding F_l^{-1} after the $\mathcal{R}$. The effect of the two filters F_l and F_l^{-1} cancels out in the overall system SIDF, affecting therefore only the HOSIDFs. It was shown that with increased $H_{\mathcal{C}}(\omega_{dis})$, the higher order harmonics excited by the n^{th} HOSIDFs could be decreased at $n\omega$. Nevertheless, some issues were exposed for the series CR architecture that hinder its implementation. In fact, F_l causes the amplification of e_r, denoted as the input signal to $\mathcal{R}$. This affects the reset instants in an unpredictable way, possibly affecting the transient behaviour but also the steady-state behaviour in case noise is present in the system. Furthermore, when implemented in discrete time, aliasing can cause the amplification of the closed-loop error when power in certain frequencies is present in the system's exogenous inputs. A novel structure, named parallel CR, was therefore developed to overcome the inherent issues of the series CR architecture. The parallel CR architecture is also based on the principle of utilizing F_l^{-1} placed in series after $\mathcal{R}$ to lower HOSIDFs, however the lead element is instead placed in parallel to $\mathcal{R}$. This avoids an amplification of e_r and thus avoids affecting the reset instants. On the other hand, the SIDF is not identical to the same PCI-PID system without CR architecture. Nevertheless, tuning guidelines were proposed that allow an even greater open-loop gain compared to the same PCI-PID system without CR architecture, at the cost of reduced suppression at frequencies right before the bandwidth.

The experiments consisted of tracking a typical reference signal of the wire bonder in presence of both feedforward and feedback control. The PCI-PID system without CR architecture showed how the systems main disturbance is suppressed more effectively compared to an equivalent PI-PID system. However, higher order harmonics led to a significant decrease in performance. Two series CR architectures were used to expand the PCI-PID system, demonstrating their effectiveness at lowering higher order harmonics. However,

one of the two series CR PCI-PID systems showed a worse performance compared to the LTI PI-PID system, evidencing that when tuned inappropriately the noise can cause significant performance degradation in systems employing the series CR architecture. Two parallel CR architectures were also used to expand the PCI-PID system. These achieved the best performance with cumulative power spectral density error reduction of up to $> 30\%$ compared to the fully LTI system.

Although this work highlighted the potential of the parallel CR architecture, it should be noted that the frequency domain NSV method cannot be utilized to analyze stability of parallel CR systems. The classical H_β-condition can be utilized instead. Nevertheless it can be argued that through future work it should be possible to augment the NSV method to the parallel CR architecture. In fact, an augmented NSV method for a reset element with two states, where only the first state resets, was presented in [7]. The structure of $\mathcal{R}$ has thus a similar characteristic to (18), where also only the first state resets. A further recommendation for future work is to incorporate the so called shaping filter, a linear filter that affects the reset instants of $\mathcal{R}$, but not its input-output relation, in the CR architecture. In [23] it was demonstrated that shaping filter are capable of bandpassing the nonlinearity of a reset element in a certain frequency region. This technique could be utilized to counteract the implementation issues that arose with the series CR architecture.

REFERENCES

[1] K. Åström and T. Hägglund, "The future of pid control," *Control Engineering Practice*, vol. 9, no. 11, pp. 1163–1175, 2001.

[2] K. Åström and R. Murray, *Feedback Systems: An Introduction for Scientists and Engineers*. Princeton University Press, 2010.

[3] H. W. Bode, *Network analysis and feedback amplifier design*. Van Nostrand, 1945.

[4] S. Skogestad and I. Postlethwaite, *Multivariable feedback control: Analysis and Design*. John Wiley, 2005.

[5] J. C. Clegg, "A nonlinear integrator for servomechanisms," *Transactions of the American Institute of Electrical Engineers, Part II: Applications and Industry*, vol. 77, no. 1, pp. 41–42, 1958.

[6] Y. Chait and C. Hollot, "On horowitz's contributions to reset control," *International Journal of Robust and Nonlinear Control*, vol. 12, pp. 335–355, 2002.

[7] A. A. Dastjerdi, "Frequency-domain analysis of "constant in gain lead in phase (cglp)" reset compensators," Ph.D. dissertation, Technische Universiteit Delft, Delft, 2021.

[8] X. Hou, A. A. Dastjerdi, N. Saikumar, and S. H. HosseinNia, "Tuning of 'constant in gain lead in phase (cglp)' reset controller using higher order sinusoidal input describing function (hosidf)," in *2020 Australian and New Zealand Control Conference (ANZCC)*, 2020, pp. 91–96.

[9] N. Karbasizadeh and H. HosseinNia, "Continuous reset element: Transient and steady-state analysis for precision motion systems," *Control Engineering Practice*, vol. 126, p. 105232, 2022.

[10] C. Cai, A. A. Dastjerdi, N. Saikumar, and S. H. HosseinNia, "The optimal sequence for reset controllers," in *2020 European Control Conference (ECC)*, 2020, pp. 1826–1833.

[11] D. Caporale, "Overcoming inherent performance limitations in industrial motion stages with reset control," Master's Thesis, Technische Universiteit Delft, 2022.

[12] K. Heinen, "Frequency analysis of reset systems containing a clegg integrator," Master's Thesis, Technische Universiteit Delft, 2018.

[13] E. Akyüz, N. Saikumar, and S. H. HosseinNia, "Reset control for vibration disturbance rejection," *IFAC-PapersOnLine*, vol. 52, no. 15, p. 525–530, 2019.

[14] L. van Eijk, "Nonlinear motion control designs and performance evaluation on an industrial motion stage," Master's Thesis, Eindhoven University of Technology, 2021.

[15] S. Beer, "Data-driven axes decoupling and motion control of bonding machines," Master's Thesis, Eindhoven University of Technology, 2019.

[16] D. Navarro, "Analysis and design of reset control systems," Ph.D. dissertation, Universidad de Murcia, Murcia, 2015.

[17] O. Beker, "Analysis of reset control systems," Ph.D. dissertation, University of Massachusetts Amherst, Amherst, 2001.

[18] O. Beker, C. Hollot, Y. Chait, and H. Han, "Fundamental properties of reset control systems," *Automatica*, vol. 40, no. 6, pp. 905–915, 2004.

[19] M. Vidyasagar, *Nonlinear Systems Analysis (2nd Ed.)*. Prentice-Hall, Inc., 1993.

[20] A. Gelb and W. E. V. Velde, *Multiple-Input Describing Functions and Nonlinear System Design*. McGraw-Hill, 1968.

[21] D. Rijlaarsdam, P. Nuij, J. Schoukens, and M. Steinbuch, "A comparative overview of frequency domain methods for nonlinear systems," *Mechatronics*, vol. 42, pp. 11–24, 2017.

[22] P. Nuij, O. Bosgra, and M. Steinbuch, "Higher-order sinusoidal input describing functions for the analysis of non-linear systems with harmonic responses," *Mechanical Systems and Signal Processing*, vol. 20, no. 8, pp. 1883–1904, 2006.

[23] N. Karbasizadeh, A. A. Dastjerdi, N. Saikumar, and S. H. HosseinNia, "Band-passing nonlinearity in reset elements," *IEEE Transactions on Control Systems Technology*, pp. 1–11, 2022.

[24] N. Saikumar, K. Heinen, and S. H. HosseinNia, "Loop-shaping for reset control systems: A higher-order sinusoidal-input describing functions approach," *Control Engineering Practice*, vol. 111, p. 104808, 2021.

[25] A. A. Dastjerdi, A. Astolfi, N. Saikumar, N. Karbasizadeh, D. Valério, and S. H. HosseinNia, "Closed-loop frequency analysis of reset control systems," *IEEE Transactions on Automatic Control*, pp. 1–8, 2022.

[26] A. A. Dastjerdi, N. Saikumar, and S. H. HosseinNia, "Optimal tuning of a class of reset controllers using higher-order describing function analysis: Application in precision motion systems," *ArXiv*, 2020.

[27] N. S. Nise, *Control Systems Engineering*, 3rd ed. USA: John Wiley & Sons, Inc., 2000.

[28] A. Barreiro, A. Baños, S. Dormido, and J. A. González-Prieto, "Reset control systems with reset band: Well-posedness, limit cycles and stability analysis," *Systems and Control Letters*, vol. 63, pp. 1–11, 2014.

[29] MathWorks, "Simulink," 2021. [Online]. Available: https://www.mathworks.com/products/simulink.html

5

USING A SHAPING FILTER TO LOWER HOSIDFS OF A PCI-PID

In this chapter the effect of a shaping filter to suppress the HOSIDFs of a PCI-PID controller at low and high frequencies will be studied. It can be derived from (2.14) that if $\mathscr{R}$ is a PCI, choosing $\varphi = 90m°$, where $m \in \mathbb{Z}^+$ is an odd value, will result in all HOSIDFs to be equal to 0. However, as with $\angle C_1 \neq 0$, also with $\angle C_s \neq 0$ the reset instances are modified. In order to avoid the issues encountered with the series CR architecture due to the amplification of the reset signal $\hat{e}_r$ (Chapter 4), it is therefore necessary to choose C_s as a lag element, i.e. $\varphi > 0° \ \forall \omega$. By selecting C_s as a lag element, the amplification of noise and the aliasing effect will both be avoided, although the change in transient response can still occur. A lag element delays the reset instance, hence potentially decreasing the total number of reset instances compared to the equivalent reset control system without C_s. Therefore, the effect on transient response is not as significant as with a lead element, and in fact approaches the transient response of the BLS for $\varphi \to 90°$. The magnitude of the HOSIDFs $|H(\omega)_n|$ given $\mathscr{R}$ is a PCI, is dependent on φ, ω and n. However, it can be determined from (2.14) that when normalized for a given n, the magnitude is identical for all ω, as depicted in Fig. 5.1. It is clear that setting $\varphi = 90°$ the reset element has no HOSIDFs, in fact behaving as its BLS. Increasing/decreasing φ increases the HOSIDFs at the same rate.

Apart from affecting the HOSIDFs, it should be taken into account that C_s has also an effect on the SIDF. In Fig. 5.2, the difference in the magnitude and phase of the SIDF and third HOSIDF of a PCI with and without C_s for different φ is shown. At $\varphi = 90°$, when the HOSIDFs are 0, the system behaves like the BLS, the gain advantage and the phase advantage given by reset control are therefore lost. As expected for $\varphi = 90°$, the gain advantage from reset is at its minimum. However, it can be seen that by increasing $\varphi > 90°$

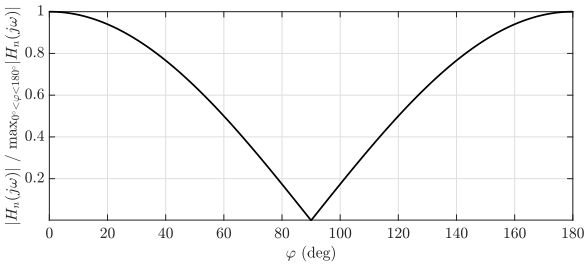

Figure 5.1: Normalized magnitude of n^{th} HOSIDFs as a function of φ, for a given ω.

it is possible to reduce the phase even further, with the minimum being $\varphi \approx 115°$. In lin-

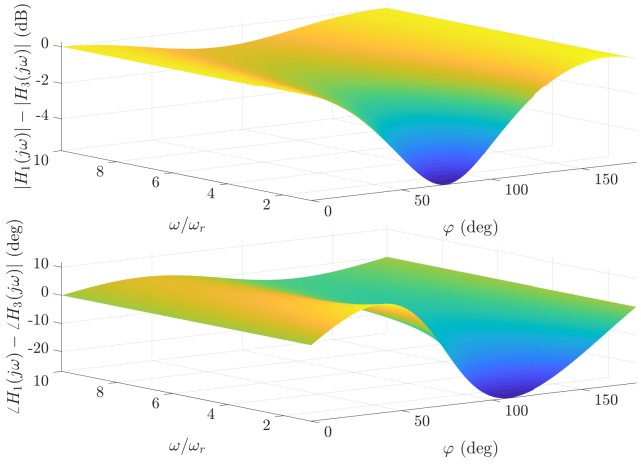

Figure 5.2: Difference between magnitude and phase of SIDF and 3^{rd} HOSIDFs as a function of φ and ω/ω_r.

ear systems the phase margin is an important metric related to stability. Although never proven, simulations and experiment suggest that this qualitative relationship holds also for the SIDF phase margin of a reset systems with $C_s = 1$ [11]. To the best of the author's knowledge, this relationship was never studied for $C_s \neq 1$. Two shaping filters C_{s_1} and C_{s_2} were designed for the previously tuned PCI-PID system with PID_1 as the LTI controller and G_1 as the plant (Chapter 4). Both shaping filters were tuned to have low HOSIDFs at low and high frequencies, thus with $\varphi \approx 90°$ in these frequency ranges. C_{s_1} was tuned to maximise the phase margin, therefore it was made sure that $\varphi(\omega_{BW}) = 65°$. On the other hand, C_{s_2} was tuned in such a way that the phase margin is minimized, hence with $\varphi(\omega_{BW}) = 115°$. C_{s_1} and C_{s_2} consist of a pure integrator, that has a phase lag of $-90°$ and a lead-lag or lag-lead element, such as F_l or F_l^{-1} in (2.28) respectively. The lead-lag el-

ement has a phase of 25° at ω_{BW}, whereas the lag-lead element has a phase of −25° at ω_{BW}. Their transfer functions are given as

$$C_{s_1} = \frac{1}{s} \times \frac{s/(\omega_{BW}/1.55)+1}{s/(1.55\omega_{BW})+1}, \quad C_{s_2} = \frac{1}{s} \times \frac{s/(1.55\omega_{BW})+1}{(\omega_{BW}/1.55)+1}. \tag{5.1}$$

The phase of the two shaping filters is plotted in Fig. 5.3. It can be noticed that the phase approaches −90° for low and high frequencies. The open-loop FRFs are plotted in Fig. 5.4.

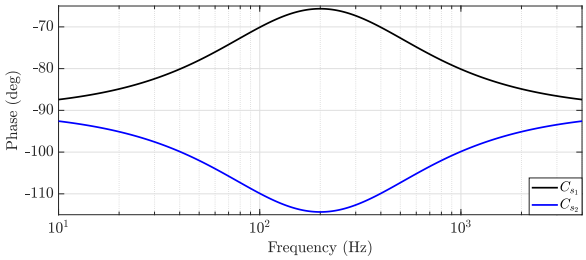

Figure 5.3: Phase-frequency plot of C_{s_1} and C_{s_2}.

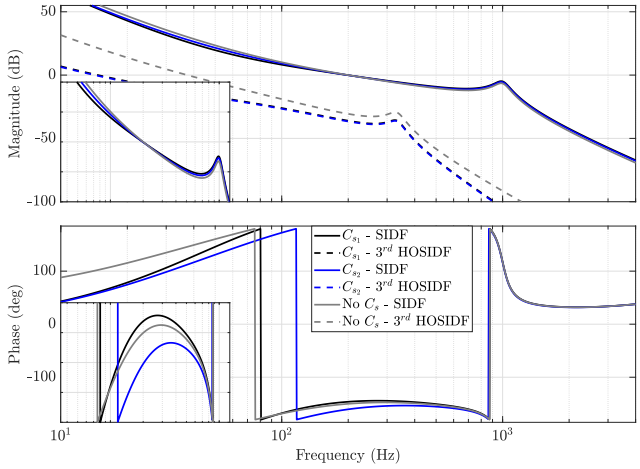

Figure 5.4: FRF of the SIDF and 3rd HOSIDF of the open-loop system with G_1 as the plant, PID_1 as the LTI controller, PCI as $\mathscr{R}$ and without C_s, with C_{s_1} and C_{s_2} as the shaping filter respectively.

The pseudosensitivities magnitudes shown in Fig. 5.5 illustrate that, contrary to the relation between the phase margin and M_S in LTI systems, the phase margin of the SIDF is

not always related to the peak of pseudosensitivity magnitude. In fact, the system with C_{s_1} has a higher pseudosensitivity magnitude peak even though the SIDF has a higher phase margin, while the opposite is true for the system employing C_{s_2}. Furthermore, the effect of C_s on the magnitude at high and low frequencies, given by the suppression of HOSIDFs, is again to be seen. On the other hand, in the frequency range [50, 150] Hz, the system with C_{s_2} shows an increased pseudosensitivity magnitude. This is given by the fact that the SIDF open-loop gain is decreased for $\varphi = [20°, 90°]$, as can be derived from Fig. 5.2.

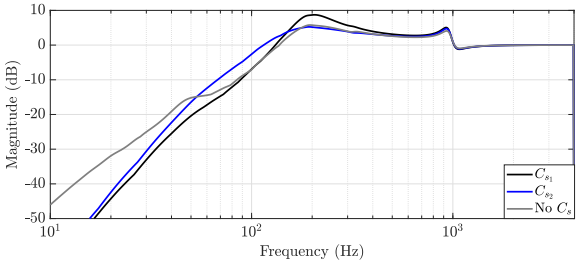

Figure 5.5: Pseudosensitivities magnitude computed through the approximate method of the closed-loop system with G_1 as the plant, PID_1 as the LTI controller, PCI as $\mathscr{R}$ and without C_s, with C_{s_1} and C_{s_2} as the shaping filter respectively.

Due to the decreased pseudosensitivity magnitude peak, the open-loop gain and bandwidth of the system can be increased to increase tracking performance, until the peak of pseudosensitivity magnitude reaches almost 6 dB. A static open-loop gain increase of 2 dB was applied to the system, by tuning a new PID controller $\text{PID}_2 = \text{PID}_1 F_{n_2} \times k_{PID_2}$, with

$$F_{n_2} = \frac{2.533 \times 10^{-8} s^2 + 7.958 \times 10^{-5} s + 1}{2.533 \times 10^{-8} s^2 + 1.415 \times 10^{-3} s + 1}, \tag{5.2}$$

being a notch filter to suppress the 1000 Hz resonance of the plant and $k_{PID_2} = 2$ dB. The notch filter is required since the increase in open-loop gain amplifies the resonance peak, as visible in the open-loop HOSIDFs and pseudosensitivity magnitude plots shown in Fig. 5.6 and Fig. 5.7 respectively. The notch filter decreases the phase margin even further, however the pseudosensitivity peak is still within the 6 dB limit. At the same time the system also achieves higher suppression at low frequencies compared to the equivalent system with PID_1.

Based on these findings, a rudimentary tuning procedure is proposed subsequently.

Tuning Procedure 5.0.1 (C_s for a PCI-PID system)

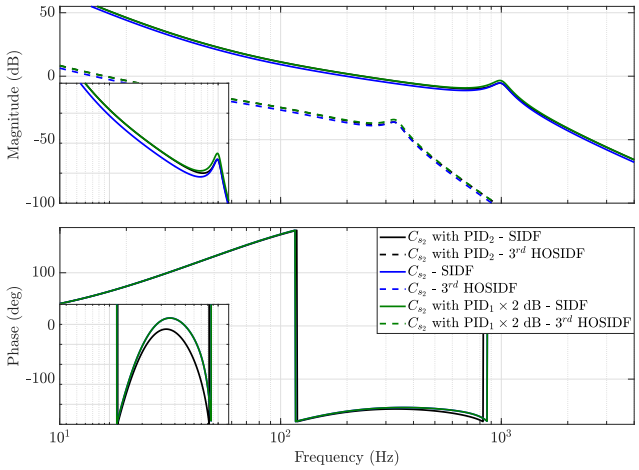

Figure 5.6: FRF of the SIDF and 3^{rd} HOSIDF of the open-loop system with G_1 as the plant, PID$_1$, PID$_2$ or PID$_1$ with increased gain as the LTI controller, PCI as $\mathscr{R}$ and with C_{s_2} as the shaping filter.

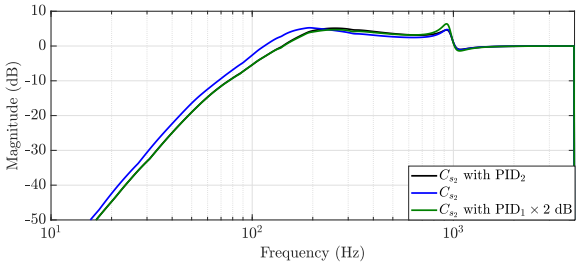

Figure 5.7: Pseudosensitivities magnitude computed through the approximate method of the closed-loop system with G_1 as the plant, PID$_1$, PID$_2$ or PID$_1$ with increased gain as the LTI controller, PCI as $\mathscr{R}$ and with C_{s_2} as the shaping filter.

- *Choose C_s as an LTI element with $\angle C_s$ approaching $-90°$ at low and high frequencies and $\approx -65°$ at ω_{BW}, e.g.: C_{s_2}.*
- *Iteratively increase the open-loop gain up to the point where the peak of the pseudosensitivity magnitude reaches the desired value. Add a notch filter in case the resonance causes a spike >6 dB in the pseudosensitivity magnitude.*

The tuning procedures ignores stability. In fact, although the designed shaping filter supposedly decreases the nonlinearity of the system, stability could not be proven using the H_β-condition for any shaping filter with $\max(\varphi) \approx 90°$. This suggests that the condition is too conservative in the case of C_s PCI-PID systems. It was shown that shaping

filters can not only significantly improve the performance of PCI-PID systems, but are also relatively straightforward to tune. It could therefore be beneficial to explore if a less conservative stability method can be utilized instead, thus allowing to more easily guarantee stability of C_s PCI-PID systems. In [62] it is stated that the stability of reset systems using the H_β-condition is independent on the reset times, therefore it is perhaps possible to expand the H_β-condition itself to prove that with certain shaping filters stability is guaranteed if the equivalent system without shaping filter is stable.

Since stability could not be guaranteed, experiments on the AB383 wire bonder could not be performed. Nevertheless, the performance of the C_s PCI-PID could be compared to the CR PCI-PID structures using Simulink simulations, as shown in the next chapter.

6

PERFORMANCE ANALYSIS VALIDATED ON SIMSCAPE MULTIBODY MODEL

A more detailed insight in the frequency and time domain performance achieved by the reset control system structures presented in Chapter 4 and Chapter 5, is given subsequently. The provided tuning procedures were utilized to tune different PCI-PID controllers for the Simscape multibody model of the motion stage. The performance of each controller was then validated through Simulink simulations performed using the same model. The structure of each controller in terms of continuous time transfer functions is displayed in Table 6.1, with

$$\text{PID} = \frac{1.0305 \times 10^6 (s+251.1)(s+326.5)(s+515.3)}{s(s+753.9)(s+1.408 \times 10^4)}$$

$$\text{PI} = 1 + \frac{1.3624(s+188.5)}{s},$$

$$\text{PCI} = 1 + \frac{60 \times 2\pi}{s},$$

$$F_{l_1} = \frac{s/(60 \times 2\pi)}{s/(200 \times 2\pi)},$$

$$F_{l_2} = \left(\frac{s/(60 \times 2\pi)}{s/(200 \times 2\pi)} \right)^2,$$

$$C_{par_1} = \left(1 + \frac{1 \times 2\pi}{s}\right) F_{l_1} - \left(1 + \frac{1 \times 2\pi}{s}\right),$$

$$C_{par_2} = \left(1 + \frac{2\times 2\pi}{s}\right) F_{l_2} - \left(1 + \frac{2\times 2\pi}{s}\right),$$
$$C_s = \frac{1}{s} \times \frac{s/(1.55\omega_{BW}) + 1}{(\omega_{BW}/1.55) + 1},$$

where $\omega_{BW} = 180\times 2\pi$. The transfer functions were discretized at $f_s = 8000$ Hz for implementation.

Table 6.1: Controllers used for simulations of the Simscape multibody model.

	C_1	C_2	C_{par}	C_s	R	γ
PCI-PID	/	PID	/	/	PCI	0
CR_1 PCI-PID	F_{l_1}	$F_{l_1}^{-1}\times$ PID	/	/	PCI	0
CR_2 PCI-PID	F_{l_2}	$F_{l_2}^{-1}\times$ PID	/	/	PCI	0
Parallel CR_1 PCI-PID	/	$1.267\times F_{l_1}^{-1}\times$ PID	C_{par_1}	/	PCI	-0.3
Parallel CR_2 PCI-PID	/	$1.462\times F_{l_2}^{-1}\times$ PID	C_{par_2}	/	PCI	-0.6
High bandwidth C_s PCI-PID	/	1.445×PID	/	C_{s_2}	PCI	0
LTI PI-PID	/	1.362×PI×PID	/	/	/	/

The resulting open-loop FRF plots are portrayed in Fig. 6.1, whereas the pseudosensitivities computed using the approximate method (Theorem II.4) are shown in Fig. 6.2. The open-loop systems have a cross-over frequency of 180 Hz, apart from the one controlled by the high bandwidth C_s PCI-PID, which was tuned to have a higher bandwidth than the base PCI-PID (210 Hz), as per the tuning rules. The phase margin of the systems is also comparable ($\approx 30°$), with the C_s PCI-PID again being the exception. This is given by the fact that for C_s PCI-PID a lower phase margin of the SIDF is required to result in an equivalent peak of pseudosensitivity as the same system without C_s. As expected all reset systems have a larger open-loop gain at the base frame connection resonance frequency ($\approx 40°$ Hz), compared to the LTI system. The parallel CR systems show the greatest open-loop gain, however also the lowest gain in the region [100,200] Hz and the highest gain at high frequencies. The pseudosensitvities suggest an equivalent behaviour to the open-loop FRF. It can be appreciated how the series CR architecture introduces spikes at high frequency. The errors resulting from simulation are portrayed in Fig. 6.3a and Fig. 6.3b in the case with and without white noise in the input n respectively. Again, the same conclusion already derived in Chapter 4 and Chapter 5 can be drawn:

- The HOSIDFs decrease the performance of the standard PCI-PID.
- The series CR architecture can be utilized to decrease HOSIDFs, however it is susceptible to noise, further decreasing the performance.

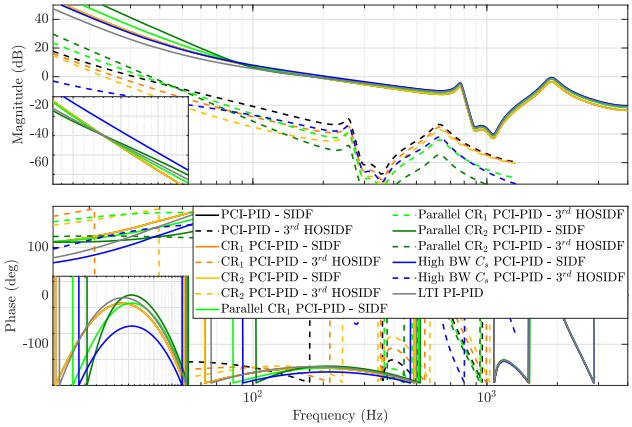

Figure 6.1: FRF of the SIDF and 3^{rd} HOSIDF of the open-loop system with the Simscape multibody model as the plant, controlled by the control systems shown in Table 6.1. The zoomed-in sections in the bottom-left show the behaviour around the cross-over region.

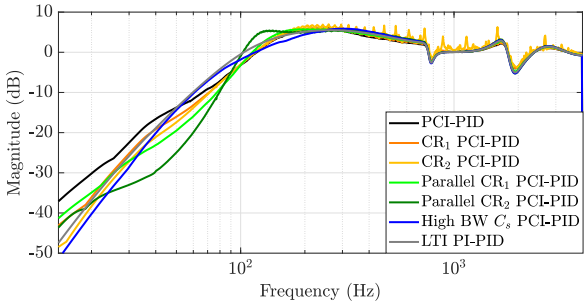

Figure 6.2: Pseudosensitivities of the closed-loop system with the Simscape multibody model as the plant, controlled by the control systems shown in Table 6.1, computed using the approximate method.

- The parallel CR architecture achieves the greatest suppression and is not sensitive to noise.
- The C_s PCI-PID is also not sensitive to noise.

In Fig. 6.3a it can be noticed that the cumulative power spectral density of the error during the settling period of the fully LTI system is significantly greater than that of any reset system, although the pseudosensitivity magnitude at the base frame connection resonance frequency is lower than that of the PCI-PID system. This is partly given by the definition of pseudosensitivites. Since they are computed based on the maximum magnitude of the error, they give a conservative estimation that can differ from the root-mean-square value of the error, which more accurately describes the power at a given

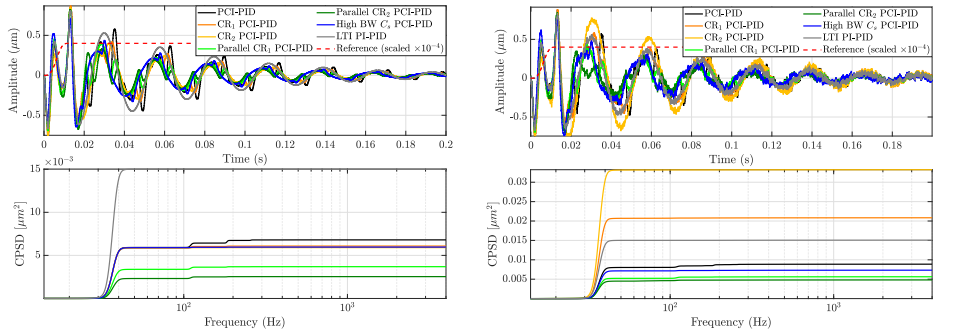

(a) (b)

Figure 6.3: Error signal and cumulative power spectral density obtained from simulations of the Simscape multibody model for a typical reference without white noise (a) and with white noise (b) in the input n.

Table 6.2: Resultant metrics from simulations of the Simscape multibody model without noise.

	$e_{t_{RMS}}$	$e_{s_{RMS}}$	$e_{t_{max}}$	$e_{s_{max}}$	T_{set}
PCI-PID	0.3333	0.1449	0.7502	0.8569	0.0451
CR_1 PCI-PID	0.3237	0.1283	0.7502	0.8685	0.0330
CR_2 PCI-PID	0.3165	0.1229	0.7502	0.8488	0.0307
Parallel CR_1 PCI-PID	0.3426	0.1183	0.6976	0.8198	0.0271
Parallel CR_2 PCI-PID	0.3162	0.1130	0.6975	0.8230	0.0242
High bandwidth C_s PCI-PID	0.3112	0.1209	0.6427	0.7159	0.0327
LTI PI-PID	0.3136	0.1704	0.6660	0.8078	0.0419

frequency. The performance metrics introduced in Section 1.2 are given for the control systems in Table 6.2. For the metric T_{set} given in (1.8) parameters $b_{min} = 0$ μm and $b_{max} = 1$ μm were utilized. The results confirm that the RMS error in the settling period can be significantly decreased with reset control, up to 44% in the case of the system employing the parallel CR_2 architecture. It should be known that all controllers were tuned to maximise the system's tracking precision, thus minimize $e_{s_{RMS}}$. The change in the RMS error in the tracking stage is comparatively only minor, with a maximal increase of 9% with respect to the LTI system, given by the parallel CR_1 architecture system. The difference in the maximal errors between different systems are also comparatively less significant, with a maximal increase of 12% for the error in the transient phase and of 7% for the error in the settling and steady-state phase. Regarding settling time performance, the resulting T_{set} values illustrate that the simple PCI-PID system has on aver-

age a greater settling time compared to the PI-PID system. This can be explained by the peaks in error signal caused by the higher order harmonics. All other reset signals have a smaller T_{set} value, once again showcasing the effectiveness of reset control

7

CONCLUSION AND FUTURE WORK RECOMMENDATIONS

7.1. CONCLUSION

In industry it is fundamental to utilize controllers which can be designed using relatively simple tuning rules. With linear controllers, loopshaping techniques allow this. However, LTI systems are affected by inherent performance limitations. In order to meet the ever-increasing demands for better performance, the adoption of nonlinear control techniques is necessary. In the case of the AB383 wire bonder, performance is given by the speed and accuracy of the motion stage, in order to increase the throughput of the machine and allow it to be utilized for smaller chips, respectively. Feedback control is mainly required to suppress a low frequency disturbance resulting from the resonance of the connection between the machine's baseframe and the environment. Relevant metrics were devised to allow the assessment of the performance quantitatively. Subsequently, the plant which was utilized to experimentally validate the findings of the project, the X-stage of the wire bonder's motion platform, was analyzed. The stage's current LTI control architecture was also described. A literature study followed, to find the structure of controllers that would best suit industrial applications. It was established that with a certain type of reset controllers the necessary nonlinearity to overcome LTI's fundamental limitations can be achieved, while also allowing frequency domain performance (open-loop HOSIDFs and closed-loop pseudosensitivities) and stability analysis (NSV method). Section 2.1.4 presented all possible types of reset controllers that allow this, analyzing their advantages and disadvantages. Out of these the FORE and PCI were deemed the most suitable. Finally, the previous implementation of reset control on the wire bonder presented in [4] was analysed, assuring that the encountered issues would be overcome in this project.

The FORE was implemented to construct a CgLp, an element capable of increasing the phase margin, of a system while having only a negligible effect on the magnitude. Using the proposed tuning procedure, a CgLp was designed that decreased the peak of (pseudo)sensitivity of a system employing an aggressive PID from 7.4 dB to 3.7 dB. It was however discovered that due to its high HOSIDFs at high frequencies, its NSV is very susceptible to high frequency resonances. This is especially relevant in the high tech industry, where the bandwidth is often maximised to increase performance, therefore bringing the bandwidth and high frequency resonances relatively closer in the frequency spectrum. It was discovered that adding a notch filter to suppress the resonance peak can lead to the satisfaction of the H_β-condition. Nevertheless, it may be the case that the required notch filter introduces more phase lag than the phase advantage of the CgLp itself.

In Chapter 4, included as a standalone paper, three different structures based on the PCI were suggested. A PCI can increase open-loop gain at low frequencies even more than an equivalent PI, thus increasing suppression of low frequency disturbances. Furthermore it has a lower phase lag compared to an equivalent LTI PI element. Nevertheless, the low frequency HOSIDFs can cause performance degradation in case of low frequency disturbances. Two different CR architectures were thus explored to reduce the HOSIDFs. The first structure, namely a series CR architecture, involves adding a lead element F_l before the reset element $\mathscr{R}$ while simultaneously adding F_l^{-1} after $\mathscr{R}$. The effect of the two filters F_l and F_l^{-1} cancels out in the overall system SIDF, affecting therefore only the HOSIDFs. It was shown that with increased $\angle F_l(\omega)$, the higher order harmonics excited by the n^{th} HOSIDFs could be decreased at $n\omega$. Nevertheless, some issues were exposed for the series CR architecture that hinder its implementation. In fact, F_l causes the amplification of e_r and $\hat{e}_r$. This affects the reset instances in an unpredictable way, possibly affecting the transient behaviour but also the steady-state behaviour in case noise is present in the system. Furthermore, when implemented in discrete time, aliasing can cause the amplification of the closed-loop error when power in certain frequencies is present in the system's exogenous inputs. A novel structure, named parallel CR, was therefore developed to overcome the inherent issues of the series CR architecture. The parallel CR architecture is also based on the principle of utilizing F_l^{-1} placed in series after $\mathscr{R}$ to lower HOSIDFs, however the lead element is instead placed in parallel to $\mathscr{R}$. This avoids an amplification of e_r and thus avoids affecting the reset instances. On the other hand, the SIDF is not identical to the same PCI-PID system without CR architecture. Nevertheless, tuning guidelines were proposed that allow an even greater open-loop gain compared to the same PCI-PID system without CR architecture, at the cost of reduced suppression at frequencies right before the bandwidth.

Experiments, consisting of tracking a typical reference signal of the wire bonder in presence of both feedforward and feedback control, were then performed with all thre PCI-

PID structures. The PCI-PID system without CR architecture showed how the systems main disturbance is suppressed more effectively compared to an equivalent PI-PID system. However, higher order harmonics led to a significant decrease in performance. Two series CR architectures were used to expand the PCI-PID system, demonstrating their effectiveness at lowering higher order harmonics. However, one of the two series CR PCI-PID systems showed a worse performance compared to the LTI PI-PID system, evidencing that, when tuned inappropriately, the noise can cause significant performance degradation in systems employing the series CR architecture. Two parallel CR architectures were also used to expand the PCI-PID system. These achieved the best performance with cumulative power spectral density error reduction of up to > 30% compared to the fully LTI system.

In Chapter 5 the final structure, a C_s PCI-PID was presented. It utilizes a shaping filter to modify the reset instances of a PCI-PID. Tuning guidelines were given to design a shaping filer that not only lowers HOSIDFs at low and high frequencies, but also decreases the magnitude peak of pseudosensitivity of the system. Nevertheless, stability could not be guaranteed, not allowing to validate the C_s PCI-PID system with real life experiments. Instead Simulink simulations were performed, comparing all PCI-PID controllers. The results confirmed the potential of these systems to suppress disturbances, achieving an RMS error reduction of 29%.

Overall, open- and closed-loop HOSIDFs were successfully put at use as a predictive performance frequency domain tool. It was demonstrated how, by reducing the magnitude of HOSIDFs, it is possible to treat reset control systems in a very similar fashion as LTI controllers, allowing loopshaping techniques to be used for design. It was thus possible to relatively easily design reset controllers that were utilized in combination with PID controllers, to improve closed-loop performance. The NSV method was instead employed to analyze the stability of reset systems. It was illustrated through the CgLp system that, contrarily to the standard H_β-condition, the NSV phase provides information on how a reset control system that does not satisfy the H_β-condition can be tuned in order to guarantee stability.

In Section 2.2, the most significant open issues that prevented the adoption of reset control in [4] were assessed as 1) The inability of the reset controllers to achieve zero-steady state error, 2) The absence of a reset controller that allows both an open-loop frequency domain predictive performance analysis and a frequency domain stability analysis method, 3) The absence of a closed-loop predictive performance analysis method. The first and last issue were overcome for all reset controllers. However, the only implemented reset controllers that allowed both a frequency domain predictive performance analysis and a frequency domain stability analysis method were the PCI-PID and series CR PCI-PID systems, two structures with significant drawbacks.

7.2. FUTURE WORK RECOMMENDATIONS

Although this work highlighted the potential of reset control, it is clear that further research is needed to to achieve the full potential that this technique has to offer. Some recommendations for future research are given subsequently:

- The sensitivity of the NSV to resonances when using a CgLp-PID system might be overcome by employing a different stability method. Otherwise, reducing the nonlinearity of the CgLp-PID system at the resonance frequency could overcome the issue. It might be worth studying if it is possible to utilize a shaping filter for this matter.
- The stability of the parallel CR architecture can currently not be analysed using the NSV method. However, an expansion of the NSV method in [8] allows to analyse stability of a SOSRE, a structure that has some similarities to the parallel CR architecture as defined in (20) of Chapter 4. It can therefore be argued that a similar expansion of the NSV method can be created for the parallel CR architecture.
- The series CR architecture can provide some implementation issues due to the effect on resetting of a lead filter before the reset element. A shaping filter can affect resetting as well, while however leading to a different response. It might be beneficial to study the effect of a shaping filter on the CR architecture, and more specifically, if it can help overcoming the series CR implementation issues.
- The stability of a C_s PCI-PID could not be guaranteed using the H_β-condition. Nevertheless, due to the fact that shaping filters tuned as proposed reduce the nonlinearity of a reset system, it can be argued that it is desirable to explore if stability can be guaranteed using a less conservative stability method. Perhaps, the it is possible to use a variation of the H_β-condition itself since in [62] it is stated that the stability of reset systems using the H_β-condition is independent on the reset times.
- Predictive performance can thus far only be evaluated regarding steady-state behaviour. In case it is desired to use reset control to improve transient behaviour instead, it is beneficial to study the relationship between reset system parameters and transient response.
- In this work the overarching goal when tuning with reset controllers was to minimize HOSIDFs at low and high frequencies. Nevertheless, it is possible that HOSIDFs can be instead utilized to increase the performance further.
- The frequency domain analysis methods employed in this work to evaluate the closed-loop HOSIDFs analytically (Theorem II.4), is based on some assumptions that are often wrong, and is thus not always accurate, especially when the system has high HOSIDFs. It would be therefore beneficial to either explore if a different

method can be used or at least study a way to determine analytically how accurate the method is based on the system's parameters.

- The open- and closed-loop HOSIDF analysis methods used in this work assume a pure sinusoidal input. The nonlinear effects of desensitisation and intermodulation were thus neglected. It could be valuable to study the impact of these nonlinear effects on the response and perhaps develop tools to incorporate them in the analysis procedure.

BIBLIOGRAPHY

[1] ASM Pacific Technology Ltd. "Asm pacific technology." (), [Online]. Available: https://www.asmpacific.com/en/. (accessed: 23.09.2021).

[2] S. Skogestad and I. Postlethwaite, *Multivariable feedback control: Analysis and Design*. John Wiley, 2005.

[3] K. Åström and T. Hägglund, "The future of pid control," *Control Engineering Practice*, vol. 9, no. 11, pp. 1163–1175, 2001.

[4] L. van Eijk, *Nonlinear motion control designs and performance evaluation on an industrial motion stage*, Master's Thesis, Eindhoven University of Technology, 2021.

[5] J. C. Clegg, "A nonlinear integrator for servomechanisms," *Transactions of the American Institute of Electrical Engineers, Part II: Applications and Industry*, vol. 77, no. 1, pp. 41–42, 1958.

[6] Y. Chait and C. Hollot, "On horowitz's contributions to reset control," *International Journal of Robust and Nonlinear Control*, vol. 12, pp. 335–355, 2002.

[7] N. Saikumar, R. K. Sinha, and S. H. Hosseinnia, ""constant in gain lead in phase" element– application in precision motion control," *IEEE/ASME Transactions on Mechatronics*, vol. 24, pp. 1176–1185, 2019.

[8] A. A. Dastjerdi, "Frequency-domain analysis of "constant in gain lead in phase (cglp)" reset compensators," Ph.D. dissertation, Technische Universiteit Delft, Delft, 2021.

[9] N. Saikumar, K. Heinen, and S. H. HosseinNia, "Loop-shaping for reset control systems: A higher-order sinusoidal-input describing functions approach," *Control Engineering Practice*, vol. 111, p. 104 808, 2021.

[10] A. A. Dastjerdi, A. Astolfi, and H. HosseinNia, "A frequency-domain stability method for reset systems," *2020 59th IEEE Conference on Decision and Control (CDC)*, pp. 5785–5791, 2020.

[11] N. Karbasizadeh and H. Hosseinnia, "Continuous reset element: Transient and steady-state analysis for precision motion systems," *Control Engineering Practice*, vol. 126, p. 105 232, 2022.

[12] N. Karbasizadeh, A. A. Dastjerdi, N. Saikumar, and S. H. HosseinNia, "Band-passing nonlinearity in reset elements," *IEEE Transactions on Control Systems Technology*, pp. 1–11, 2022.

[13] X. Hou, A. A. Dastjerdi, N. Saikumar, and S. H. Hosseinnia, "Tuning of 'constant in gain lead in phase (cglp)' reset controller using higher order sinusoidal input describing function (hosidf)," in *2020 Australian and New Zealand Control Conference (ANZCC)*, 2020, pp. 91–96.

[14] K. Heinen, *Frequency analysis of reset systems containing a clegg integrator*, Master's Thesis, Technische Universiteit Delft, 2018.

[15] Digital Science. "Dimensions.ai [software]." (2018), [Online]. Available: https://app.dimensions.ai/discover/publication?search_mode=content&search_text=reset%20control&search_type=kws&search_field=text_search. (accessed: 04.11.2021).

[16] K. Åström and R. Murray, *Feedback Systems: An Introduction for Scientists and Engineers*. Princeton University Press, 2010, ISBN: 9781400828739.

[17] H. W. Bode, *Network analysis and feedback amplifier design*. Van Nostrand, 1945.

[18] K. Aström, "Limitations on control system performance," *European Journal of Control*, vol. 6, no. 1, pp. 2–20, 2000.

[19] M. M. Seron, J. H. Braslavsky, and G. C. Goodwin, *Fundamental Limitations in Filtering and Control*, 1st. Springer Publishing Company, Incorporated, 2011.

[20] J. Freudenberg, R. Middleton, and A. Stefanpoulou, "A survey of inherent design limitations," in *Proceedings of the 2000 American Control Conference*, vol. 5, Feb. 2000, pp. 2987–3001.

[21] M. Schuettler and T. Stieglitz, "Microassembly and micropackaging of implantable systems," in *Implantable Sensor Systems for Medical Applications*, ser. Woodhead Publishing Series in Biomaterials, A. Inmann and D. Hodgins, Eds., Woodhead Publishing, 2013, pp. 108–149.

[22] G. E. Moore, "Cramming more components onto integrated circuits, reprinted from electronics, volume 38, number 8, april 19, 1965, pp.114 ff.," *IEEE Solid-State Circuits Society Newsletter*, vol. 11, no. 3, pp. 33–35, 2006.

[23] O. Burkacky, M. de Jong, A. Mittal, and N. Verma. "Value creation: How can the semiconductor industry keep outperforming?" (2021), [Online]. Available: https://www.mckinsey.com/industries/semiconductors/our-insights/value-creation-how-can-the-semiconductor-industry-keep-outperforming. (accessed: 04.11.2021).

[24] S. Beer, *Data-driven axes decoupling and motion control of bonding machines*, Master's Thesis, Eindhoven University of Technology, 2019.

[25] The MathWorks Inc., *Simscape multibody*, Feb. 2021. [Online]. Available: https://www.mathworks.com/products/simmechanics.html.

[26] R. M. Schmidt, G. Schitter, A. Rankers, and J. van Eijk, *The Design of High Performance Mechatronics: High-Tech Functionality by Multidisciplinary System Integration*, 2nd. IOS Press, 2014.

[27] K. J. Aström and B. Wittenmark, *Computer Controlled Systems: Theory and Design*. Prentice Hall, 1984.

[28] Z. Gao, "From linear to nonlinear control means: A practical progression," *ISA Transactions*, vol. 41, no. 2, pp. 177–189, 2002.

[29] T. Samad, S. Mastellone, P. Goupil, A. van Delft, A. Serbezov, and K. Brooks, "Ifac industry committee update, initiative to increase industrial participation in the control community," *Newsletters april 2019*, 2019.

[30] J. Rawlings and D. Mayne, *Model Predictive Control: Theory and Design*. Nob Hill Publishing, 2008.

[31] J. Slotine and W. Li, *Applied Nonlinear Control*. Englewood Cliffs, NJ: Prentice-Hall, 1991.

[32] K. Tanaka and H. O. Wang, *Fuzzy Control Systems Design and Analysis*. John Wiley & Sons, Ltd, 2001, ISBN: 9780471224594.

[33] M. Heertjes and M. Steinbuch, "Stability and performance of a variable gain controller with application to a dvd storage drive," *Automatica*, vol. 40, pp. 591–602, Apr. 2004.

[34] W. Aangenent, M. Molengraft, and M. Steinbuch, "Nonlinear control of a linear motion system," *Journal of Nutrition Health & Aging*, vol. 38, Jul. 2005.

[35] D. Deenen, M. Heertjes, W. Heemels, and H. Nijmeijer, "Hybrid integrator design for enhanced tracking in motion control," in *2017 American Control Conference (ACC)*, 2017, pp. 2863–2868.

[36] D. Navarro, "Analysis and design of reset control systems," Ph.D. dissertation, Universidad de Murcia, Murcia, 2015.

[37] O. Beker, "Analysis of reset control systems," Ph.D. dissertation, University of Massachusetts Amherst, Amherst, 2001.

[38] A. Baños and A. Barreiro, *Reset Control Systems*. Springer, Oct. 2012, vol. 9.

[39] L. Zaccarian, D. Nesic, and A. Teel, "First order reset elements and the clegg integrator revisited," in *Proceedings American Control Conference*, vol. 1, Jul. 2005, pp. 563–568.

[40] D. Nešić, L. Zaccarian, and A. R. Teel, "Stability properties of reset systems," *Automatica*, vol. 44, no. 8, pp. 2019–2026, 2008.

[41] A. Barreiro, A. Baños, S. Dormido, and J. A. González-Prieto, "Reset control systems with reset band: Well-posedness, limit cycles and stability analysis," *Systems and Control Letters*, vol. 63, pp. 1–11, 2014.

[42] B. Kieft, S. H. HosseinNia, and N. Saikumar, "Reset band for mitigation of quantization induced performance degradation," in *2021 European Control Conference (ECC)*, 2021, pp. 2465–2472.

[43] A. Baños, S. Dormido, and A. Barreiro, "Limit cycles analysis of reset control systems with reset band," *Nonlinear Analysis Hybrid Systems*, vol. 5, pp. 163–173, May 2011.

[44] S. van Loon, "Hybrid control for performance improvement of linear systems," Proefschrift, Ph.D. dissertation, Mechanical Engineering, Jan. 2016.

[45] J. Zheng, Y. Guo, M. Fu, Y. Wang, and L. Xie, "Improved reset control design for a pzt positioning stage," in *2007 IEEE International Conference on Control Applications*, 2007, pp. 1272–1277.

[46] B. Kieft, S. H. HosseinNia, and N. Saikumar, "Time regularization as a solution to mitigate quantization induced performance degradation," in *2021 European Control Conference (ECC)*, 2021, pp. 2458–2464.

[47] N. S. Nise, *Control Systems Engineering*, 3rd. USA: John Wiley & Sons, Inc., 2000.

[48] J. Schoukens, R. Pintelon, T. Dobrowiecki, and Y. Rolain, "Identification of linear systems with nonlinear distortions," *Automatica*, vol. 41, pp. 491–504, Mar. 2005.

[49] D. Rijlaarsdam, P. Nuij, J. Schoukens, and M. Steinbuch, "A comparative overview of frequency domain methods for nonlinear systems," *Mechatronics*, vol. 42, pp. 11–24, 2017.

[50] A. Pavlov, N. Wouw, and H. Nijmeijer, "Frequency response functions and bode plots for nonlinear convergent systems," in *Proceedings of the IEEE Conference on Decision and Control*, Jan. 2007, pp. 3765–3770.

[51] Y. Guo, L. Xie, and Y. Wang, *Analysis and Design of Reset Control Systems*. The Institution of Engineering and Technology, Nov. 2015.

[52] M. Vidyasagar, *Nonlinear Systems Analysis (2nd Ed.)* Prentice-Hall, Inc., 1993.

[53] A. Gelb and W. E. V. Velde, *Multiple-Input Describing Functions and Nonlinear System Design*. McGraw-Hill, 1968.

[54] P. Nuij, O. Bosgra, and M. Steinbuch, "Higher-order sinusoidal input describing functions for the analysis of non-linear systems with harmonic responses," *Mechanical Systems and Signal Processing*, vol. 20, no. 8, pp. 1883–1904, 2006.

[55] T. M. Inc., *System Identification Toolbox*, Natick, Massachusetts, United State, 2019. [Online]. Available: https://www.mathworks.com/help/ident/.

[56] N. Karbasizadeh and S. H. HosseinNia, *Complex-order reset control system*, 2022. DOI: 10.48550/ARXIV.2205.01378.

[57] R. Buitenhuis, *Frequency-domain modelling of reset control systems using an impulsive description*, Master's Thesis, Technische Universiteit Delft, 2020.

[58] K. Krishnan and I. Horowitz, "Synthesis of a non-linear feedback system with significant plant-ignorance for prescribed system tolerances," *International Journal of Control*, vol. 19, pp. 689–706, 1974.

[59] H. Hu, Y. Zheng, Y. Chait, and C. Hollot, "On the zero-input stability of control systems with clegg integrators," in *Proceedings of the 1997 American Control Conference*, vol. 1, 1997, pp. 408–410.

[60] Q. Chen, C. Hollot, and Y. Chait, "Stability and asymptotic performance analysis of a class of reset control systems," in *Proceedings of the 39th IEEE Conference on Decision and Control*, vol. 1, 2000, 251–256 vol.1.

[61] C. Prieur, I. Queinnec, S. Tarbouriech, and L. Zaccarian, "Analysis and synthesis of reset control systems," *Foundations and Trends in Systems and Control*, vol. 6, pp. 117–338, Jan. 2018.

[62] O. Beker, C. Hollot, Y. Chait, and H. Han, "Fundamental properties of reset control systems," *Automatica*, vol. 40, no. 6, pp. 905–915, 2004.

[63] G. Zhao, J. Wang, and K. Li, "On stability analysis and synthesis of reset control systems with output uncertainties," in *Proceedings of the 33rd Chinese Control Conference*, 2014, pp. 3965–3969.

[64] T. Loquen, D. Nesic, C. Prieur, S. Tarbouriech, A. R. Teel, and L. Zaccarian, "Piecewise quadratic lyapunov functions for linear control systems with first order reset elements," *IFAC Proceedings Volumes*, vol. 43, pp. 807–812, 2010.

[65] D. Cheng, X. Hu, and T. Shen, "$\mathscr{L}_2$-gain synthesis," in *Analysis and Design of Nonlinear Control Systems*, Berlin, Heidelberg: Springer Berlin Heidelberg, 2010, pp. 403–429.

[66] W. H. T. M. Aangenent, G. Witvoet, W. Heemels, van de M.J.G. Molengraft, and M. Steinbuch, "Performance analysis of reset control systems," *International Journal of Robust and Nonlinear Control*, vol. 20, pp. 1213–1233, 2010.

[67] G. Witvoet, W. Aangenent, W. Heemels, M. van de Molengraft, and M. Steinbuch, "$\mathscr{H}_2$ Performance analysis of reset control systems," in *2007 46th IEEE Conference on Decision and Control*, 2007, pp. 3278–3284.

[68] W. H. T. M. Aangenent, G. Witvoet, W. Heemels, R. van de Molengraft, and M. Steinbuch, "An lmi-based $\mathscr{L}_2$ gain performance analysis for reset control systems," *2008 American Control Conference*, pp. 2248–2253, 2008.

[69] S. van Loon, W. Heemels, and A. Teel, "Improved $\mathscr{L}_2$-gain analysis for a class of hybrid systems with applications to reset and event-triggered control," in *53rd IEEE Conference on Decision and Control*, 2014, pp. 1221–1226.

[70] J. Carrasco, A. Baños, and A. Barreiro, "Stability of reset control systems with inputs," in *2008 Mediterranean Conference on Control and Automation - Conference Proceedings*, 2008, pp. 1496–1501.

[71] Y. Guo and L. Xie, "Quadratic stability of reset control systems with delays," in *Proceedings of the 10th World Congress on Intelligent Control and Automation*, 2012, pp. 2268–2273.

[72] J. Carrasco, A. Baños, and A. Schaft, "A passivity-based approach to reset control systems stability," *Systems & Control Letters*, vol. 59, pp. 18–24, Jan. 2010.

[73] A. Banos, J. Carrasco, and A. Barreiro, "Reset times-dependent stability of reset control systems," *IEEE Transactions on Automatic Control*, vol. 56, no. 1, pp. 217–223, 2011.

[74] S. van Loon, K. Gruntjens, M. Heertjes, N. van de Wouw, and W. Heemels, "Frequency-domain tools for stability analysis of reset control systems," *Automatica*, vol. 82, pp. 101–108, 2017.

[75] M. Heertjes, K. Gruntjens, S. Loon, N. Wouw, and M. Heemels, "Experimental evaluation of reset control for improved stage performance," *IFAC-PapersOnLine*, vol. 49, pp. 93–98, 2016.

[76] K. Gruntjens, M. Heertjes, S. Van Loon, N. Van De Wouw, and W. Heemels, "Hybrid integral reset control with application to a lens motion system," in *2019 American Control Conference (ACC)*, 2019, pp. 2408–2413.

[77] A. Bacciotti, "External stabilizability of nonlinear systems with some applications," *International Journal of Robust and Nonlinear Control*, vol. 8, no. 1, pp. 1–10, 1998.

[78] O. Beker, C. Hollot, Q. Chen, and Y. Chait, "Stability of a reset control system under constant inputs," in *Proceedings of the 1999 American Control Conference*, vol. 5, 1999, 3044–3045 vol.5.

[79] A. Baños and A. Vidal, "Definition and tuning of a pi+ci reset controller," in *2007 European Control Conference (ECC)*, 2007, pp. 4792–4798.

[80] A. Vidal and A. Baños, "Reset compensation for temperature control: Experimental application on heat exchangers," *Chemical Engineering Journal*, vol. 159, no. 1, pp. 170–181, 2010.

[81] A. Baños and A. Vidal, "Design of reset control systems: The pi+ci compensator," *Journal of Dynamic Systems Measurement and Control*, vol. 134, Jun. 2012.

[82] I. Horowitz and P. Rosenbaum, "Non-linear design for cost of feedback reduction in systems with large parameter uncertainty," *International Journal of Control*, vol. 21, no. 6, pp. 977–1001, 1975.

[83] G. Zhao and C. Hua, "Improved high-order-reset-element model based on circuit analysis," *IEEE Transactions on Circuits and Systems II: Express Briefs*, vol. 64, no. 4, pp. 432–436, 2017.

[84] G. Zhao, D. Nešić, Y. Tan, and C. Hua, "Overcoming overshoot performance limitations of linear systems with reset control," *Automatica*, vol. 101, pp. 27–35, 2019.

[85] A. Palanikumar, N. Saikumar, and S. H. HosseinNia, "No more differentiator in pid: Development of nonlinear lead for precision mechatronics," in *2018 European Control Conference (ECC)*, 2018, pp. 991–996.

[86] L. Hazeleger, M. Heertjes, and H. Nijmeijer, "Second-order reset elements for stage control design," in *2016 American Control Conference (ACC)*, 2016, pp. 2643–2648.

[87] Y. Li, G. Guo, and Y. Wang, "Reset control for midfrequency narrowband disturbance rejection with an application in hard disk drives," *IEEE Transactions on Control Systems Technology*, vol. 19, no. 6, pp. 1339–1348, 2011.

[88] ——, "Nonlinear mid-frequency disturbance compensation in hard disk drives," *IFAC Proceedings Volumes*, vol. 38, pp. 31–36, 2005.

[89] M. S. Bahnamiri, N. Karbasizadeh, A. A. Dastjerdi, N. Saikumar, and S. H. HosseinNia, "Tuning of cglp based reset controllers: Application in precision positioning systems," *IFAC-PapersOnLine*, vol. 53, no. 2, pp. 8997–9004, 2020.

[90] N. Saikumar, R. K. Sinha, and H. HosseinNia, "Resetting disturbance observers with application in compensation of bounded nonlinearities like hysteresis in piezo-actuators," *Control Engineering Practice*, vol. 82, pp. 36–49, 2019.

[91] A. A. Dastjerdi and S. H. HosseinNia, "A frequency-domain tuning method for a class of reset control systems," *IEEE Access*, vol. 9, pp. 40 950–40 962, 2021.

[92] N. Karbasizadeh, A. A. Dastjerdi, N. Saikumar, D. Valerio, and S. H. Hossein Nia, "Benefiting from linear behaviour of a nonlinear reset-based element at certain frequencies," *2020 Australian and New Zealand Control Conference (ANZCC)*, 2020.

[93] C. Cai, A. A. Dastjerdi, N. Saikumar, and S. HosseinNia, "The optimal sequence for reset controllers," in *2020 European Control Conference (ECC)*, 2020, pp. 1826–1833.

[94] N. Saikumar, D. Valerio, and S. H. HosseinNia, "Complex order control for improved loop-shaping in precision positioning," *2019 IEEE 58th Conference on Decision and Control (CDC)*, 2019.

[95] D. Caporale, *Reset control frequency analysis tools*, https://www.mathworks.com/matlabcentral/fileexchange/116440-reset-control-frequency-analysis-tools, 2022.

A

COMPUTATIONAL ANALYSIS TOOLS

In the following appendix some of the developed MATLAB-Simulink tools are presented.

A.1. SIMULINK IMPLEMENTATION OF A RESET CONTROL SYSTEM

The set of state space equation describing the dynamics of a reset controller were shown in Section 2.1. These were integrated in a Simulink model of the expended architecture as given in Fig. A.1.

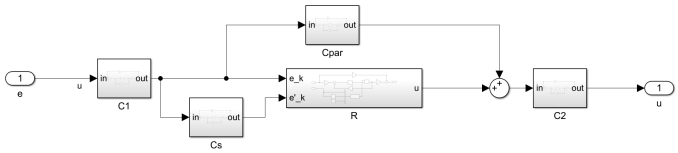

Figure A.1: Simulink block diagram of the expanded architecture including C_{par}.

The content of the the Simulink block 'R', which includes the reset controller, is shown in Fig. A.2. It can be noticed that the block uses state-space form in order to approximate the discrete time implementation of $\mathscr{R}$ as given in (22) of Chapter 4. The reset action is implemented by the `Matrix Multiply` block, which scales x_r by either I if the reset condition is not triggered or A_ρ if the reset condition is triggered. The determination whether the reset condition is triggered occurs through the algorithm im-

plemented in the MATLAB function `trigger.mat` [95], in the Simulink `Interpreted MATLAB Function` block 'trigger', which can be characterized as pseudocode with the snippet

```
if e'_k*e'_k-1 ≥ 0
    tr_k = eye(length(Arho));
else
    tr_k = Arho;
end
```

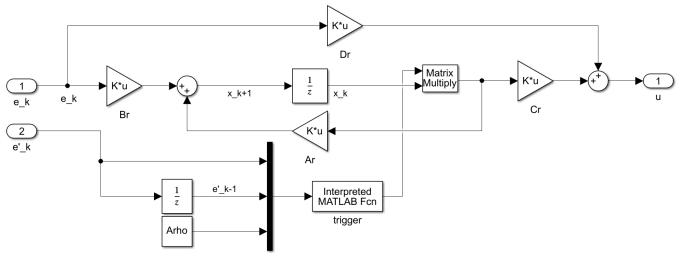

Figure A.2: Simulink block diagram of the reset controller.

A.2. OPEN-LOOP HOSIDFS

The MATLAB function `hosidfOL.mat` [95] computes the open-loop HOSIDFs for an extended architecture structure including C_{par}, based on (2.14) and (2.17). However the HOSIDFs are computed as $H_n(j\omega/n)$ instead of $H_n(j\omega)$. This is due to the fact that FRF data of G is only provided for frequencies ω, thus as $G(jn\omega)$ and the open-loop HOSIDFs are given by $H_n(j\omega) * G(jn\omega)$.

A.3. APPROXIMATE CLOSED-LOOP HOSIDFS

The MATLAB function `hosidfCL.mat` [95] computes the closed-loop HOSIDFs and the resulting pseudosensitivity for an extended architecture structure including C_{par} using the approximate method based on (2.18) and (2.19). It is possible to choose the sampling frequency of the closed-loop error signal to analyse the aliasing effect. In order to compute the closed-loop HOSIDFs it is necessary to first compute the open-loop HOSIDFs at frequency ω, `hosidfOL.mat` can thus not be utilized. Instead a new function `hosidfOL_interp.mat` [95] is utilized. In case FRF data is provided for G, linear

interpolation is used to find the value of $G(jn\omega)$.

A.4. NYQUIST STABILITY VECTOR

The MATLAB function `NSV.mat` [95] computes the Nyquist stability vector for an extended architecture structure excluding C_{par}.